UNIVERSITY OF CALIFORNIA

Los Angeles

Protein Arginine Methyltransferases: Catalytic Mechanisms and Crosstalk in Epigenetics

A dissertation submitted in partial satisfaction of the requirements for the degree Doctor of Philosophy in Biochemistry and Molecular Biology

by

Kanishk Jain

2018

ABSTRACT OF THE DISSERTATION

Protein Arginine Methyltransferases: Catalytic Mechanisms and Crosstalk in Epigenetics

by

Kanishk Jain

Doctor of Philosophy in Biochemistry and Molecular Biology

University of California, Los Angeles, 2018

Professor Steven G. Clarke, Chair

Over the last decade, protein arginine methyltransferases (PRMTs) have emerged as key regulators in epigenetic processes and have been shown to be crucial targets for drug therapies in various types of cancers. As drug-development is progressing, however, it is vital to understand the biochemical nature of these enzymes and what makes them different from other posttranslational modifiers in the epigenetic landscape. To that end, the studies conducted in this work provide novel insights into how PRMTs specify the products they make, how one of the mammalian PRMTs—PRMT7—exhibits a peculiar preference for sub-physiological temperatures, and the first evidence of positive cooperativity observed in PRMTs and potential crosstalk among them. Specifically, a model has been developed which describes the unique aspects of PRMT active sites in way that highlights the role of sterics and overall volume differences between the different types of PRMTs and allows them to produce different methylarginine derivates. Secondly, biophysical techniques in this work show that human PRMT7 preference for colder, sub-physiological temperatures may be caused due to incredibly minute

structural changes that need to be more finely measured *in vivo* and replicated *in vitro*. Finally, as the field of epigenetic research expanded and the general knowledge of enzymes in this area has grown, more and more evidence for the regulation of these regulators in the way of enzyme crosstalk has been documented. In the case of PRMTs, however, this work shows for the first time that both PRMT1 and PRMT5 display positive cooperativity when methylating histone H4 N-terminal peptides; furthermore, PRMT5's ability to methylate histone H4 R3 seems to be greatly affected by a prior methylation of H4 R17—a modification carried out by PRMT7.

The dissertation of Kanishk Jain is approved.

Joseph Ambrose Loo

Amander Therese Clark

Steven G. Clarke, Committee Chair

University of California, Los Angeles

2018

DEDICATION

I would like to dedicate this work firstly to my family.

To my father, Ashok, and mother, Anjul, who have sacrificed so much in their lives to afford their children every opportunity to succeed in a country foreign to them. Their never-ending love and support have allowed me to become the person I am today.

To my sister, Megha, from whom I learned to be confident and ambitious about the things I want in life.

To my oldest friend, Thuy, for being a stalwart and loving friend since the first day we met. Her commitment to intellectual excellence has always inspired me.

To my brothers from other mothers: John, Mike, Nick, Sean, and Zack. I'm so lucky to have met you guys.

To my high school AP Chemistry teacher, Mrs. Ina Koppel, who sparked my love for chemistry. I'm so grateful to have had a wonderful educator such as her.

TABLE OF CONTENTS

LIST OF FIGURES

LIST OF TABLES

ACKNOWLEDGEMENTS

Firstly, I would like to thank Dr. Steven Clarke for his years of mentorship in both my scientific and personal pursuits. He has always made me feel like a colleague and I have learned much from his guidance. I also want to acknowledge the significant role Dr. Jonathan Lowenson has had in my graduate career. He has been a steadfast source of knowledge, guidance, and jokes in the lab; I truly believe I would not have accomplished half of the things I have without his generous help! Furthermore, I would like to thank and acknowledge all of the present and past members of the lab with whom I've worked, especially fellow graduate student Rebeccah A. Warmack and Dr. Alexander N. Patananan and Dr. Maria Dzialo. I have been lucky enough to mentor some bright undergraduate (Cyrus Jin) and graduate students (Troy Lowe) and also want to acknowledge their assistance in the work represented here. Members of the Clubb lab, both past and current, have provided me with tremendous help throughout graduate school, so I would also like to acknowledge their aid by thanking Dr. Alex Jacobitz, Dr. Brendan Amer, Dr. Michele Kattke, Dr. Grace Huang, Ramsay Macdonald, Scott McConnell, Jason Gosschalk, Christopher Sue, and Orlando Martinez.

I would like to thank the members of my dissertation committee—Dr. David S. Eisenberg, Dr. Joseph A. Loo, Dr. Amander T. Clark, and Dr. Douglas Black—for their invaluable advice and guidance throughout my graduate career.

This work was partly supported by a Ruth L. Kirschstein National Research Award (GM007185), particularly Chapters 3, 4, and 6, and an Audree Fowler Fellowship for Protein Science (2018), particularly Chapter 5.

Chapter 3 of this dissertation is a manuscript of the publication entitled "A glutamate/aspartate switch controls product specificity in a protein arginine methyltransferase" in the *Proceedings of the National Academy of Sciences USA* (volume 113, pages 2068-2073). I

would like to acknowledge the first author Erik W. Debler and the co-authors Rebeccah A. Warmack, You Feng, Steven G. Clarke, Gunter Blobel, and Peter Stavropoulos.

Chapter 4 of this dissertation is a manuscript of the publication entitled “Protein arginine methyltransferase product specificity is mediated by distinct active-site architectures” in the *Journal of Biological Chemistry* (volume 291, pages 18299-18308). I would like to thank the other authors on this publication: Rebeccah A. Warmack, Erik W. Debler, Andrea Hadjikyriacou, Peter Stavropoulos, and Steven G. Clarke.

Analytical ultracentrifugation work in Chapter 5 was done with the aid of Dr. Martin L. Phillips in the UCLA-DOE & Biochemistry Shared Instrumentation Core Facility. Some of the circular dichroism data was collected with the help of Troy Lowe.

Chapter 6 of this dissertation is a manuscript of the publication entitled “Epigenetic control via allosteric regulation of mammalian protein arginine methyltransferases” in the *Proceedings of the National Academy USA* (volume 114, pages 10101-10106). I would like to thank the other authors: Cyrus Y. Jin and Steven G. Clarke.

VITA

2009-2013	Bachelor of Science in Chemistry with a concentration in Biochemistry University of Virginia, Charlottesville, VA
2013-2018 (expected)	Doctor of Philosophy in Biochemistry and Molecular Biology University of California, Los Angeles, Los Angeles, CA
2013-2014	Teaching Assistant, Department of Chemistry and Biochemistry University of California, Los Angeles, Los Angeles, CA
2014	Hanson-Dow Award for Teaching Excellence, Department of Chemistry and Biochemistry, University of California, Los Angeles, Los Angeles, CA
2015	Candidate in Philosophy in Biochemistry and Molecular Biology University of California, Los Angeles, Los Angeles, CA
2015-2018	Cellular and Molecular Biology Pre-Doctoral Training Grant, Trainee University of California, Los Angeles, Los Angeles, CA
2017-2018	Audree Fowler Fellowship in Protein Science University of California, Los Angeles, Los Angeles, CA
2018	Roberts A. Smith Research Award for Excellence in Biochemistry University of California, Los Angeles, Los Angeles, CA

PUBLICATIONS

Kanishk Jain, Cyrus Y. Jin, and Steven G. Clarke. “Epigenetic control via allosteric regulation of mammalian protein arginine methyltransferases.” *Proc. Natl. Acad. Sci. U.S.A*. 2017 Sep 114(38):10101-10106.

Lucie Kafkova, Erik W. Debler, John C. Fisk, **Kanishk Jain,** Steven G. Clarke, and Laurie K. Read. “The major protein arginine methyltransferase in *Trypanosoma brucei* functions as an enzyme-prozyme complex.” *J. Biol. Chem.* 2017 Feb 292(6): 2089-2100.

Kanishk Jain, Rebeccah A. Warmack, Erik W. Debler, Andrea Hadjikyriacou, Pete Stavropoulos, and Steven G. Clarke. “Protein arginine methyltransferase product specificity is mediated by distinct active-site architectures.” *J. Biol. Chem.* 2016 Aug 291(35): 18299-18308.

Erik W. Debler, **Kanishk Jain**, Rebeccah A. Warmack, You Feng, Steven G. Clarke, Gunter Blobel, and Pete Stravropoulos. “A glutamate/aspartate switch controls product specificity in a protein arginine methyltransferase.” *Proc. Natl. Acad. Sci. U.S.A*. 2016 Feb 113(8): 2068-2073

Chapter 1

Plan of the Dissertation

Through biochemical and biophysical techniques, the research in this dissertation aims to increase our understanding of the catalytic mechanisms of the major protein arginine methyltransferases (PRMTs) and how their functions are regulated biochemically. To these ends, I utilized the combined power of enzyme kinetics and structural biology to probe the fundamental properties of PRMTs.

Chapter 2 contains a concise summary of what is known about PRMTs to date and reviews, briefly, how the work in this dissertation has contributed to our knowledge of PRMTs.

The focus of Chapters 3 and 4 is on PRMT product specificity and its determinants. The nine mammalian PRMTs can be grouped into three categories based on the type of methylarginine derivative they produce—type I for asymmetric dimethylarginine (ADMA) and monomethylarginine (MMA), type II for symmetric dimethylarginine (SDMA) and MMA, and type III for only MMA. Until recently, the factors that determined how each PRMT was able to specifically produce one derivative over the other was not well understood. The publications in Chapters 3 and 4, with the collaboration of Dr. Erik W. Debler, Dr. Peter Stavropoulos, and Dr. Gunter Blobel at the Rockefeller University, and Dr. You Feng, Rebeccah A. Warmack, and Dr. Andrea Hadjikyriacou at UCLA, I was able to come with a steric/volume-centric model for the architectural determinants of PRMT product specificity. This model suggests that the active-site architectures of type I, II, and III enzymes differ in specific ways to allow for volume changes in regions which select for the production of specific methylarginine derivates.

Chapter 5 focuses on trying to understand the peculiar temperature preference for activity by mammalian PRMT7. Previous work done in the lab has shown that mammalian PRMT7 is almost inactive at physiological temperatures (37°C) while being optimally active between 15-25°C (1, 2). In order to understand why this occurs *in vitro*, I used a series of biochemical and biophysical approaches including circular dichroism and analytical ultracentrifugation. With the aid of Troy Lowe and Dr. Martin L. Phillips, I was able to observe that while enzymologically

PRMT7 displays a strong preference for colder temperatures, structural changes in the enzyme as a function of temperature are miniscule. This suggests that structural changes which may be affecting PRMT7's activity at different temperatures are fairly small relative to the large changes that are detectable using methods such as circular dichroism (CD) spectroscopy and analytical ultracentrifugation (AUC).

In Chapter 6, I explore the possibility for crosstalk and regulation among different PRMTs. It is known that many PRMTs methylate similar or the same residues on histones and these PTMs have different epigenetic outcomes (1–4). Specifically, in the case of PRMT5 and PRMT7, recent biological studies have suggested a possible avenue for PRMT7-regulated PRMT5 activity by way of methylating residue Arg-3 on histone H4 (3, 5–7). By analyzing the kinetics of PRMT5 activity on histone H4 unmethylated and methylated peptides and with the help of Cyrus Y. Jin, I was able to determine that PRMT5-mediated methylation of Arg-3 is regulated by the methylation of Arg-17 on the same peptide by PRMT7. Additionally, I discovered that both PRMT5 and PRMT1, the major PRMTs in the cell, exhibit positive cooperativity in methylating histone H4 peptides, something hitherto unknown.

Finally, Chapter 7 contains my concluding remarks and thoughts on future experiments to expand our understanding of PRMT biochemistry.

REFERENCES

1. Feng, Y., Maity, R., Whitelegge, J. P., Hadjikyriacou, A., Li, Z., Zurita-Lopez, C., Al-Hadid, Q., Clark, A. T., Bedford, M. T., Masson, J. Y., and Clarke, S. G. (2013) Mammalian protein arginine methyltransferase 7 (PRMT7) specifically targets RXR sites in lysine- and arginine-rich regions. *J. Biol. Chem.* **288**, 37010–37025
2. Feng, Y., Hadjikyriacou, A., and Clarke, S. G. (2014) Substrate specificity of human protein arginine methyltransferase 7 (PRMT7): the importance of acidic residues in the double E loop. *J. Biol. Chem.* **289**, 32604–32616
3. Blanc, R. S., and Richard, S. (2017) Arginine methylation: the coming of age. *Mol. Cell*. **65**, 8–24
4. Herrmann, F., Pably, P., Eckerich, C., Bedford, M. T., and Fackelmayer, F. O. (2009) Human protein arginine methyltransferases in vivo--distinct properties of eight canonical members of the PRMT family. *J. Cell Sci.* **122**, 667–677
5. Karkhanis, V., Wang, L., Tae, S., Hu, Y. J., Imbalzano, A. N., and Sif, S. (2012) Protein arginine methyltransferase 7 regulates cellular response to DNA damage by methylating promoter histones H2A and H4 of the polymerase δ catalytic subunit gene, POLD1. *J. Biol. Chem.* **287**, 29801–29814
6. Dhar, S. S., Lee, S.-H., Kan, P.-Y., Voigt, P., Ma, L., Shi, X., Reinberg, D., and Lee, M. G. (2012) Trans-tail regulation of MLL4-catalyzed H3K4 methylation by H4R3 symmetric dimethylation is mediated by a tandem PHD of MLL4. *Genes Dev.* **26**, 2749–2762
7. Migliori, V., Müller, J., Phalke, S., Low, D., Bezzi, M., Mok, W. C., Sahu, S. K., Gunaratne, J., Capasso, P., Bassi, C., Cecatiello, V., De Marco, A., Blackstock, W., Kuznetsov, V., Amati, B., Mapelli, M., and Guccione, E. (2012) Symmetric dimethylation of H3R2 is a newly identified histone mark that supports euchromatin maintenance. *Nat. Struct. Mol. Biol.* **19**, 136–144

Chapter 2

Introduction to Protein Arginine Methyltransferases (PRMTs)

Protein arginine methyltransferases

Recent cancer research has implicated various methyltransferases and their posttranslational methylation of proteins in the genesis and proliferation of tumors (1, 2). A prominent group of these enzymes are protein arginine methyltransferases (PRMTs), which include a family of nine related enzymes in mammals (1, 3). These enzymes are grouped together as members of the seven-β strand methyltransferases due to their characteristic seven consecutive β-strand fold. Using the cofactor *S*-adenosylmethionine (AdoMet), PRMTs methylate terminal nitrogen atoms on arginine residue side chains of their substrates. Arginine methylation of histones, carried out by PRMTs, has been shown to regulate transcription and epigenetic processes (2, 4–7). The nine mammalian PRMTs are divided into three types (**Figure 1**) based on the types of methylation they perform: type I PRMTs generate monomethyl and asymmetric dimethylarginine (MMA and ADMA respectively), type II enzymes generate MMA and symmetric dimethylarginine (SDMA), and type III enzymes generate only MMA products.

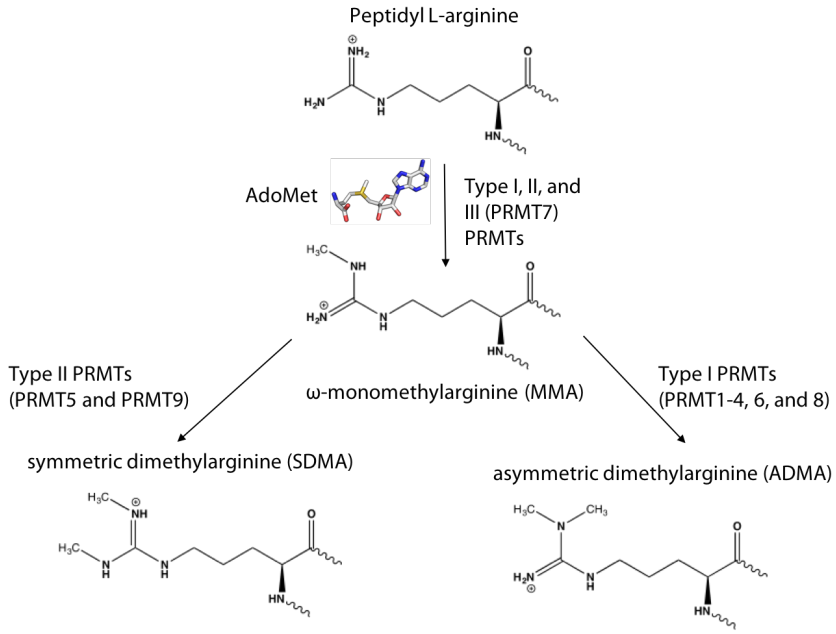

Figure 1. Scheme of arginine methylation carried out by PRMTs. ADMA and MMA produced by type I (PRMT1-4, 6, and 8), SDMA and MMA produced by type II (PRMT5 and 9), and only MMA produced by type II (PRMT7) enzymes.

Catalytic activity

Methylation can drastically change the local chemical environment in a protein by introducing a degree of hydrophobicity and extra electron density, potentially shielding the guanidino group's positive charge (5). Additionally, methyl groups can change the pattern of hydrogen bonding between an arginine and its bonding partners. The popular view in this area is

that methylation decreases the number of potential H-bonds which can be formed by replacing the guanidine protons (5). However, computational and structural studies have shown the emergence of a new type of H-bond: the CH···O bond (8, 9). CHO bonds are weaker than the conventional H-bond, but in the case of arginine methylation, the addition of a single methyl group may actually increase the number of possible H-bonds by two rather than lower that number. So far, the exact contribution methyl groups on arginine residues have on hydrogen bonding patterns is not clearly understood in the realm of biochemistry.

The catalytic seven-β strand fold of the PRMTs contains AdoMet-binding motifs and a substrate binding loop referred to as the "double E loop" due to the glutamates flanking a series of well conserved residues (1, 6, 10) (**Figure 2**). These glutamate residues are important in attracting and sustaining substrate-enzyme binding interactions since the substrates for PRMTs (i.e. histones, splicing factors, etc.) usually contain positively charged regions. Recent studies have shown the second of these glutamate residues to be a crucial determinant of type I versus type III product specificity (11) (see Chapter 3). Additionally, the "THW" loop, composed of a threonine-histidine-tryptophan segment in type I PRMTs, and with a conserved tryptophan residue in the other PRMTs, aids in the stabilization of the positively charged arginine guanidino group through cation-π and hydrogen-bonding interactions. The

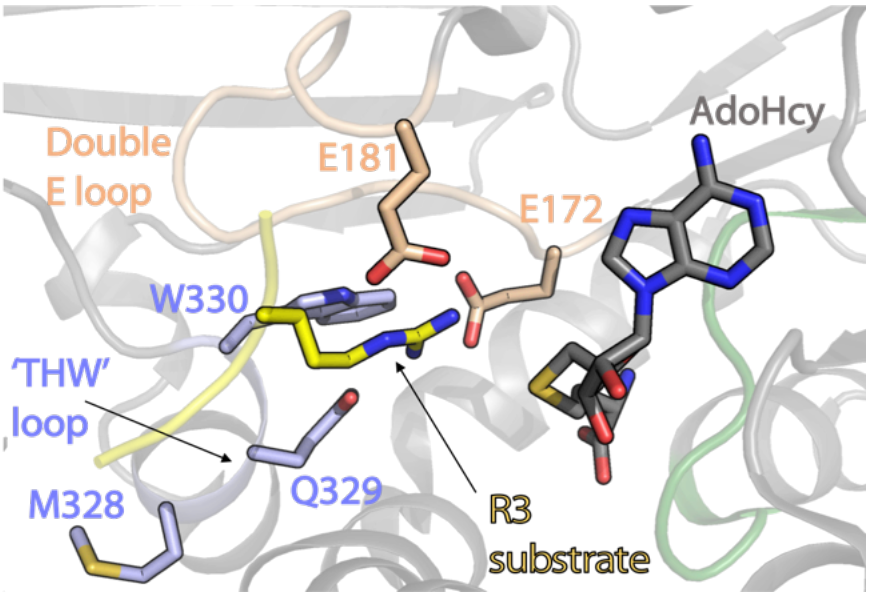

Figure 2. Active site of PRMT7 from *Trypanosoma brucei*. Major structural features of the PRMT active site are shown in this image of PRMT7 (PDB 4M38). The green moiety represents the AdoMet/AdoHcy binding domain, the pink region represents the double E loop substrate binding motif, the purple region represents the "THW" loop (present as MQW in this protein), and the yellow peptide represents the structure of a histone H4 N-terminal peptide with residue Arg-3 as the substrate residue.

"THW" loop has been shown to contribute in the type II SDMA producing activity of PRMTs; when this loop was mutated in a type III PRMT to mimic the sterics of a type II enzyme, the mutated enzyme was able to produce SDMA (12) (see Chapter 4). Taken together, these results have allowed for the development of a model for understanding PRMT product specificity that reveals active site sterics as well as total volume parameters to be major players.

Structural biology of PRMTs

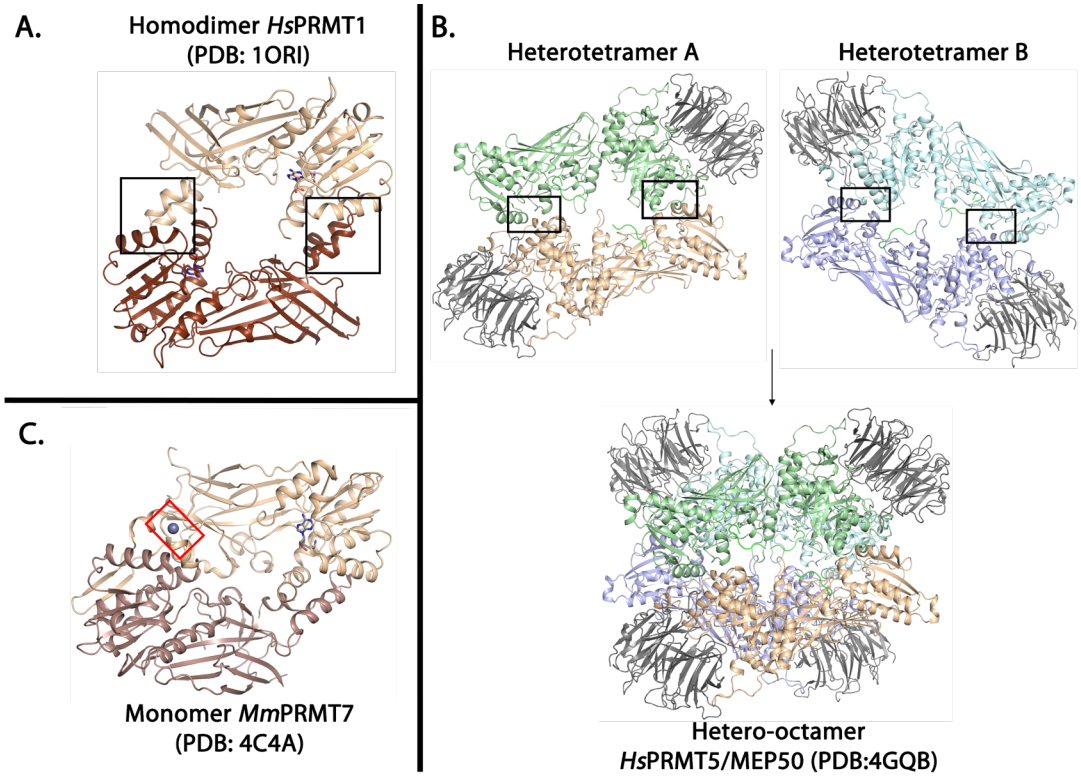

Figure 3. Oligomerized structures of the three main PRMT types. A) Human PRMT1 (PDB:1ORI) is shown here as a homodimer with one protomer in wheat and the other in brown. The dimerization arms are represented by black boxes. B) Human PRMT5/MEP50 (PDB: 4GQB) complexes are shown as heterotetramers (top) and a hetero-octamer (bottom). All MEP50 subunits are colored gray, each of the four individual PRMT5 subunits is colored green, wheat, cyan, and purple. The dimerization arms are represented by black boxes. C) Mouse PRMT7 (PDB: 4C4A) is shown here in the monomeric "homodimer-like" representation, with the N-terminal domain colored in wheat and the C-terminal domain colored in brown. The Zn-finger like domain around which the N and C-terminal domains hinge is shown in the red box with the Zn ion as purple sphere. All images were analyzed and processed in PyMOL (Schrodinger, LLC).

Type I PRMTs, classified as ADMA and MMA producers, consist of PRMT1-4, 6, and 8. Structural studies done on type I PRMTs have revealed them to exist in catalytically active homodimers in solution (13–15) (**Figure 3A**). Of these enzymes, PRMT1 is responsible for the

majority of asymmetric dimethylation of arginine residues on proteins in the cell (16) and as such, has been used as an exemplary type I enzyme in this work.

PRMT5 is the predominant type II enzyme, producing the bulk of SDMA modifications in the cell—particularly on histones and proteins required in transcriptional regulation (2, 17–21). Like type I PRMTs, PRMT5 also oligomerizes. However, unlike the former group of PRMTs, PRMT5 forms a homotetramer in solution and further associates with binding partners such as MEP50. (methylosome protein 50) to form a hetero-octameric functionally active structure that catalyzes the production of SDMA and MMA (18) (**Figure 3B**).

In the group of the nine mammalian PRMT family members, only one known type III PRMT exists —PRMT7. Mammalian PRMT7 is distinct from the major dimethylating enzymes in its family because it does not dimerize. However, the PRMT7 gene contains a gene duplication which results in two tandem methyltransferase domains that fold together around a central Zn-finger-like domain to resemble the tertiary configuration of a homodimer (22) (**Figure 3C**); it should be noted here that PRMT9 also has similar gene duplication and is a demethylating enzyme, though little is known about its structure (23). Furthermore, mutational studies show the C-terminal domain to be catalytically inactive but crucial for overall activity of the enzyme (22, 24). Interestingly, *in vitro* methylation studies with mammalian PRMT7 have shown the enzyme to prefer colder, non-physiological temperatures (25, 26).

PRMTs and disease

A number of studies have shown that PRMTs are highly overexpressed in various cancer tissues (1, 27–29) (**Table 1**). Specifically, overexpression of PRMT5 and PRMT7 has been associated with cancer metastasis (3, 27, 30, 31). PRMT7 has been linked to breast cancer progression (27, 30) and appears to be involved in cell-proliferating processes such as maintaining pluripotency (32) and response to DNA damage (31).

Overexpression of PRMT5 has been shown to promote tumor cell growth and has already been identified as a potential therapeutic target for glioblastoma (3, 33). Symmetric dimethylation

of arginine-3 of histone H4 by PRMT5 represses gene expression (34–36). For example, a plant homeodomain (PHD_{4-6}) recognizes and binds the unmethylated and ADMA versions of histone H4 at arginine 3 but not the SDMA version. The lack of binding to the SDMA version leads to repression of several MLL4-related genes (Mixed Lineage Leukemia 4). PRMT5's role in gene regulation has been highlighted in several works on embryonic stem cells (ESCs) of both the human and mouse variety. In both cases, PRMT5 is required for proliferation, and in the case of mESCs, it is needed for pluripotency as well (37, 38).

Table 1. Aberrant expression of PRMTs in various human cancers. Material adapted from Poulard and colleagues (39).

PRMTs	Aberrant expression in human cancers
PRMT1	breast, bladder, leukemia, lung, and colon cancers
PRMT2	breast and colon cancers
PRMT3	breast cancer
PRMT4	prostate and lung cancer
PRMT5	prostate, colorectal, lung, liver, and breast cancer
PRMT6	bladder, lung, and breast cancer
PRMT7	breast cancer and leukemia
PRMT8	breast, ovarian, and gastric
PRMT9	Not determined

Emergence of crosstalk among PRMTs

PRMT7 and PRMT5 stand out among the other PRMTs for very different reasons. PRMT7 is uniquely able to produce only MMA (7, 8) whereas all other mammalian PRMTs produce either ADMA or SDMA. Dimethylated arginine residues can be recognized by a variety of reader proteins (36) and the production of only MMA by PRMT7 indicates that additional reader proteins may exist that specifically recognize the singly methylated species. This novel mode of cellular recognition would dramatically change our understanding of regulation by methylation.

Additionally, PRMT5 and PRMT7 share histone and ribonucleoprotein substrates such as splicing complexes (i.e. U2 snRNP assembly) (8), indicating the possibility of crosstalk between the two enzymes via methylation. Many histone tails contain multiple sites of methylation and by performing amino acid analysis, we have determined that PRMT5 and PRMT7 methylate different

arginine residues on the same protein (i.e. Arg-3 on histone H4 for PRMT5 and Arg-17 and Arg-19 on histone H4 for PRMT7) (25, 26). This biochemical observation has been replicated consistently *in vivo* and in various disease models (2, 31, 35, 36, 40–42). Given that mammalian PRMT7 methylates distinctly different residues on the same histone tails that PRMT5 methylates, we have sought to understand how these enzymes could potentially engage in indirect regulation through their methylation activity (43) (see Chapter 6). What has remained unclear for a long time is whether PRMT7 regulates the activity of PRMT5 by methylating the same exact residue or some other region of the same substrate; in other words, does PRMT7 activity directly or indirectly control PRMT5 activity? Work described in Chapter 6 seeks to provide insight into how PRMTs interact with one another enzymologically in order to simulate the cellular environment where many other PRMTs are present and many post-translational modifications and regulatory procedures are occurring. The potential for PRMT interplay *in vivo* could lead to new perspectives on how methylation modulates biomolecular function.

REFERENCES

1. Yang, Y., and Bedford, M. T. (2013) Protein arginine methyltransferases and cancer. *Nat. Rev. Cancer*. **13**, 37–50

2. Blanc, R. S., and Richard, S. (2017) Arginine methylation: the coming of age. *Mol. Cell*. **65**, 8–24

3. Bao, X., Zhao, S., Liu, T., Liu, Y. Y., Liu, Y. Y., and Yang, X. (2013) Overexpression of PRMT5 promotes tumor cell growth and is associated with poor disease prognosis in epithelial ovarian cancer. *J. Histochem. Cytochem.* **61**, 206–217

4. Walsh, G., and Jefferis, R. (2006) Post-translational modifications in the context of therapeutic proteins. *Nat. Biotechnol.* **24**, 1241–12452

5. Fuhrmann, J., Clancy, K. W., and Thompson, P. R. (2015) Chemical biology of protein arginine modifications in epigenetic regulation. *Chem. Rev.* **115**, 5413–5461

6. Bedford, M. T., and Clarke, S. G. (2009) Protein arginine methylation in mammals: who, what, and why. *Mol. Cell*. **33**, 1–13

7. Peng, C., and Wong, C. C. (2017) The story of protein arginine methylation: characterization, regulation, and function. *Expert Rev. Proteomics*. **14**, 157–170

8. Yesselman, J. D., Horowitz, S., Brooks, C. L., and Trievel, R. C. (2015) Frequent side chain methyl carbon-oxygen hydrogen bonding in proteins revealed by computational and stereochemical analysis of neutron structures. *Proteins*. **83**, 403–410

9. Desiraju, G. R. (2005) C-H...O and other weak hydrogen bonds. From crystal engineering to virtual screening. *Chem. Commun. (Camb).* 10.1039/b504372g

10. Herrmann, F., Pably, P., Eckerich, C., Bedford, M. T., and Fackelmayer, F. O. (2009) Human protein arginine methyltransferases in vivo--distinct properties of eight canonical

members of the PRMT family. *J. Cell Sci.* **122**, 667–677

11. Debler, E. W., Jain, K., Warmack, R. A., Feng, Y., Clarke, S. G., Blobel, G., and Stavropoulos, P. (2016) A glutamate/aspartate switch controls product specificity in a protein arginine methyltransferase. *Proc. Natl. Acad. Sci. U. S. A.* **113**, 2068–2073

12. Jain, K., Warmack, R. A., Debler, E. W., Hadjikyriacou, A., Stavropoulos, P., and Clarke, S. G. (2016) Protein arginine methyltransferase product specificity Is mediated by distinct active-site architectures. *J. Biol. Chem.* **291**, 18299–18308

13. Zhang, X., and Cheng, X. (2003) Structure of the predominant protein arginine methyltransferase PRMT1 and analysis of its binding to substrate peptides. *Structure*. **11**, 509–520

14. Cura, V., Marechal, N., Troffer-Charlier, N., Strub, J.-M., van Haren, M. J., Martin, N. I., Cianférani, S., Bonnefond, L., and Cavarelli, J. (2017) Structural studies of protein arginine methyltransferase 2 reveal its interactions with potential substrates and inhibitors. *FEBS J.* **284**, 77–96

15. Zhou, R., Xie, Y., Hu, H., Hu, G., Patel, V. S., Zhang, J., Yu, K., Huang, Y., Jiang, H., Liang, Z., Zheng, Y. G., and Luo, C. (2015) Molecular Mechanism underlying PRMT1 Dimerization for SAM Binding and Methylase Activity. *J. Chem. Inf. Model.* **55**, 2623–2632

16. Dhar, S., Vemulapalli, V., Patananan, A. N., Huang, G. L., Di Lorenzo, A., Richard, S., Comb, M. J., Guo, A., Clarke, S. G., and Bedford, M. T. (2013) Loss of the major Type I arginine methyltransferase PRMT1 causes substrate scavenging by other PRMTs. *Sci. Rep.* **3**, 1311

17. Wang, M., Xu, R.-M., and Thompson, P. R. (2013) Substrate specificity, processivity, and kinetic mechanism of protein arginine methyltransferase 5. *Biochemistry*. **52**, 5430–5440

18. Antonysamy, S., Bonday, Z., Campbell, R. M., Doyle, B., Druzina, Z., Gheyi, T., Han, B.,

Jungheim, L. N., Qian, Y., Rauch, C., Russell, M., Sauder, J. M., Wasserman, S. R., Weichert, K., Willard, F. S., Zhang, A., and Emtage, S. (2012) Crystal structure of the human PRMT5:MEP50 complex. *Proc. Natl. Acad. Sci.* **109**, 17960–17965

19. Antonysamy, S. (2017) The structure and function of the PRMT5:MEP50 complex. in *Sub-cellular biochemistry*. **83**, 185–194

20. Yang, Y., Hadjikyriacou, A., Xia, Z., Gayatri, S., Kim, D., Zurita-Lopez, C., Kelly, R., Guo, A., Li, W., Clarke, S. G., and Bedford, M. T. (2015) PRMT9 is a type II methyltransferase that methylates the splicing factor SAP145. *Nat. Commun.* **6**, 6428

21. Pesiridis, G. S., Diamond, E., and Van Duyne, G. D. (2009) Role of pICLn in methylation of Sm proteins by PRMT5. *J. Biol. Chem.* **284**, 21347–21359

22. Cura, V., Troffer-Charlier, N., Wurtz, J. M., Bonnefond, L., and Cavarelli, J. (2014) Structural insight into arginine methylation by the mouse protein arginine methyltransferase 7: a zinc finger freezes the mimic of the dimeric state into a single active site. *Acta Crystallogr. D. Biol. Crystallogr.* **70**, 2401–2412

23. Hadjikyriacou, A., Yang, Y., Espejo, A., Bedford, M. T., and Clarke, S. G. (2015) Unique features of human protein arginine methyltransferase 9 (PRMT9) and its substrate RNA splicing factor SF3B2. *J. Biol. Chem.* **290**, 16723–16743

24. Miranda, T. B., Miranda, M., Frankel, A., and Clarke, S. (2004) PRMT7 is a member of the protein arginine methyltransferase family with a distinct substrate specificity. *J. Biol. Chem.* **279**, 22902–22907

25. Feng, Y., Maity, R., Whitelegge, J. P., Hadjikyriacou, A., Li, Z., Zurita-Lopez, C., Al-Hadid, Q., Clark, A. T., Bedford, M. T., Masson, J. Y., and Clarke, S. G. (2013) Mammalian protein arginine methyltransferase 7 (PRMT7) specifically targets RXR sites in lysine- and arginine-rich regions. *J. Biol. Chem.* **288**, 37010–37025

26. Feng, Y., Hadjikyriacou, A., and Clarke, S. G. (2014) Substrate specificity of human protein arginine methyltransferase 7 (PRMT7): the importance of acidic residues in the double E loop. *J. Biol. Chem.* **289**, 32604–32616

27. Baldwin, R. M., Haghandish, N., Daneshmand, M., Amin, S., Paris, G., Falls, T. J., Bell, J. C., Islam, S., and Côté, J. (2015) Protein arginine methyltransferase 7 promotes breast cancer cell invasion through the induction of MMP9 expression. *Oncotarget*. **6**, 3013–3032

28. Koh, C. M., Bezzi, M., Low, D. H. P., Ang, W. X., Teo, S. X., Gay, F. P. H., Al-Haddawi, M., Tan, S. Y., Osato, M., Sabò, A., Amati, B., Wee, K. B., and Guccione, E. (2015) MYC regulates the core pre-mRNA splicing machinery as an essential step in lymphomagenesis. *Nature*. **523**, 96–100

29. Hu, D., Gur, M., Zhou, Z., Gamper, A., Hung, M.-C., Fujita, N., Lan, L., Bahar, I., and Wan, Y. (2015) Interplay between arginine methylation and ubiquitylation regulates KLF4-mediated genome stability and carcinogenesis. *Nat. Commun.* **6**, 8419

30. Yao, R., Jiang, H., Ma, Y., Wang, L., Wang, L., Du, J., Hou, P., Gao, Y., Zhao, L., Wang, G., Zhang, Y., Liu, D.-X., Huang, B., and Lu, J. (2014) PRMT7 induces epithelial-to-mesenchymal transition and promotes metastasis in breast cancer. *Cancer Res.* **74**, 5656–5667

31. Karkhanis, V., Wang, L., Tae, S., Hu, Y. J., Imbalzano, A. N., and Sif, S. (2012) Protein arginine methyltransferase 7 regulates cellular response to DNA damage by methylating promoter histones H2A and H4 of the polymerase δ catalytic subunit gene, POLD1. *J. Biol. Chem.* **287**, 29801–29814

32. Wang, Y.-C., Peterson, S. E., and Loring, J. F. (2014) Protein post-translational modifications and regulation of pluripotency in human stem cells. *Cell Res.* **24**, 143–160

33. Yan, F., Alinari, L., Lustberg, M. E., Martin, L. K., Cordero-Nieves, H. M., Banasavadi-

Siddegowda, Y., Virk, S., Barnholtz-Sloan, J., Bell, E. H., Wojton, J., Jacob, N. K., Chakravarti, A., Nowicki, M. O., Wu, X., Lapalombella, R., Datta, J., Yu, B., Gordon, K., Haseley, A., Patton, J. T., Smith, P. L., Ryu, J., Zhang, X., Mo, X., Marcucci, G., Nuovo, G., Kwon, C. H., Byrd, J. C., Chiocca, E. A., Li, C., Sif, S., Jacob, S., Lawler, S., Kaur, B., and Baiocchi, R. A. (2014) Genetic validation of the protein arginine methyltransferase PRMT5 as a candidate therapeutic target in glioblastoma. *Cancer Res.* **74**, 1752–1765

34. Sun, L., Wang, M., Lv, Z., Yang, N., Liu, Y., Bao, S., Gong, W., and Xu, R.-M. (2011) Structural insights into protein arginine symmetric dimethylation by PRMT5. *Proc. Natl. Acad. Sci.* **108**, 20538–20543

35. Dhar, S. S., Lee, S.-H., Kan, P.-Y., Voigt, P., Ma, L., Shi, X., Reinberg, D., and Lee, M. G. (2012) Trans-tail regulation of MLL4-catalyzed H3K4 methylation by H4R3 symmetric dimethylation is mediated by a tandem PHD of MLL4. *Genes Dev.* **26**, 2749–2762

36. Migliori, V., Müller, J., Phalke, S., Low, D., Bezzi, M., Mok, W. C., Sahu, S. K., Gunaratne, J., Capasso, P., Bassi, C., Cecatiello, V., De Marco, A., Blackstock, W., Kuznetsov, V., Amati, B., Mapelli, M., and Guccione, E. (2012) Symmetric dimethylation of H3R2 is a newly identified histone mark that supports euchromatin maintenance. *Nat. Struct. Mol. Biol.* **19**, 136–144

37. Tee, W.-W., Pardo, M., Theunissen, T. W., Yu, L., Choudhary, J. S., Hajkova, P., and Surani, M. A. (2010) Prmt5 is essential for early mouse development and acts in the cytoplasm to maintain ES cell pluripotency. *Genes Dev.* **24**, 2772–2777

38. Gkountela, S., Li, Z., Chin, C. J., Lee, S. a, and Clark, A. T. (2014) PRMT5 is required for human embryonic stem cell proliferation but not pluripotency. *Stem Cell Rev.* **10**, 230–9

39. Poulard, C., Corbo, L., and Le Romancer, M. (2016) Protein arginine methylation/demethylation and cancer. *Oncotarget*. **7**, 67532–67550

40. Blanc, R. S., Vogel, G., Chen, T., Crist, C., and Richard, S. (2016) PRMT7 preserves satellite cell regenerative capacity. *Cell Rep.* **14**, 1528–1539

41. Ying, Z., Mei, M., Zhang, P., Liu, C., He, H., Gao, F., and Bao, S. (2015) Histone arginine methylation by PRMT7 controls germinal center formation via regulating Bcl6 transcription. *J. Immunol.* **195**, 1538–1547

42. Blanc, R. S., and Richard, S. (2017) Regenerating muscle with arginine methylation. *Transcription*. 10.1080/21541264.2017.1291083

43. Jain, K., Jin, C. Y., and Clarke, S. G. (2017) Epigenetic control via allosteric regulation of mammalian protein arginine methyltransferases. *Proc. Natl. Acad. Sci. U. S. A.* **114**, 10101–10106

Chapter 3

A glutamate/aspartate switch controls product specificity in a protein arginine methyltransferase

The work described in this chapter has been reproduced from:

Erik W. Debler, Kanishk Jain, Rebeccah A. Warmack, You Feng, Steven G. Clarke, Gunter Blobel, and Pete Stravropoulos. “A glutamate/aspartate switch controls product specificity in a protein arginine methyltransferase.” *Proc. Natl. Acad. Sci. U.S.A*. 2016 Feb 113(8): 2068-73.

ABSTRACT

Trypanosoma brucei PRMT7 is a protein arginine methyltransferase that strictly monomethylates various substrates, thus classifying it as a type III PRMT. Yet, the molecular basis of its unique product specificity has remained elusive. Here we present the structure of *Tb*PRMT7 in complex with its cofactor product *S*-adenosyl-L-homocysteine (AdoHcy) at 2.8Å resolution and identify a glutamate residue critical for its monomethylation behavior. *Tb*PRMT7 is comprised of the conserved methyltransferase and β-barrel domains, an N-terminal extension, and a dimerization arm. The active site at the interface of the N-terminal extension, methyltransferase and β-barrel domains is stabilized by the dimerization arm of the neighboring protomer, providing a structural basis for dimerization as a prerequisite for catalytic activity. Mutagenesis of active-site residues highlights the importance of Glu181, the second of the two invariant glutamate residues of the double E loop that coordinate the target arginine in substrate peptides/proteins and increase its nucleophilicity. Strikingly, mutation of Glu181 to aspartate converts *Tb*PRMT7 into a type I PRMT producing asymmetric dimethylarginine (ADMA). Isothermal titration calorimetry (ITC) using a histone H4 peptide showed that the Glu181Asp mutant has markedly increased affinity for monomethylated peptide with respect to the wild type, suggesting that the enlarged active site can favorably accommodate monomethylated peptide and provide sufficient space for ADMA formation. In conclusion, these findings yield valuable insights into the product specificity and the catalytic mechanism of protein arginine methyltransferases and have important implications for the rational (re)design of PRMTs.

SIGNIFICANCE STATEMENT

Posttranslational modifications in proteins profoundly modulate their function, and enzymes that generate these modifications therefore have key regulatory roles in a wide array of biological processes. Protein arginine methyltransferases (PRMTs) attach methyl group(s) to arginines and differ in their product specificity, as they form either monomethyl arginine (MMA), asymmetric (ADMA) or symmetric dimethyl arginine (SDMA), which each relay specific biological signals. Although the members of the PRMT family are structurally highly homologous, the precise molecular basis of their product specificity has not been determined. Based on our structure of *Tb*PRMT7, which explicitly forms MMA, we identified a glutamate residue as a key determinant of its product specificity and we were able to engineer a PRMT7 mutant capable of ADMA formation.

INTRODUCTION

Posttranslational modifications of proteins can affect their structure, catalytic activity, and molecular interactions (1). Methylation of the guanidino group of arginine residues represents a prominent subset of these reactions (2). Histone arginine methylation is associated with gene silencing and activation (3); the modification of arginine residues in a variety of non-histone proteins including splicing and transcription factors can regulate their activity (4, 5).

Most of the enzymes that catalyze arginine methylation are designated PRMTs (protein arginine methyltransferases) and require the cofactor *S*-adenosyl-L-methionine (AdoMet) as the methyl donor (6). Four types of arginine methylation products have been described: ω-N^G-monomethylarginine (MMA), asymmetric ω-N^G-N^G dimethylarginine (ADMA), symmetric ω-N^G-$N^{G'}$ dimethylarginine (SDMA) and δ-N^G-methylarginine (6, 7). Accordingly, PRMTs can be categorized into four groups: Type I PRMTs catalyze ADMA formation, type II PRMTs catalyze SDMA formation, type III PRMTs catalyze MMA formation and type IV PRMTs catalyze δ-N^G-methylarginine formation. Type I, II, and III PRMTs are widely distributed in nature, while type IV PRMTs appear to be limited to yeasts and plants (8). Interestingly, while type I and II enzymes catalyze MMA production in addition to their dimethyl products, type III enzymes are the only PRMTs that produce MMA alone. To date, only one methyltransferase, PRMT7, has been reported to have type III activity in mice, humans, and trypanosomes (9-13). The function of PRMT7 has been linked to cancer metastasis (4, 14, 15), DNA damage (16), pluripotency (17), and parasite infection (18).

All PRMTs that have been structurally characterized to date share a conserved catalytic core of about 300-350 residues comprising an AdoMet-binding methyltransferase and a β-barrel domain. Another common feature of PRMTs is the dimerization of the catalytic core that is realized in most cases by non-covalent association of two protomers. Covalent linkage of two PRMT modules has also been observed (19-22). Although representative structures of type I, II, and III

enzymes have been determined (13, 19, 20, 23-25), our understanding of product specificity in these enzymes remains fragmentary. In order to unravel the molecular basis of the strict MMA activity of PRMT7 enzymes, we determined the x-ray crystal structure of *Trypanosoma brucei* PRMT7, which was recently reported in two different crystal forms (13). While this former study established its dimeric state in solution (13), we generated a dimerization-deficient mutant where active-site residues remain intact and demonstrated that dimerization is necessary for catalysis. Importantly, we performed extensive mutational analysis and identified and proved for the first time that Glu181 is a key residue for monomethylation by *Tb*PRMT7. We carried out isothermal titration calorimetry to characterize peptide binding to wild-type and mutant proteins and assayed product formation. Collectively, these studies provide new insights into the catalytic mechanism and product specificity of this class of enzymes.

RESULTS

*Tb*PRMT7 is a type III PRMT that forms only monomethylarginine

*Tb*PRMT7 exclusively produces MMA with protein substrates including histones and the trypanosomal RNA binding protein 16 (*Tb*RBP16) (12). *Tb*PRMT7 also effectively methylates a peptide corresponding to the amino acid sequence of the N-terminal 21 residues of human histone H4; however, when the arginine residue at position 3 was replaced by an MMA residue, little or no methylation was observed (13), suggesting that Arg-3 was the prominent site of methylation in this peptide and that the enzyme was unable to catalyze the addition of a second methyl group on this residue to form SDMA or ADMA. However, the sensitivity of the latter assay was low.

In order to rule out any possible dimethylation, we used *Tb*RBP16 and human histone H4 peptides (residues 1-21) as substrates in an amino acid analysis method that could detect specific dimethylated substrates on a sub-femtomole level. We were able to demonstrate the complete inability of *Tb*PRMT7 to produce dimethylarginine species with *Tb*RBP16 under conditions where 0.01% of such methylated species would be detected (Fig. 1*A*); sensitivity is based on the ratio of the background radioactivity to the MMA peak radioactivity. We next demonstrated that a histone $H4^{1-21}$ peptide acetylated at its N-terminus is also an excellent substrate for *Tb*PRMT7 and yields only MMA where 0.02% of a dimethylated product would be detected (Fig. 1*B*). Finally, we were able to directly test for dimethylation using the corresponding peptide that had MMA substituted for arginine at position 3 ($H4^{1-21}$ R3MMA); the presence of only monomethylated H4 peptide provides a direct substrate for any dimethylation reaction and limits any competition for methylation between unmethylated and monomethylated species. Again, no production of dimethylated arginine species was detected under conditions where 0.5% would be readily detected (Fig. 1*C*). Only a small increase in MMA over the background of automethylation was observed (perhaps due to methylation at arginine-17 and/or arginine-19), indicating that the major site of methylation on this peptide is at arginine-3 (Fig. 1*C*).

Overall structure of *Tb*PRMT7

In order to obtain a detailed picture of the active site at atomic resolution, we set out to determine the x-ray crystal structure of *Tb*PRMT7. Limited proteolysis on the full-length protein identified a stable, N-terminally truncated fragment spanning residues 32-390, referred to as *Tb*PRMT7 in the remainder of the manuscript for convenience. Notably, its catalytic activity is comparable to that of full-length protein. In order to obtain phase information for the *de novo* structure determination, the protein was derivatized with seleno-methionine. The 2.8Å crystal structure was solved using the single anomalous dispersion (SAD) phasing technique and refined to an R_{free}/R_{work} = 26.1/ 22.1%. For details of the data collection and refinement statistics, see *Supporting Informtation (SI)*, Table S1.

In an independent study, Wang et al. identified a similar core fragment of *Tb*PRMT7 (residues 36-378) and determined its crystal structure in two different crystal forms (13). Despite the alternative crystal packing, *Tb*PRMT7 adopts the same compact, roughly rhombus-shaped homodimer, in which two protomers are arranged in an antiparallel fashion with a twofold symmetry axis perpendicular to the rhombus (Fig. 2*B*) (13). Since the dimeric *Tb*PRMT7-AdoHcy complexes are essentially identical in the different crystal forms with an RMSD of 0.5Å for 670 Cα atoms, confirming the validity of the dimeric structure, only key features of the overall structure are recapitulated below.

The structured core of a *Tb*PRMT7 protomer resembles that of other PRMTs and consists of four modules: An N-terminal extension (residues 32-77), the AdoHcy-containing methyltransferase domain (residues 78-202), and the β-barrel domain (residues 203-390) that contains a protruding dimerization arm (residues 224-238) (Fig. 2*B*) (13, 23, 24). The two active sites that would bind the methyl donor AdoMet and the target arginine of the substrate are located ~36Å apart on the same face of the homodimer. The total buried surface area between the two protomers amounts to 7,560 $Å^2$ as calculated by the PISA server (26) and is primarily formed by

the N-terminal extension and the dimerization arm and to a smaller degree by helices αE, αH', and αK at the center of the dimer (Fig. 2*B*).

Dimerization is necessary for *Tb*PRMT7 catalytic activity

Using multi angle-light scattering, we confirmed that *Tb*PRMT7 exists as a dimer in solution (*SI*, Fig. S1), consistent with the large interface observed in the crystal structure and consistent with previous results from small-angle x-ray scattering (13). In order to assess the importance of dimerization for catalysis, we created a mutant that is deficient in dimerization while keeping the active site intact. To this end, we replaced residues 224 to 235 of the dimerization arm with glycines. This dimerization arm mutant was exclusively monomeric in solution, indicating that the mutant is still properly folded, while its catalytic activity was greatly reduced (Table 1). These data strongly suggest a requirement of dimerization for efficient catalysis. We confirmed this correlation with a second mutant, in which the N-terminal extension (residues 1-77 including helix αY) was truncated (*Tb*PRMT7ΔN mutant). Again, dimerization is abolished with a concomitant loss in catalytic activity (Table 1). However, since helix αY of the N-terminal extension directly contributes several residues to the active site (see below), the effect of helix αY removal cannot be solely ascribed to the dimerization deficiency.

Active site of *Tb*PRMT7

The active site of *Tb*PRMT7 is formed by the methyltransferase domain, helix αY in the N-terminal extension, and a short motif of the β-barrel (Fig. 3). The cofactor product AdoHcy is well defined in the electron density map, adopts its canonical conformation observed in AdoMet-dependent methyltransferases, and engages in highly conserved interactions with the methyltransferase domain (24). AdoHcy sits in the lower part of the binding pocket with the methionine moiety at the bottom, while the upper part of the cavity is poised for accommodating the incoming arginine of the substrate. The strongly negative electrostatic surface potential of the binding pocket is complementary to a substrate harboring a positively charged arginine residue

(*SI*, Fig. S2). Since the methyl group of AdoMet is transferred from its sulfur atom to a terminal nitrogen atom of the target arginine during catalysis, the residues adjacent to the sulfur atom of AdoHcy are expected to be most relevant for governing product specificity in *Tb*PRMT7. The two conserved eponymous glutamate residues Glu172 and Glu181 as well as Ile173 of the double E loop in the methyltransferase domain form one side of the binding pocket (27), opposed by Phe71 and His72 of helix αY in the N-terminal extension on the other side. The bottom of the pocket is formed by Met75 of helix αY, while Gln329 and Trp330 of helix αK in the β-barrel domain are wedged between the methyltransferase and β-barrel domains. The latter two residues are part of the THW motif termed after the threonine, histidine, and tryptophan residues predominantly found in type I PRMTs. In PRMT7 enzymes, however, methionine and glutamine substitute for the threonine and histidine residues. Comparison with the *Tb*PRMT7-AdoHcy complex of the other crystal form (PDB code 4M37) reveals that almost all active-site residues adopt identical positions and rotamers, with slight deviations observed for Met75, Glu172, Glu181, and Gln329.

Active-site mutations decrease type III methylation activity

In order to investigate the impact of individual residues on the methylation activity, mutations were made at key residues in the active site, e.g. the double E loop and THW motif (27). Using *Tb*RBP16 as a substrate, MMA production was assayed by amino acid analysis (Table 1). Several of the mutants displayed similar levels of MMA as wild-type *Tb*PRMT7, including mutants for three residues in the double E loop (Ile173Val, Ile173Leu/Phe174Leu, and Gly180Tyr), a mutant of the THW motif (Gln329His), and two mutants in helix αY (Phe71Ala and Met75Phe). While these mutations did not markedly affect activity, the remaining mutants displayed severe losses in activity, highlighting the significance of these amino acids in catalysis. Notably, no ADMA or SDMA product was formed in any of these mutants under conditions where 0.02% would have been detected.

A mutation in the double E loop converts *Tb*PRMT7 into an ADMA-producing enzyme

The ability of PRMTs to dimethylate arginines to form either SDMA or ADMA relies on sufficient space within the active site to accommodate not only the unmodified, but also the larger monomethylated arginine residue for subsequent dimethylation (28). Notably, none of the mutants yielded any ADMA or SDMA with *Tb*RBP16 or the $H4^{1-21}$ peptide. Many of these mutants showed significantly decreased activity, making it difficult to observe any level of possible dimethylarginine products. In order to overcome this limitation, the activity of certain mutants was tested with an already methylated H4 peptide at Arg3 ($H4^{1-21}$R3MMA). When $H4^{1-21}$R3MMA is used as a substrate with mutant Glu181Asp, we demonstrated production of both MMA and ADMA (Fig. 4*C*). The MMA formed here presumably results from the methylation of the unmodified arginine-17 and/or arginine-19 residues. With the unmodified $H4^{1-21}$ peptide, the Glu181Asp mutant shows strictly type III activity (Fig. 4 *A* and *B*).

A similar mutational study of the first glutamate in *Tb*PRMT7's double E loop (Glu172Asp) did not reveal any production of dimethylated arginine species. The side chain carboxyl atoms of the first glutamate residue in the*Tb*PRMT7 double E loop (Glu172) have lower B-values than those of the second glutamate (Glu181), consistent with the deeper burial of Glu172 in the protein interior and its larger number of interactions with neighboring residues than the more solvent-exposed Glu181. A similar situation occurs for the first and second glutamate residues in the double E loop of other PRMTs (*SI*, Table S2). To further confirm the production of ADMA, thin layer chromatography (TLC) was performed with acid hydrolysates of the methylation reaction and methylarginine standards. Radioactivity from TLC slices confirms that the Glu181Asp mutant does produce both MMA and ADMA with the $H4^{1-21}$R3MMA peptide (Fig. 4*D*).

The *Tb*PRMT7 Glu181Asp mutant has a higher affinity for the monomethylated peptide than wild-type *Tb*PRMT7

In order to analyze peptide binding to the wild-type and mutant Glu181Asp enzymes, we performed isothermal titration calorimetry (ITC) with $H4^{1-21}$ and $H4^{1-21}$R3MMA peptides (Fig. 5). Consistent with a strong electrostatic interaction, binding of the $H4^{1-21}$ peptide to *Tb*PRMT7 is highly dependent on ionic strength, with relatively strong binding (K_D = 2.7 μM) at low salt concentration (20 mM NaCl) and essentially no binding at 300 mM NaCl (K_D = 0.4 M) (*SI*, Table S3). The wild-type *Tb*PRMT7 enzyme binds its substrate $H4^{1-21}$ with higher affinity (K_d = 2.7 μM) than its monomethylation product $H4^{1-21}$R3MM (K_d = 9.0 μM), thermodynamically favoring product release. While the affinity for the unmodified $H4^{1-21}$ peptide (K_d = 2.0 μM) is essentially unchanged in the Glu181Asp mutant with respect to the wild-type enzyme, this mutant strikingly has increased binding affinity for the methylated peptide (K_d = 1.5 vs. 9.0 μM of the wild-type). Thus, the Glu181Asp mutant favors binding of the bulkier $H4^{1-21}$R3MM peptide, which can be rationalized by providing a more spacious binding pocket, stabilizing the MMA substrate-enzyme interactions and enabling dimethylation.

DISCUSSION

We determined the crystal structure of a protein arginine methyltransferase, PRMT7 from *T. brucei*, in complex with the methyl donor product AdoHcy and performed biochemical and mutational analyses to elucidate its catalytic mechanism and the structural basis of its exquisite product specificity. Although various suggestions have been made for the role of specific residues in the active site of PRMTs and although a constricted active site has recently been suggested as the basis for MMA activity in different crystal forms of *Tb*PRMT7 (13, 27), little is known experimentally about key residues that direct which methylarginine derivative is produced. This product specificity is crucial to the function of these enzymes, because proteins that bind methylated substrates (so-called “methyl readers”) differentially recognize ADMA and SDMA (3, 29), and potentially MMA. Thus, defining the exact components of catalysis and product specificity for this class of enzymes has become increasingly important. Although it has not been established that the mammalian and trypanosomal PRMT7 enzymes have the same function, the degree of sequence identity (28% over the full-length *Tb*PRMT7 protein compared to human PRMT7), its strict monomethylating behavior, and its robust enzymatic activity make the protozoan enzyme a facile system to study the biochemistry of type III PRMTs.

Notably, *Tb*PRMT7 and mammalian PRMT7 have a distinct structural organization (9, 10, 13, 20). While the mammalian enzymes contain two PRMT cores in tandem, the trypanosomal enzyme contains only one PRMT core. However, our light scattering analysis (*SI*, Fig. S1) as well as previous small-angle x-ray scattering studies (13) showed that *Tb*PRMT7 forms a homodimer in solution. The juxtaposition of the two tandem PRMT cores in mouse and roundworm PRMT7 crystal structures recapitulates the dimeric *Tb*PRMT7 architecture, sharing a similar overall quaternary structure (19, 20). Although only one PRMT module is catalytically active in *Mm*PRMT7 and *Ce*PRMT7 (19, 20), our data (Table 1) as well as those of others suggest that

dimerization of PRMT7 cores – either by a non-covalent assembly or by juxtaposition of two units as part of one polypeptide – is a prerequisite for catalytic activity (19, 20).

Another difference between mammalian and trypanosomal PRMT7 enzymes pertains to their substrate specificity (9, 10, 13, 20). Human PRMT7, for example, has a substrate specificity for RXR motifs surrounded by basic residues, such as Arg17 and Arg19 in $H4^{1-21}$ (9, 10), while our experiments with wild-type *Tb*PRMT7 and the $H4^{1-21}$ peptide demonstrate that arginine methylation does not occur at this motif. By contrast, Arg3 is the major site of methylation in this peptide by *Tb*PRMT7 (Fig. 1), as indicated by the lack of MMA production above automethylation levels with the $H4^{1-21}$ peptide monomethylated at Arg3. Furthermore, the absence of any additional methylated species confirms the inability of *Tb*PRMT7 to catalyze dimethylation reactions.

Site-directed mutagenesis experiments involving residues of the *Tb*PRMT7 active site have given insight into key structural players of this enzyme's function. Several of the mutations are located in known PRMT motifs – including Gln329Ala in the THW motif as well as Glu172Gln and Glu181Gln in the double E loop (13, 27). The importance of the double E loop in determining PRMT activity has been widely reported (27), as the methylated nitrogen atoms of the arginine(s) in substrate proteins are coordinated through these two glutamate residues (13, 24, 25). These results demonstrate the importance of these residues on the activity of the *Tb*PRMT7 enzyme.

By analyzing the effects certain residues have on *Tb*PRMT7 in a biochemical and structural context, we have identified Glu181 as a crucial molecular component of this enzyme's unique catalysis (Fig. 4). In so doing, we have also expanded the current understanding of how type I and type III enzymes behave and why their methylation behavior differs from one another. A comparison of the distance between the two glutamate residues of the double E loop shows that the glutamates of the type III PRMTs are generally closer together (8.4Å on average for *Tb*PRMT7, PDB codes 4M36, 4M37, 4M38, 5EKU; 6.8Å for *Ce*PRMT7, 3WST, 3X0D; 8.7Å for

*Mm*PRMT7, 4C4A) than those in type I PRMTs (e.g. 12.5Å in *Rn*PRMT1, 1ORI; 13.2Å in *Mm*PRMT6, 4C07; 8.5Å in *Hs*PRMT4, 4IKP) (*SI*, Fig. S3), consistent with the previous finding that *Tb*PRMT7 features a smaller guanidine binding pocket with respect to type I and type II PRMTs (13). The Glu181Asp mutation effectively shortens the side chain at that position by one carbon-carbon bond, increasing the distance between the flanking residues of the double E loop. An enlarged cavity would resemble the larger type I enzyme cavities more closely and allow for the recognition of an already methylated species, resulting in subsequent dimethylation. Indeed, our binding studies show a marked increase in affinity in the Glu181Asp mutant for a methylated substrate ($H4^{1-21}$R3MMA) with respect to the wild-type enzyme (Fig. 5). The Glu181Asp mutation still maintains the same charge at that position, allowing for similar interactions between the enzyme and the substrate's arginine, albeit at a weaker level. These findings provide a model for predicting the structural determinants of type I methylation, mediated by enzymes with longer distances between glutamates of the double E loop, versus type III methylation, mediated by enzymes with relatively shorter distances between the glutamates of the double E loop (about 1-2 Å shorter).

Product specificity plays also an important role in histone lysine methyltransferases (HKMTs), as mono-, di-, and trimethylation of lysines relay different biological signals and hence must be strictly controlled. A comparison between the structures of the lysine monomethyltransferase SET7/9 and the trimethyltransferase DIM-5 revealed that the different product specificity can be ascribed to a switch between a tyrosine in SET7/9 for a phenylalanine residue in DIM-5 (30, 31). In detail, DIM-5 contains Phe281 in close proximity to the ε-amino group of the target lysine. In SET7/9, Tyr305 occupies the equivalent position of Phe281 in DIM-5. The addition of the hydroxyl group in Tyr305 narrows the substrate channel and sterically hinders the insertion of a dimethylated ε-amino group at the target lysine, resulting in strict monomethylation activity of SET7/9. Strikingly, the Phe281Tyr mutation in DIM-5 results in the alteration of product

specificity from a trimethylated lysine to a mono- and dimethylated product, whereas the reverse mutation of Tyr305Phe in SET7/9 abolished the strict monomethylation activity and allowed for the formation of di- and trimethylated product. This tyrosine/phenylalanine switch in HKMTs depicts the importance of the absence or presence of a single non-hydrogen atom in the active site for product specificity and recapitulates our finding of an analogous glutamate/aspartate switch that controls product specificity in PRMTs.

In conclusion, our biochemical and structural analyses have defined the components that restrict type III PRMTs to only monomethylate its target arginines and, more generally, provided insights into the attributes that direct PRMT-mediated catalysis. This knowledge will not only be useful for the prediction of the methylation behavior of novel, thus far uncharacterized members of this family, but will also prove valuable in the rational (re)design of other PRMTs.

SHORT METHODS

The details of molecular cloning, expression, purification, crystallization, x-ray diffraction data collection, structure determination, isothermal titration calorimetry, multiangle light scattering, and amino acid analysis of protein and peptide substrates are described in the *SI*. In short, *Tb*PRMT7 was expressed in *E. coli* with a N-terminal His-tag. Recombinant proteins were purified using several chromatographic techniques. The structure was solved by SAD from seleno-L-methionine-labeled crystals.

ACKNOWLEDGEMENTS

We thank H. Rust (The Scripps Research Institute) and P. Thompson (UMass Medical School) for providing the $H4^{1-21}$ and $H4^{1-21}$R3MMA peptides, L. Read (SUNY Buffalo) for providing the expression vector for *Tb*RBP16, M. Dzialo (UCLA) for help with amino acid analysis, D. Berman (Rockefeller University) for help with protein expression and purification, D. King (UC Berkeley) for mass spectrometry analysis, M. Becker and R. Fischetti (APS) and W. Shi (NSLS) for support during data collection, and the Structural Biology and the High-Throughput Screening and Spectroscopy Resource Centers at Rockefeller University for support. X-ray data were measured at the GM/CA beamline 23ID-D at APS, supported by funds from NCI (ACB-12002) and NIGMS (AGM-12006), and at beamline X29 at NSLS, supported by NIH grants P41GM103473 and P30-EB-00998. EWD was a Frey Fellow of the Damon Runyon Cancer Research Foundation (DRG-1977-08). This work was also supported by grants from NIH including GM026020 (SGC) and a Ruth L. Kirschstein National Service Award GM007185 (KJ and RAW).

TABLES AND FIGURES

Table 1. Type III enzymatic activity of WT and mutant *Tb*PRMT7 enzymes

Enzyme	Percentage Type III Activity
Wild-Type	**100**
Automethylation	1.3
Dimerization mutants	
224-235 mutated to 12 Glycines	0.16
1-74 deletion	0.0055
Double EE loop mutants	
G180Y	119
I173L F174L	109
I173V	102
G180N	58
E172D	21
E181D	14.2
I173A	8.6
I173G	1.9
E181Q	1.1
E172D E181D	0.32
E172Q	0.17
I173P F174M	0.04
G175D M177E	0.02
THW loop mutants	
Q329H	99.6
Q329F	90.1
Q329A	14.1
W330A	46
Helix αY mutants	
F71A	96.1
M75F	94.5
M75A	5.2

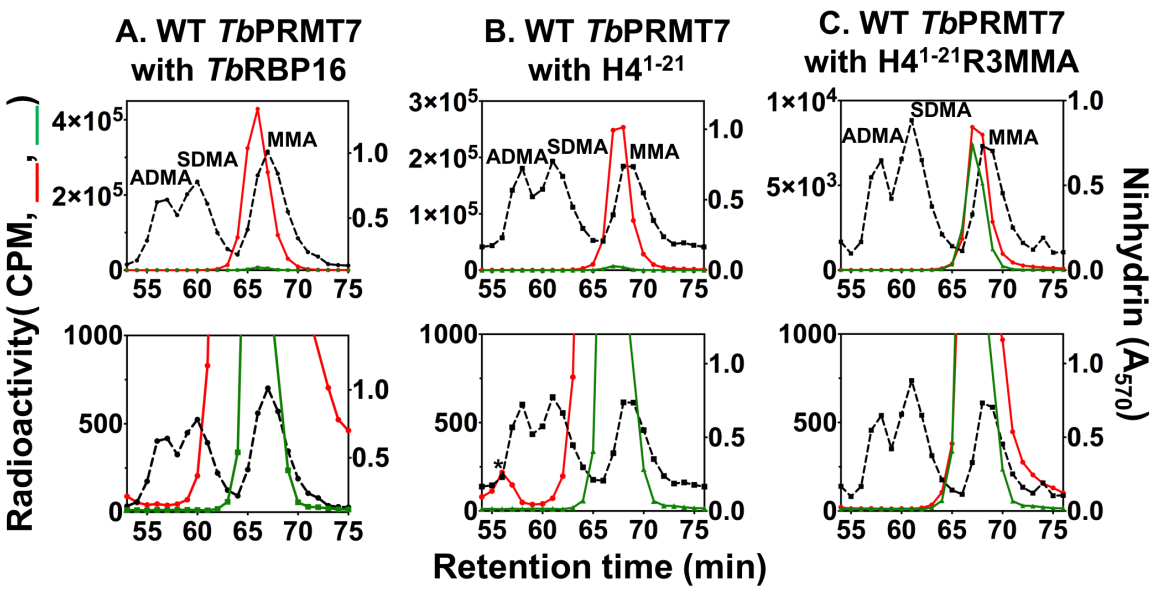

Fig. 1. *Tb*PRMT7 displays Type III PRMT activity. *Tb*PRMT7 was incubated with [*methyl*-^{3}H]-AdoMet and (*A*) *Tb*RBP16; (*B*) an *N*-acetyl peptide corresponding to residues 1-21 of human histone H4 (H4$^{1-21}$); or (*C*) the H4$^{1-21}$ peptide with MMA substituted for arginine at position 3 (H4$^{1-21}$R3MMA). Protein or peptides from the incubation were hydrolyzed and mixed with amino acid standards of ADMA, SDMA, and MMA and then analyzed via high-resolution cation-exchange chromatography. The red lines indicate the radioactivity of ^{3}H-methyl groups for complete reactions. The green lines indicate the radioactivity from a single control reaction where the enzyme alone was incubated with [*methyl*-^{3}H]-AdoMet as an automethylation control and is shown in each panel. The elution of the amino acid standards was determined by ninhydrin reactivity and is shown as a black dashed line. In each case, the lower panel represents an enlargement to show lower levels of methylation. Isotopically labeled ADMA, SDMA, and MMA elute about a minute earlier than the non-isotopically labeled standards due to the effect of tritium on the pKa's of the methylarginine species (11, 32). The asterisked small radioactive peak in the lower panel of panel 1B migrates about 1 min earlier than expected for [^{3}H]ADMA – the identity of this material is unknown.

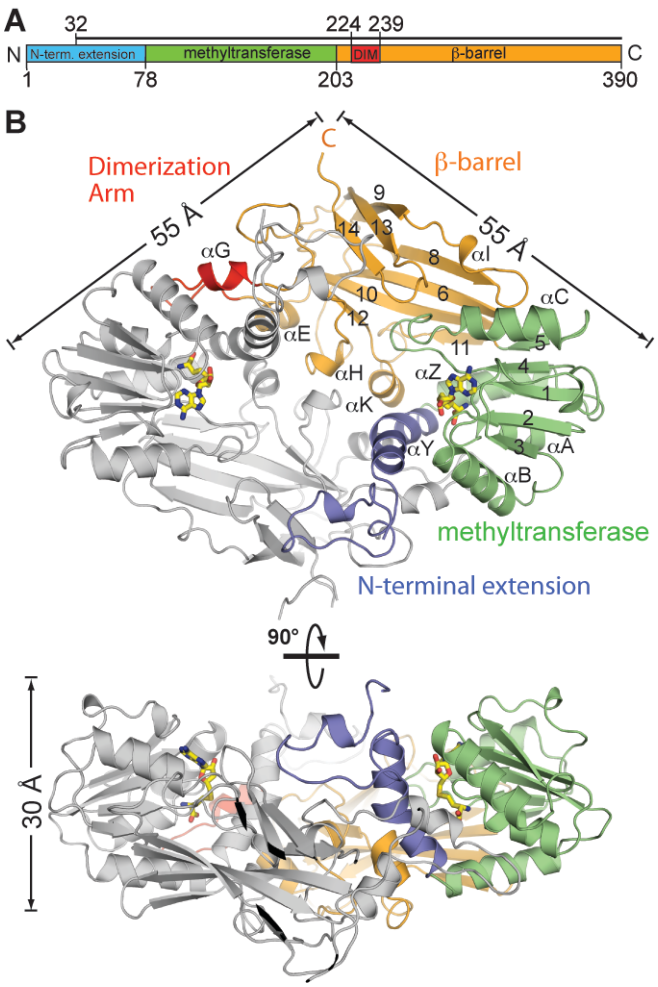

Fig. 2. Overview of *Tb*PRMT7 in complex with AdoHcy. (*A*) Domain organization of *Tb*PRMT7. Domain boundaries are indicated by residue numbers. The bar above the domain structure denotes the crystallized fragment. DIM; dimerization arm. (*B*) Ribbon representation of the *Tb*PRMT7 dimer, using the same color code for the domains as in panel (*A*). The second protomer of the *Tb*PRMT7 dimer is shown in grey. AdoHcy is displayed in yellow stick representation. A 90° rotated view is shown below. Labeling of α-helices and β-strands follows the convention of earlier structures (23, 24).

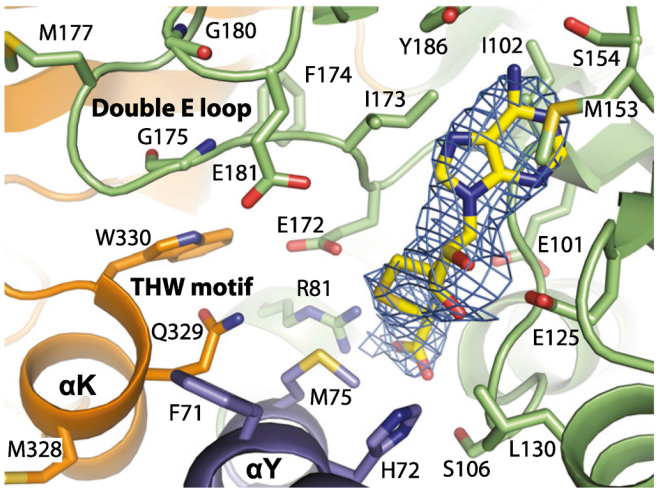

Fig. 3. Active site of *Tb*PRMT7. Electron density of AdoHcy and key residues in the active site are shown.

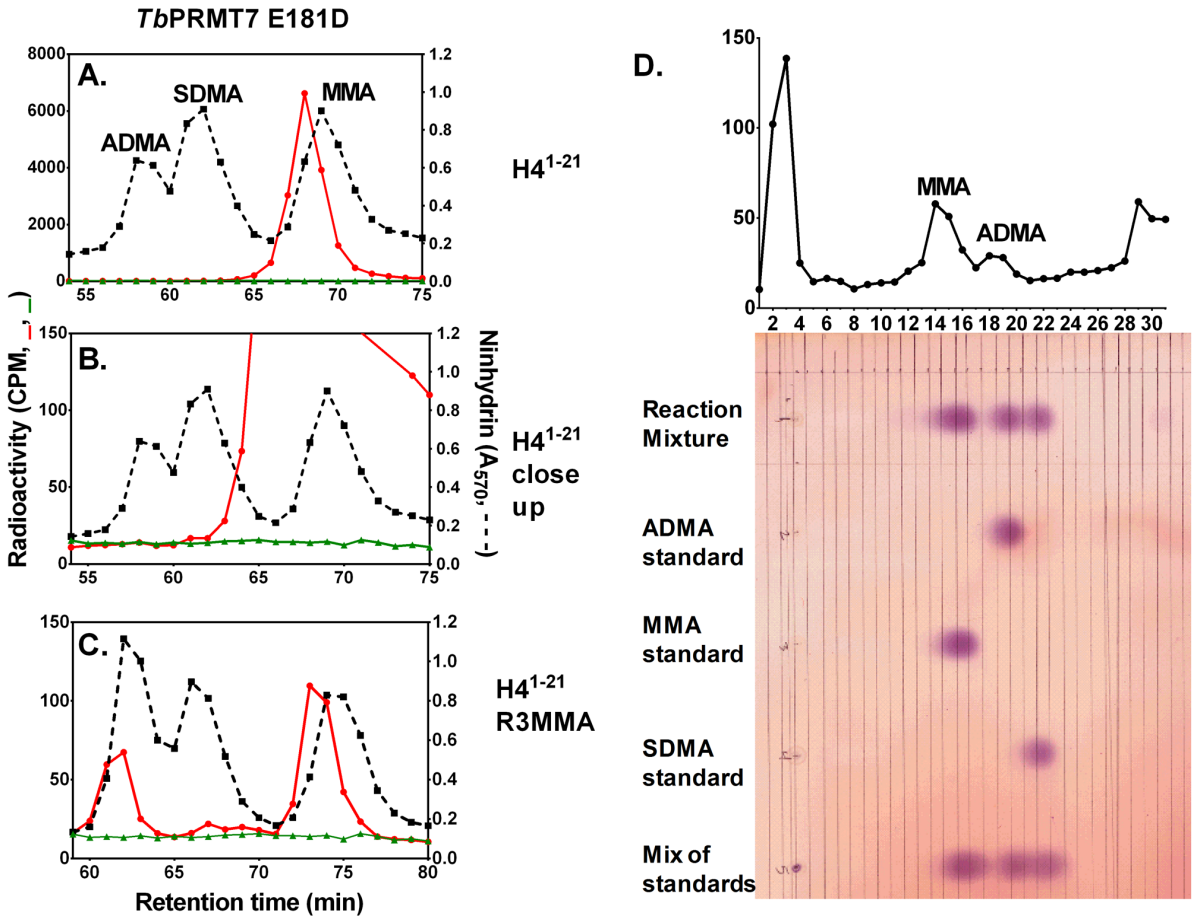

Fig. 4. An active-site mutation in the double E loop of *Tb*PRMT7 produces ADMA. *Tb*PRMT7 Glu181Asp was incubated with [*methyl*-^{3}H]-AdoMet and (*A, B*) the H4$^{1-21}$ peptide or (*C, D*) the H4$^{1-21}$R3MMA peptide. Hydrolysates of the peptide products were mixed with amino acid standards of ADMA, SDMA, and MMA and were analyzed via high-resolution cation exchange chromatography (*A-C*) or thin layer chromatography (TLC) (*D*). Red lines in panels (*A-C*) indicate the radioactivity of ^{3}H-*methyl* groups for complete reactions. The green lines indicate the radioactivity from a single control reaction where the enzyme alone was incubated with [*methyl*-^{3}H]-AdoMet as an automethylation control and is shown in each panel. (*B*) An enlargement of the radioactive data in panel (*A*). The elution of the amino acid standards was determined by ninhydrin reaction, shown in black dashes. Isotopically labeled ADMA and MMA elute about a minute earlier than the non-isotopically labeled standards. (*D*) TLC for hydrolysates of the reaction mixture and

individual and mixed standards of ADMA, MMA, and SDMA. The upper portion shows the radioactivity corresponding to the TLC slices of the reaction mixture lane; the lower portion shows the ninhydrin staining of the TLC plate.

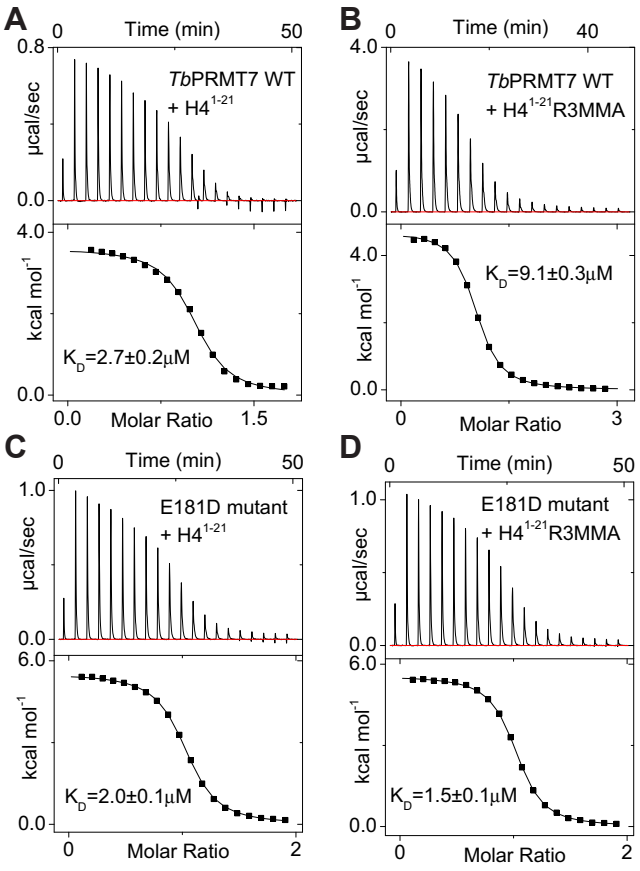

Fig. 5. Isothermal titration calorimetry of *Tb*PRMT7 wild type (*A,B*) and Glu181Asp mutant (*C,D*) with $H4^{1-21}$ and $H4^{1-21}$R3MMA, respectively.

SUPPORTING INFORMATION (SI)

SI Methods

Peptide substrates

Histone $H4^{1-21}$ (Ac-SGRGKGGKGLGKGGAKRHRKV) and histone $H4^{1-21}$R3MMA (Ac-SGR[me]GKGGKGLGKGGAKRHRKV) peptides were kind gifts from Drs. Heather Rust and Paul Thompson (The Scripps Research Institute and University of Massachusetts Medical School, respectively). The plasmid for expression of *Tb*RBP16 (UniProt: Q9XY40) was a kind gift from Dr. Laurie Read (SUNY Buffalo).

Protein expression and purification

DNA fragments of *Tb*PRMT7 were amplified by PCR from genomic DNA, cloned into a pET28a vector (Novagen) containing an N-terminal PreScission protease (GE Healthcare) cleavable His_6-tag, overexpressed in *E. coli* BL21-CodonPlus(DE3)-RIL cells (Stratagene), and grown in LB media containing appropriate antibiotics. Mutations in *Tb*PRMT7 were introduced by overlap extension PCR mutagenesis. Protein expression was induced at $OD_{600} \approx 0.6$ with 0.5 mM isopropyl-β-D-thiogalactoside at 18 °C for 16 h. The cells were harvested by centrifugation at 7,500 x *g* and 4 °C and lysed with a cell disrupter (Avestin) in a buffer containing 20 mM Tris, pH 8.0, 300 mM NaCl, 5 mM β-mercaptoethanol, 0.5 mM phenylmethylsulfonyl fluoride (Sigma), 2 μM bovine lung aprotinin (Sigma), and complete EDTA-free protease inhibitor cocktail (Roche). After centrifugation at 35,000 x *g* for 45 min, the cleared lysate was loaded onto a Ni-NTA column (Qiagen) and eluted with an imidazole gradient. Protein-containing fractions were pooled, dialyzed against a buffer containing 20 mM Tris, pH 8.0, 100 mM NaCl, and 5 mM dithiothreitol (DTT), and subjected to cleavage with PreScission protease (GE Healthcare) for 12 h at 4 °C. Following His_6-tag removal, the cleaved protein was bound to a heparin column (GE Healthcare) and eluted with a NaCl gradient. Protein-containing fractions were pooled, concentrated, and purified on a HiLoad

Superdex 200 16/60 gel filtration column (GE Healthcare) in a buffer containing 20 mM Hepes, pH 7.5, 150 mM NaCl, and 0.5 mM tris(2-carboxyethyl)phosphine (TCEP). His-tagged *Tb*RBP16 was expressed and purified as previously described (33), but the His-tag was removed.

Crystallization, data collection, structure determination, and refinement

For formation of the complex with the AdoHcy, 20 mg/ml of purified *Tb*PRMT7 was mixed in a 1:2 molar ratio with AdoHcy and incubated for 1 h on ice. The crystallization solution consisted of 30% PEG 400, 0.2 M $MgCl_2$, and 0.1 M Tris, pH 8.0. Crystals grew in space group $P3_221$ at room temperature within two weeks. X-ray diffraction data were collected at the X29 beamline at the National Synchrotron Light Source (NSLS) at the Brookhaven National Laboratory (BNL). Diffraction data were processed in HKL2000 (34). The structure was solved by the single anomalous dispersion (SAD) phasing technique in the program AutoSol of the PHENIX package (35), using data obtained from seleno-L-methionine-labeled crystals. The asymmetric unit contained one dimer. Model building was performed in O (36) and Coot (37). The final model spanning residues 38-384 was refined in Phenix (35) to an R_{free} of 26.1 % with excellent stereochemistry as assessed by MolProbity (38). Details for data collection and refinement statistics are summarized in Table S1. Figures were generated using PyMOL (Schrödinger, LLC), the electrostatic potential was calculated with APBS (39). Atomic coordinates and structure factors have been deposited with the Protein Data Bank under PDB code 5EKU.

Multi-angle light scattering

Purified proteins were characterized by multi-angle light scattering following size-exclusion chromatography (40). Protein at 50 µM was injected onto a Superdex 200 10/300 GL size-exclusion chromatography column (GE Healthcare) equilibrated in a buffer containing 20 mM HEPES pH 7.5, 150 mM NaCl, and 0.5 mM TCEP. The chromatography system was connected in series with an 18-angle light scattering detector (DAWN HELEOS) and refractive index detector

(OptilabrEX) (Wyatt Technology). Data were collected every second at a flow rate of 0.25 mL/min at 25 °C. Data analysis was carried out using the program ASTRA, yielding the molar mass and mass distribution (polydispersity) of the sample.

Isothermal titration calorimetry

ITC measurements were performed at 15°C using a MicroCal auto-iTC200 calorimeter (MicroCal, LLC). Protein was incubated with twofold molar excess of AdoHcy for 1 h at room temperature. Protein and peptide samples were then extensively dialyzed against a buffer containing 20 mM HEPES, pH 7.5, 20 mM NaCl, and 0.5 mM TCEP. 2 µL of 1-4 mM peptide was injected into 0.2 mL of 0.1-0.4 mM protein in the chamber every 150 s. Baseline-corrected data were analyzed with ORIGIN software.

Amino acid analysis of protein and peptide substrates

Unless otherwise described, 5 µg of the *Tb*RBP16 protein or 10 µM of the peptide substrates were methylated with 1.2 µg of wild-type *Tb*PRMT7 or the indicated amount of mutant *Tb*PRMT7 by incubating the mixture with 0.7 µM of *S*-adenosyl-[*methyl*-^{3}H]-L-methionine ([*methyl*-^{3}H]-AdoMet) (PerkinElmer Life Sciences; stock solution of 7 µM (78.2 Ci/mmol) in 10 mM H_2SO_4/EtOH (9:1, v/v)) in 50 mM HEPES pH 7.5, 100 mM NaCl, 1 mM DTT, and 5% glycerol at 25 °C for 16 h in a total volume of 60 µl. When *Tb*RBP16 was used as the substrate, 60 µL 25% trichloroacetic acid (w/v) and 20 µg bovine serum albumin were added to the reaction after completion and the mixture was incubated at 25 °C for 30 min, followed by centrifugation at 4000 x *g* for 30 min at 25 °C. The resulting pellet was washed with -20 °C acetone before acid hydrolysis. Alternatively, when peptides were used as substrates, the reactions were quenched with 4 µL 25% trichloroacetic acid (w/v). For reactions that were used for thin layer chromatography (TLC), the peptides were purified via RP-HPLC. For reactions that were used for cation exchange chromatography, peptides were purified using OMIX C18 Zip-Tips® with elution in 15 µL of trifluoroacetic acid/acetonitrile/water (0.1:50:50). In both cases, elution solvent was

removed by vacuum centrifugation. Acid hydrolysis of all samples was performed with 50 µL 6 M HCl at 110 °C for 20 h *in vacuo*. Once the acid was removed via vacuum centrifugation, the dried sample pellets were dissolved in 50 µL of water.

For samples analyzed by cation exchange chromatography, 1 µmol each of ω-MMA (acetate salt; Sigma, M7033), SDMA (di-(p-hydroxyazobenzene)-p-sulfonate salt; Sigma, D0390), and ADMA (hydrochloride salt; Sigma, D4268) were added as internal standards and chromatography was then performed as previously described but using a buffer at pH 5.21 instead of 5.27 (10). The positions of the non-radioactive methylarginine standards were determined by detecting the absorbance of 50 µL fraction aliquots at 570 nm after being reacted with ninhydrin, and radioactivity of the remaining 950 µL from each fraction was determined through liquid scintillation, using the average of three 5- to 20-min counting cycles, as described (10). For samples analyzed by TLC, 10 µmol each of ω-MMA, SDMA, and ADMA were added to the peptide pellets. This mixture was dried via vacuum centrifugation and acid hydrolyzed as described above. 10 µmol of the three standards were also acid hydrolyzed individually and as a group. The dried hydrolysates were resuspended in 10 µL of water. Each reaction hydrolysate and individual standard hydrolysate was spotted onto silica plates (Polygram Sil G/UV_{254}; Macherey-Nagel, 805203) in 1-µL aliquots. Once the spots were dried, each plate was run in a 3:1 ethanol:water solvent mixture for about 8 h. After air-drying, the plate was dipped momentarily in a ninhydrin solution (15 mg/ml ninhydrin dissolved in 97% butanol, 3% glacial acetic acid). The plate was again allowed to air dry and then heated at 90 °C for 15 s. Visible ninhydrin spots were outlined and the plate was sectioned into 5 mm wide slices. The silica from each slice was mixed with 500 µL water and vortexed for 2 h. This material was added to 5 mL of scintillation fluid to detect radioactivity using the average of three 20-min cycles.

SI TABLES AND FIGURES

Table S1. Data collection and refinement statistics.

Data collection	
Synchrotron	NSLS[a]
Beamline	X29
Space group	$P3_221$
Cell dimensions	
a, b, c (Å)	a=b= 157.6, c= 97.4
α, β, γ (°)	$\alpha=\beta=90, \gamma=120$
Wavelength (Å)	1.072
Resolution (Å)[b]	50.0-2.80 (2.90-2.80)
No. of unique reflections	34,624 (3,417)
R_{sym} (%)[b]	0.096 (88.6)
CC1/2	0.997 (0.716)
CC*	0.999 (0.914)
$\langle I / \sigma I \rangle$[b]	12.1 (1.8)
Completeness (%)[b]	100.0 (99.7)
Redundancy[b]	5.8 (5.8)
Refinement	
Resolution (Å)	50.0 – 2.80
No. of reflections	34,586
Test set	3380
R_{work} / R_{free} (%)	22.1 / 26.1
No. of atoms	5,564
R.m.s deviations	
Bond lengths (Å)	0.004
Bond angles (°)	0.9
<B-Value>	
Protein (Å^2)	80.0
AdoHcy (Å^2)	110.1
MolProbity Score/Percentile	1.68/100
Ramachandran plot[c]	
Favored (%)	96.33
Allowed (%)	3.52
Outliers (%)	0.15

[a]NSLS, National Synchrotron Light Source, Brookhaven National Laboratory

[b]Highest-resolution shell is shown in parentheses.

[c]As determined by MolProbity.

Table S2. B-values of side-chain carboxyl groups from the glutamates of the double E loops in PRMTs indicate the first glutamate to be more rigid than the last one. "**1st glutamate"** and **"2nd glutamate"** refer to the first and last glutamates in the double E loop, respectively. **CD**, **OE1,** and **OE2** refer to the delta carbon and terminal epsilon oxygen atoms of the glutamates, respectively. *Rn: Rattus norvegicus; Hs: Homo sapiens; Mm: Mus musculus; Tb: Trypanosoma brucei; Ce: Caenorhabditis elegans.*

	B-values (Å²)					
	Carboxylate carbon		**Carboxylate oxygens**			
	CD		**OE1**		**OE2**	
Enzymes	**1st glutamate**	**2nd glutamate**	**1st glutamate**	**2nd glutamate**	**1st glutamate**	**2nd glutamate**
***Tb*PRMT7** (Type III, PDB 4M38)	23.84	29.06	22.19	36.35	27.89	33.01
***Mm*PRMT7** (Type III, PDB 4C4A)	37.39	46.01	40.03	47.35	25.11	47.83
***Ce*PRMT7** (Type III, PDB 3X0D)	51.31	98.59	54.21	87.5	52.8	104.58
***Rn*PRMT1** (Type I, PDB 1ORI)	46.41	54.71	46.7	54.98	48.97	57.55
***Rn*PRMT4** (Type I, PDB 3B3F)	33.2	37.81	31.63	41.91	34.66	38.35
***Mm*PRMT4** (Type I, PDB 2V7E)	40.67	44.13	41.76	44.47	39.65	44.44
***Hs*PRMT4** (Type I, PDB 4IKP)	37.45	37.69	38.11	38.29	37.28	38.34
***Hs*PRMT6** (Type I, PDB 4HC4)	29.46	46.09	30.96	48.51	39.56	49.09
***Mm*PRMT6** (Type I, PDB 4C07)	11.17	23.02	19.55	23.96	16.78	25.63
***Hs*PRMT5** (Type II, PDB 4GQB)	68.06	56.21	55.82	57.61	52.32	50.64

Table S3. Summary of ITC results. The dissociation constant (K_D), binding enthalpy (ΔH), and the stoichiometry (N) were derived by curve fitting using a single-site model, while the entropy (ΔS) was calculated from these values.

Protein	Peptide	[NaCl] (mM)	K_D (μM)	ΔH (kcal/mol)	N	ΔS (cal/mol/K)
WT	$H4^{1-21}$	20	2.7 ±0.2	3.59 ±0.03	1.00 ±0.01	37.9
WT	$H4^{1-21}$	150	50 ±3	1.41 ±0.03	1.00 ±0.02	24.6
WT	$H4^{1-21}$	300	400,000	n.a.	1.00 (fixed)	n.a.
WT	$H4^{1-21}$	500	no binding	n.a.	n.a.	n.a.
WT	$H4^{1-21}$R3MMA	20	9.1 ±0.3	4.70 ±0.02	1.00 ±0.01	39.4
Glu181Asp mutant	$H4^{1-21}$	20	2.03 ±0.05	5.52 ±0.01	1.00 ±0.01	45.2
Glu181Asp mutant	$H4^{1-21}$R3MMA	20	1.50 ±0.03	5.55 ±0.01	0.99 ±0.01	45.9

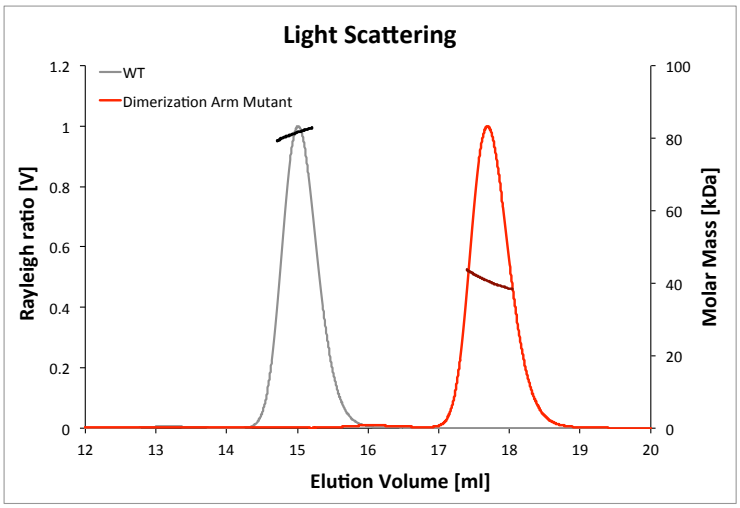

Fig. S1. Dimerization of *Tb*PRMT7. Molecular mass determination and Rayleigh ratio of wild-type *Tb*PRMT7 (light and dark grey, respectively) and of the dimerization arm mutant (light and dark red, respectively) by multi-angle light scattering (MALS) coupled to size exclusion chromatography (Superdex 200 10/300 column, GE Healthcare). Wild-type *Tb*PRMT7 forms a dimer, while the dimerization arm mutant is monomeric.

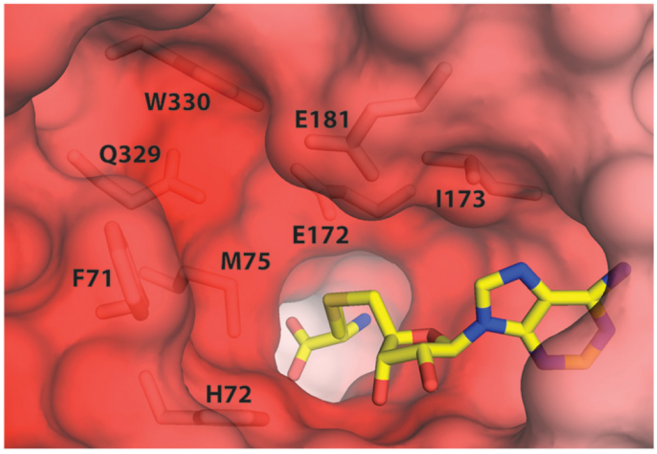

Fig. S2. Electrostatic surface potential of the active site shown between -20 kT/e (red) and +20kT/e (blue).

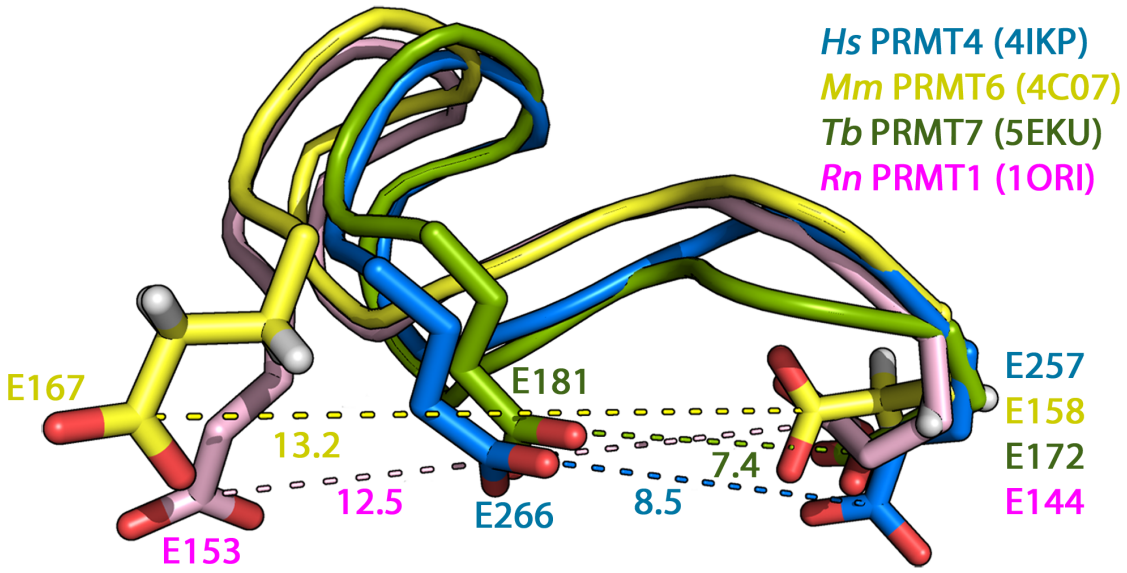

Fig. S3. *Tb*PRMT7's active site is generally smaller than that of type I enzymes. A structural alignment of the double E loops of *Tb*PRMT7 (PDB 5EKU, chainA) and type I PRMTs with *Rn*PRMT1 (PDB 1ORI, chainA), *Hs*PRMT4 (PDB 4IKP, chain A), and *Mm*PRMT6 (PDB 4C07, chain A) is shown with indicated coloring to match each E loop to its organism and enzyme. Distances between the glutamates of each E loop are given in Ångströms. Dashed lines are colored to match the pairs of glutamate residues in each enzyme.

REFERENCES

1. Walsh G & Jefferis R (2006) Post-translational modifications in the context of therapeutic proteins. *Nat Biotechnol* 24:1241-1252.
2. Carr SM, Poppy Roworth A, Chan C, & La Thangue NB (2015) Post-translational control of transcription factors: methylation ranks highly. *FEBS J*.
3. Dhar SS*, et al.* (2012) Trans-tail regulation of MLL4-catalyzed H3K4 methylation by H4R3 symmetric dimethylation is mediated by a tandem PHD of MLL4. *Genes Dev* 26:2749-2762.
4. Baldwin RM*, et al.* (2015) Protein arginine methyltransferase 7 promotes breast cancer cell invasion through the induction of MMP9 expression. *Oncotarget* 6:3013-3032.
5. Biggar KK & Li SS (2015) Non-histone protein methylation as a regulator of cellular signalling and function. *Nat Rev Mol Cell Biol* 16:5-17.
6. Bedford MT & Clarke SG (2009) Protein arginine methylation in mammals: who, what, and why. *Mol Cell* 33:1-13.
7. Herrmann F, Pably P, Eckerich C, Bedford MT, & Fackelmayer FO (2009) Human protein arginine methyltransferases in vivo--distinct properties of eight canonical members of the PRMT family. *J Cell Sci* 122:667-677.
8. Niewmierzycka A & Clarke S (1999) S-Adenosylmethionine-dependent methylation in Saccharomyces cerevisiae. Identification of a novel protein arginine methyltransferase. *J Biol Chem* 274:814-824.
9. Feng Y, Hadjikyriacou A, & Clarke SG (2014) Substrate specificity of human protein arginine methyltransferase 7 (PRMT7): the importance of acidic residues in the double E loop. *J Biol Chem* 289:32604-32616.

10. Feng Y*, et al.* (2013) Mammalian protein arginine methyltransferase 7 (PRMT7) specifically targets RXR sites in lysine- and arginine-rich regions. *J Biol Chem* 288:37010-37025.

11. Zurita-Lopez CI, Sandberg T, Kelly R, & Clarke SG (2012) Human protein arginine methyltransferase 7 (PRMT7) is a type III enzyme forming omega-NG-monomethylated arginine residues. *J Biol Chem* 287:7859-7870.

12. Fisk JC*, et al.* (2009) A type III protein arginine methyltransferase from the protozoan parasite Trypanosoma brucei. *J Biol Chem* 284:11590-11600.

13. Wang C*, et al.* (2014) Structural determinants for the strict monomethylation activity by trypanosoma brucei protein arginine methyltransferase 7. *Structure* 22:756-768.

14. Yao R*, et al.* (2014) PRMT7 induces epithelial-to-mesenchymal transition and promotes metastasis in breast cancer. *Cancer Res* 74:5656-5667.

15. Yang Y & Bedford MT (2013) Protein arginine methyltransferases and cancer. *Nat Rev Cancer* 13:37-50.

16. Karkhanis V*, et al.* (2012) Protein arginine methyltransferase 7 regulates cellular response to DNA damage by methylating promoter histones H2A and H4 of the polymerase delta catalytic subunit gene, POLD1. *J Biol Chem* 287:29801-29814.

17. Wang YC, Peterson SE, & Loring JF (2014) Protein post-translational modifications and regulation of pluripotency in human stem cells. *Cell Res* 24:143-160.

18. Ferreira TR*, et al.* (2014) Altered expression of an RBP-associated arginine methyltransferase 7 in Leishmania major affects parasite infection. *Mol Microbiol*.

19. Hasegawa M, Toma-Fukai S, Kim JD, Fukamizu A, & Shimizu T (2014) Protein arginine methyltransferase 7 has a novel homodimer-like structure formed by tandem repeats. *FEBS Lett* 588:1942-1948.

20. Cura V, Troffer-Charlier N, Wurtz JM, Bonnefond L, & Cavarelli J (2014) Structural insight into arginine methylation by the mouse protein arginine methyltransferase 7: a zinc finger freezes the mimic of the dimeric state into a single active site. *Acta Crystallogr D Biol Crystallogr* 70:2401-2412.

21. Yang Y*, et al.* (2015) PRMT9 is a type II methyltransferase that methylates the splicing factor SAP145. *Nat Commun* 6:6428.

22. Hadjikyriacou A, Yang Y, Espejo A, Bedford MT, & Clarke SG (2015) Unique Features of Human Protein Arginine Methyltransferase 9 (PRMT9) and Its Substrate RNA Splicing Factor SF3B2. *J Biol Chem* 290:16723-16743.

23. Weiss VH*, et al.* (2000) The structure and oligomerization of the yeast arginine methyltransferase, Hmt1. *Nat Struct Biol* 7:1165-1171.

24. Zhang X, Zhou L, & Cheng X (2000) Crystal structure of the conserved core of protein arginine methyltransferase PRMT3. *EMBO J* 19:3509-3519.

25. Sun L*, et al.* (2011) Structural insights into protein arginine symmetric dimethylation by PRMT5. *Proc Natl Acad Sci U S A* 108:20538-20543.

26. Krissinel E & Henrick K (2007) Inference of macromolecular assemblies from crystalline state. *J Mol Biol* 372:774-797.

27. Fuhrmann J, Clancy KW, & Thompson PR (2015) Chemical biology of protein arginine modifications in epigenetic regulation. *Chem Rev* 115:5413-5461.

28. Lee HW, Kim S, & Paik WK (1977) S-adenosylmethionine: protein-arginine methyltransferase. Purification and mechanism of the enzyme. *Biochemistry* 16:78-85.

29. Migliori V*, et al.* (2012) Symmetric dimethylation of H3R2 is a newly identified histone mark that supports euchromatin maintenance. *Nat Struct Mol Biol* 19:136-144.

30. Xiao B*, et al.* (2003) Structure and catalytic mechanism of the human histone methyltransferase SET7/9. *Nature* 421:652-656.

31. Zhang X*, et al.* (2003) Structural basis for the product specificity of histone lysine methyltransferases. *Mol Cell* 12:177-185.

32. Gottschling H & Freese E (1962) A tritium isotope effect on ion exchange chromatography. *Nature* 196:829-831.

33. Hayman ML & Read LK (1999) Trypanosoma brucei RBP16 is a mitochondrial Y-box family protein with guide RNA binding activity. *J Biol Chem* 274:12067-12074.

34. Otwinowski Z & Minor W (1997) Processing of X-Ray Diffraction Data Collected in Oscillation Mode. *Methods Enzymol* 276:307-326.

35. Adams PD*, et al.* (2011) The Phenix software for automated determination of macromolecular structures. *Methods* 55:94-106.

36. Jones TA, Zou J-Y, Cowan SW, & Kjeldgaard M (1991) Improved methods for building protein models in electron density maps and the location of errors in these models. *Acta Crystallogr A* 47:110-119.

37. Emsley P, Lohkamp B, Scott WG, & Cowtan K (2010) Features and development of Coot. *Acta Crystallogr D Biol Crystallogr* 66:486-501.

38. Davis IW*, et al.* (2007) MolProbity: all-atom contacts and structure validation for proteins and nucleic acids. *Nucleic Acids Res* 35:W375-383.

39. Baker NA, Sept D, Joseph S, Holst MJ, & McCammon JA (2001) Electrostatics of nanosystems: application to microtubules and the ribosome. *Proc Natl Acad Sci U S A* 98:10037-10041.

40. Wyatt PJ (1997) Multiangle light scattering: The basic tool for macromolecular characterization. *Instrum Sci Technol* 25:1-18.

Chapter 4

Protein arginine methyltransferase product specificity is mediated by distinct active-site architectures

The work described in this chapter has been reproduced from:

Kanishk Jain, Rebeccah A. Warmack, Erik W. Debler, Andrea Hadjikyriacou, Pete Stavropoulos, and Steven G. Clarke. “Protein arginine methyltransferase product specificity is mediated by distinct active-site architectures.” *J. Biol. Chem.* 2016 Aug 291(35): 18299-308

ABSTRACT

In the family of protein arginine methyltransferases (PRMTs) that predominantly generate either asymmetric or symmetric dimethylarginine (ADMA or SDMA), PRMT7 is unique in producing solely monomethylarginine (MMA) products. The type of methylation on histones and other proteins dictates changes in gene expression, and numerous studies have linked altered profiles of methyl marks with disease phenotypes. Given the importance of specific inhibitor development, it is crucial to understand the mechanisms by which PRMT product specificity is conferred. We have focused our attention on active-site residues of PRMT7 from the protozoan *Trypanosoma brucei*. We have designed 26 single and double mutations in the active site, including residues in the Glu-X_8-Glu (double E) loop and the Met-Gln-Trp sequence of the canonical Thr-His-Trp (THW) loop known to interact with the methyl-accepting substrate arginine. Analysis of the reaction products by high-resolution cation exchange chromatography combined with the knowledge of PRMT crystal structures suggests a model where the size of two distinct subregions in the active site determines PRMT7 product specificity. A dual mutation of Glu181 to Asp in the double E loop and Gln329 to Ala in the canonical THW loop enables the enzyme to produce SDMA. Consistent with our model, the mutation of Cys431 to His in the THW loop of human PRMT9 shifts its product specificity from SDMA towards MMA. Together with previous results, these findings provide a structural basis and a general model for product specificity in PRMTs, which will be useful for the rational design of specific PRMT inhibitors.

INTRODUCTION

Methylation of proteins is a major type of posttranslational modification involved in the regulation of a variety of cellular processes mediated by protein-protein interactions including splicing, transcription, translation, and signaling (1–3). Recent studies have implicated arginine methylation in altering the metabolic landscape of the cell, linking it to cancer metastasis (4–6), DNA damage (7), pluripotency (8), and parasite infection (9, 10). Catalysis of arginine methylation on the terminal nitrogen atoms of the guanidine group is mediated by a family of enzymes designated as protein arginine methyltransferases (PRMTs). Most of these enzymes harbor a conserved ~310-residue core that comprises the methyltransferase domain conserved in *S*-adenosylmethionine (AdoMet)-dependent methyltransferases and a β-barrel domain unique to the PRMT family. These enzymes can be further categorized based on which methylarginine product they catalyze: type I PRMTs catalyze the production of ω-N^G-monomethylarginine (MMA) and asymmetric ω-N^G-N^G-dimethylarginine (ADMA), type II PRMTs catalyze the production of MMA and symmetric ω-N^G-$N^{G'}$-dimethylarginine (SDMA), type III PRMTs catalyze the production of only MMA, and type IV PRMTs catalyze δ-N^G-monomethylarginine production (11). Notably, most PRMTs fall under the first three types of PRMTs. Type IV enzymes have only been reported in yeast and plants, although presence of free δ-N^G-monomethylarginine has been reported in human plasma in a recent proteomic study (12).

ADMA and SDMA methyl marks on histones are recognized by different “reader” proteins and can lead to distinct downstream outcomes. For example, whether a particular arginine residue on histone tails is asymmetrically or symmetrically dimethylated can lead to gene repression or activation (13–17). However, few studies have been conducted to determine the role of MMA marks (18). It has been proposed that MMA marks are used mainly as precursors for dimethylation by the various type I and II PRMTs (17, 19).

Given the biological significance of the type of methylated arginine derivative formed, it is important to understand how product specificity is determined in PRMTs. It has been suggested

that small variations in the structure of the active site of these enzymes govern the methylation activity type (2, 3, 20–23). While previous studies utilizing site-directed mutagenesis have given some support for this hypothesis, efforts to efficiently change the activity type of PRMTs have not yet been fruitful. Two such studies using moderately sensitive analytical techniques have been reported for PRMT1 (14) and PRMT5 (24), but have not put forth a general model for the factors that guide product specificity for the three main types of PRMTs.

Using an approach where MMA, ADMA, and SDMA can be detected with sub-femtomole sensitivity, we have been able to demonstrate the transformation of a PRMT7 from *Trypanosoma brucei* (*Tb*PRMT7) from an enzyme that strictly produces MMA to one also forming ADMA by replacing a glutamate residue in the double E loop (E181) with an aspartate residue (25) (Fig 1). The double E loop is a conserved feature of PRMTs that has been shown to directly interact with the methyl-accepting arginine residue (2, 11). *Tb*PRMT7 had been initially characterized for a possible role in the transcriptional control of gene expression in this organism (26). Here, we have focused on *Tb*PRMT7 because it displays robust type III activity and has been amenable to structural analysis (25–27). Within this work, we further examine the effects of key active-site residues on the enzymatic activity of *Tb*PRMT7 through mutagenesis and highly sensitive amino acid analysis techniques to demonstrate the importance of the THW loop (MQW for *Tb*PRMT7) (2) (Fig. 1). Complementary studies with PRMT9 from *Homo sapiens*, previously characterized as a type II enzyme (28, 29), corroborate our PRMT7 results. Based on this evidence, we propose a structural model for how PRMTs can limit their activities to type I, type II, or type III methylation.

RESULTS

A *Tb*PRMT7 active-site double mutation, E181D/Q329A, converts the enzyme to an SDMA-producing PRMT

Given the ability of the double E loop E181D mutation of *Tb*PRMT7 to alter the methylation type (25), six *Tb*PRMT7 double mutants were generated with the E181D background to probe the effects of further increasing the size of the active site. Notably, the double mutant E172D/E181D was previously tested and found inactive (25) (Table 1). The additional substitutions in the six new double mutants comprised M75A, Q329A, Q329N, W330A, F71A, and I173G, each with the E181D mutation, based on their immediate vicinity to the sulfur atom of AdoHcy from which the methyl group of AdoMet is transferred to the arginine residue in protein and peptide substrates (Fig. 1). Using [*methyl*-^{3}H]AdoMet as a cofactor, we analyzed the hydrolyzed products of arginine methylation with high-resolution cation exchange chromatography. Four of these double mutants showed little or no activity towards either the H4$^{1-21}$ peptide, comprised of the acetylated 21 N-terminal residues of the human histone H4 protein (data not shown), or the acetylated H4$^{1-21}$ R3MMA peptide, ω-monomethylated at the third arginine (Table 1). The H4$^{1-21}$ R3MMA peptide was used in order to enhance the detection of dimethylarginine derivatives by providing a substrate where a single methylation reaction at the primary site of modification could result in dimethylation of the peptide. Strikingly, one of the double mutants, E181D/Q329A, produced SDMA when incubated with the H4$^{1-21}$ R3MMA peptide (Fig. 2*A* and *B*). The small amount of MMA produced in the reaction of the E181D/Q329A mutant with the H4$^{1-21}$ R3MMA peptide is most likely due to methylation of the secondary R17 and R19 sites on the histone peptide since the level of radioactivity here is higher than the level recorded for the enzyme alone (Fig. 2*B*). Importantly, while this enzyme contains the ADMA-producing mutation E181D (25), as well as a Q329A mutation in the THW loop, no ADMA formation was detected. SDMA production catalyzed by the E181D/Q329A mutant was confirmed by TLC analysis where the radioactive product co-migrated with the non-radioactive SDMA standard (Fig. 2*C*). The wild-type *Tb*PRMT7 does not produce

any dimethylarginine products with either $H4^{1-21}$ or $H4^{1-21}$ R3MMA peptide (Fig. 3). The single Q329A mutant shows no evidence of dimethylarginine formation (Table 1).

_Tb_PRMT7 E181D/Q329A shows higher binding affinity for the monomethylated histone $H4^{1-21}$ peptide than for the unmethylated peptide

Using isothermal titration calorimetry (ITC) with $H4^{1-21}$ and $H4^{1-21}$ R3MMA peptides, we previously demonstrated that the wild-type *Tb*PRMT7 enzyme binds its substrate $H4^{1-21}$ with higher affinity than its monomethylated product, $H4^{1-21}$ R3MMA, while the ADMA-producing *Tb*PRMT7 E181D mutant has markedly increased affinity for $H4^{1-21}$ R3MMA that even surpasses that for $H4^{1-21}$ (25). Similarly, we measured the affinity of the SDMA-producing *Tb*PRMT7 E181D/Q329A enzyme and found that this mutant displays higher affinity for $H4^{1-21}$ R3MMA (K_D = 46.7 μM) vs. its unmethylated counterpart $H4^{1-21}$ (K_D = 80.6 μM) (Fig. 4). Thus, the two mutant enzymes capable of dimethylation consistently favor binding of the bulkier $H4^{1-21}$R3MMA peptide, which can be rationalized by providing a more spacious binding pocket, stabilizing the MMA substrate-enzyme interactions and enabling dimethylation.

Active-site mutations lead to decreases in type III PRMT7 activity and shifts in recognition site specificity

Overall, we have reacted 26 single and double mutants of *Tb*PRMT7 with the $H4^{1-21}$ R3MMA peptide to test whether active-site mutations could display changes in the methylation type when presented with a primed monomethylarginine (Table 1). These mutations were generated based on their location in the active site of *Tb*PRMT7*,* including residues in the double E loop, the AdoMet binding motif, the THW loop, and an N-terminal extension (helix αY). The majority of the active-site mutations result in decreases in enzyme activity. However, monomethylation is still observed, indicating that the modification of R17 and R19 on the substrate peptide is occurring, as R3 is already methylated in this peptide. This finding suggests that there may be a change in recognition site specificity from glycine-arginine rich regions to arginine

residues in basic regions (26, 30). Notably, the THW (MQW) loop mutant Q329H showed significant increases in MMA production. Most remarkably, the double mutant E181D/Q329A produced both MMA and SDMA, as described above.

A mutation in the THW loop of human PRMT9, a type II PRMT, shifts product specificity from SDMA towards MMA

The human PRMT9 has recently been characterized as a type II PRMT, joining PRMT5 as an enzyme that catalyzes SDMA production (28, 29). This methyltransferase contains a Thr-Cys-Trp (TCW) sequence in place of the canonical Thr-His-Trp (THW) residues (28). In order to further investigate the role of spatial restrictions conferred by key active-site residues, the cysteine residue was mutated to a bulkier histidine residue in order to mimic type I and type III PRMTs. These mutant and wild-type enzymes were reacted with a GST fusion of the splicing factor SF3B2, a known substrate of PRMT9 (28). Comparison of wild-type and mutant activities reveals an impressive eight-fold increase in MMA production and almost complete elimination of SDMA production (<0.037%) (Fig. 5).

***Rattus norvegicus* PRMT1 M48F mutant enzyme does not produce SDMA with histone H4 peptides**

A previous study (24) reported a mutation in rat PRMT1 at Met48, a residue conserved in the αY helix of many PRMTs, to Phe. This change led to the apparent production of SDMA along with ADMA and MMA, the wild-type products of a type I PRMT, as determined by *o*-phthalaldehyde-derivatized RPLC and LC-MS analysis. However, it appeared that the degree of dimethylarginine formation was quite different when analyzed by these two methods. In our studies with *Tb*PRMT7, the homologous mutation, M75F, showed no change in PRMT7's type III activity with substrates including RBP16 (25) and the $H4^{1-21}$ R3MMA peptide (Table 1). To validate the PRMT1 mutant activity (24), we compared the product specificity of the wild-type human PRMT1 (Fig. 6*A*) with the $H4^{1-21}$ and $H4^{1-21}$ R3MMA peptides to that of the rat PRMT1 Met48Phe enzyme (Fig. 6*B*). We chose these peptides because $H4^{1-21}$ has been shown to be a robust

PRMT1 substrate (31, 32). However, in contrast to the earlier work (24), we were unable to distinguish any difference in the product specificity of the wild-type human PRMT1 and the rat PRMT1 M48F mutant with the H4 peptide substrates using high-resolution cation exchange chromatography (Fig. 6). With both enzymes, only MMA and ADMA were formed under conditions where we could detect SDMA at a level of less than 0.4% of the radioactivity in ADMA. Significantly, in the presence of an already methylated substrate such as $H4^{1-21}$ R3MMA, the rat PRMT1 M48F was still unable to produce any SDMA (Fig. 6*B*). Additionally, there is MMA production above automethylation levels for wild-type human PRMT1 and rat PRMT1 M48F when given $H4^{1-21}$ R3MMA as a substrate. The MMA being produced with this peptide would be expected to occur at positions R17 and R19. These results indicate that the residue M48 may not be involved in mediating product specificity in mammalian PRMT1.

DISCUSSION

Different methylarginine marks can be recognized by distinct reader proteins (17) and often behave as epigenetic switches, affecting the activation or silencing of certain genes (15, 16). Given the significance of ADMA and SDMA marks, it has become increasingly important to understand how product specificity arises to generate these residues. Having previously demonstrated the conversion of *Tb*PRMT7, a strictly MMA producing type III enzyme, into a type I enzyme forming ADMA by mutation (25), we now present another *Tb*PRMT7 mutant that is capable of producing SDMA, exhibiting the product specificity of type II PRMTs (Fig. 2). Biochemical and mutational analyses of the enzyme's catalytic activity reveal that SDMA production occurs when it is presented with an already monomethylated substrate, demonstrating that this mutant of PRMT7, in contrast to the wild-type, is able to recognize a monomethylated molecule as a substrate and carry out further methylation. In fact, the E181D/Q329A mutant enzyme binds $H4^{1-21}$ R3MMA with a higher affinity than the corresponding unmethylated peptide (Fig. 4). This observation illustrates that although the activity of the E181D/Q329A mutant is low, it still behaves, on the catalytic level, as a type II PRMT.

We also examined a mammalian PRMT1 mutant enzyme that was previously reported to produce SDMA along with its wild-type products, ADMA and MMA (24). We were unable to observe any symmetric dimethylation on histone H4 peptide substrates from this rat PRMT1 mutant enzyme (M48F) (Fig. 6). Coupled with our results from amino acid analysis of a homologous mutation in *Tb*PRMT7 (M75F; Table 1) and its mutation to alanine (M75A; Table 1) (25), our work did not confirm any role of M48 in affecting PRMT1 product specificity in the mammalian enzyme. It should be noted that the H4 peptide substrates used in our study differ from the GGRGGFGGRGGFGGRGGFG peptide used previously (24). Additionally, immunoblot analysis revealed that the reverse mutation in the PRMT5 enzymes of humans and *Caenorhabditis elegans*, where the corresponding wild-type residue is a phenylalanine (F327M and F379M, respectively) caused asymmetric dimethylation of human histone H4 (14). It would

be interesting to examine these mutants with our more sensitive amino acid analysis techniques in order to determine any changes in product specificity more precisely.

Our previous mutagenesis results (25), coupled with those discussed here, highlight the major features of the PRMT active site which may control mono- and dimethylation specificity. Conceptually, the active site of PRMTs, defined by the double E loop, the THW loop, and the AdoMet/AdoHcy cofactor, can be divided into two subregions, one of which is located between the two glutamate residues of the double E loop and above the substrate arginine (subregion A), while subregion B is adjacent to the THW loop and the region underneath the substrate arginine as displayed in Fig. 7. Our analysis reveals that the nature of these two subregions correlates well with – and therefore seems predictive of – product specificity in PRMTs. Specifically, type I PRMTs contain an open subregion A and a spatially restricted subregion B (Fig. 7*A*). The nature of these subregions in type II active sites is reversed with respect to type I PRMTs, with an open subregion B and a restricted subregion A (Fig. 7*B*). PRMT7's active site by contrast contains two restricted subregions, combining the restraining features of subregions A (type I) and B (type II) of the other two types of PRMTs (Fig. 7*C*). These spatial restrictions may be the key for PRMT7 to only monomethylate its substrates, thus classifying it as a type III PRMT enzyme.

The E181D mutation of *Tb*PRMT7 increases the space within subregion A of the active site by a single carbon-carbon bond where the substrate arginine is stabilized. The distance between the glutamates of the double E loop, however, is not the essential factor in SDMA production because the glutamates of human PRMT5, the major SDMA producer in the cell, are actually closer together than even those in *Tb*PRMT7 (Fig. 7*B* and *C*). The methylation type alteration can be largely attributed to the Q329A mutation, which, in combination with E181D, may result in the opening up of subregion B in the active site underneath the substrate arginine. It is important to note that the Q329A single mutant did not produce SDMA, suggesting that the THW loop may not be the sole contributor in determining type II methylation. Human PRMT5 has a serine residue in place of the corresponding glutamine residue in *Tb*PRMT7 that is located at a

greater distance (5.2 Å vs. 3.0 Å; Fig. 8) from the substrate arginine than the glutamine of *Tb*PRMT7 and is also pointed away from the active site (Fig. 7). In our *Tb*PRMT7 E181D/Q329A construct, the glutamine to alanine substitution removes an acetamide moiety in subregion B. This active-site alteration now allows for methylated arginines to bind more favorably and is better suited to accommodate a methylated nitrogen atom near the THW loop, allowing the other terminal nitrogen atom (positioned near the double E loop) to become methylated. A specific role of the THW loop in determining PRMT product specificity was first suggested in two recent reviews from the Thompson group (2, 20).

In support of the importance of the THW loop in determining type II PRMT product specificity, the mutation of C431H in human PRMT9 shows a significant decrease in SDMA production relative to the wild-type enzyme (Fig. 5). Although no structure has been determined for this enzyme, the cysteine to histidine mutation introduces a bulkier moiety into the THW loop potentially contributing to further crowding in the active site, which in turn may prevent SDMA production. The concomitant marked increase in MMA production of the PRMT9 is consistent with a partially processive methylation mechanism, a characteristic of type I PRMTs (33).

Structural alignments of known type I, II, and III PRMTs show that the geometries of the active sites are highly conserved within each PRMT type (Fig. 9 and Table 2). While our proposed model will benefit from further validation through structural studies of novel PRMTs and additional mutant enzymes, our results illustrate how small changes in the active site of PRMTs can markedly alter their catalytic specificity and thus aid in creating a spectrum of methylarginine species that may differentially mediate various biological pathways.

The emerging role of PRMTs in cancer (4, 5, 34, 35) has profoundly spurred the research into PRMT inhibitors (36). One of the major issues in this field, however, has been the promiscuity of many PRMT inhibitors derived from small-molecule library screening (37). Approaches based on finding bisubstrate analogs that mimic the cofactor and the substrate arginine have the disadvantages of promiscuity and additionally, due to their highly charged nature, limited

bioavailability precluding their administration as oral drugs (37). In light of such obstacles in the development of small-molecule inhibitors of PRMTs involved in various diseases, it is our hope that our model will facilitate the rational design of specific and potent PRMT inhibitors by providing detailed insight into the distinct active-site architectures of the three types of PRMTs.

EXPERIMENTAL PROCEDURES

Peptide substrates

Histone $H4^{1-21}$ (Ac-SGRGKGGKGLGKGGAKRHRKV) and histone $H4^{1-21}$ R3MMA (Ac-SGR[me]GKGGKGLGKGGAKRHRKV) peptides were kind gifts from Heather Rust (The Scripps Research Institute, Jupiter, FL) and Paul Thompson (University of Massachusetts Medical School, Worcester, MA). Peptides used for ITC analysis were purchased from AnaSpec.

Protein expression and purification

*Tb*PRMT7 wild-type and mutant enzymes were cloned, expressed, and purified as previously described (25). GST-PRMT9 wild-type, GST-PRMT9 C431H mutant, and GST-SF3B2 (401-550) fragment were expressed and purified as described previously (28).

Human PRMT1 (*Hs*PRMT1) was expressed from a pET28b(+) vector with a short N-terminal His-tag obtained from Dr. Paul Thompson (University of Massachusetts Medical School, Worcester, MA) (38). Rat PRMT1 (*Rn*PRMT1) M48F was expressed from a pET28b(+) vector obtained from Dr. Joan Hevel (Utah State University, Logan, UT) (24). Both constructs were expressed in *Escherichia coli* BL21(DE3) cells (Invitrogen) and grown in LB media containing kanamycin at 37 °C to an OD_{600} of ~ 0.6. Expression was induced with 1 mM isopropyl-β-D-thiogalactoside (IPTG; GoldBio) at 18 °C for 16 h. The cells were then harvested by centrifugation at 5,000 x *g* and 4 °C. The harvested cells were lysed using an EmulsiFlex cell homogenizer (Avestin) in 50 mM HEPES (pH 8.0), 300 mM NaCl, 0.5 mM phenylmethylsulfonyl fluoride (Sigma), and complete EDTA-free protease inhibitor mixture (Pierce). Lysed cells were centrifuged at 15,000 rpm for 50 min at 4 °C. The clarified lysate was loaded onto a 5-mL HisTrap HP Ni^{2+} column (GE Healthcare). The column was washed with 10 column volumes of the lysis buffer including 50 mM imidazole-HCl (pH 8.0) and the protein was eluted with a 50-500 mM imidazole-HCl (pH 8.0) gradient. The eluted protein's purity was verified through SDS-PAGE analysis to be > 95% (M_r ~ 40.6 kDa). The protein was then dialyzed against a storage buffer containing 50 mM HEPES (pH 8.0), 1 mM DTT, and 15% glycerol (v/v).

Isothermal titration calorimetry

ITC measurements were performed at 15 °C using a MicroCal auto-iTC200 calorimeter (MicroCal, LLC). Protein was incubated with two-fold molar excess of AdoHcy for 1 h at room temperature. Protein and peptide samples were then extensively dialyzed against a buffer containing 20 mM HEPES, pH 7.5, 20 mM NaCl, and 0.5 mM TCEP. 2 µL of 1-4 mM peptide was injected into 0.2 mL of 0.1-0.4 mM protein in the chamber every 150 s. Baseline-corrected data were analyzed with ORIGIN software.

Amino acid analysis of protein and peptide substrates

In vitro methylation assays and amino acid analysis using the *Tb*PRMT7 wild-type and mutant enzymes were performed as previously described (25) in a buffer of 50 mM HEPES pH 8.0, 10 mM NaCl, 1 mM DTT, and 5% glycerol in a final volume of 60 µL. Assays and amino acid analysis using human PRMT9 were also carried out as previously described (28, 29). For methylation assays with PRMT1, human and rat PRMT1 were used. The wild-type control was done with human PRMT1 and the mutant reactions were done with rat PRMT1 M48F. In both cases, 2.5 µg of PRMT1 and either 50 µM $H4^{1-21}$ or $H4^{1-21}$ R3MMA peptide were incubated at 37 °C for 3 h in a mixture containing 0.7 µM of *S*-adenosyl-[*methyl*-^{3}H]-L-methionine ([*methyl*-^{3}H]-AdoMet) (PerkinElmer Life Sciences; stock solution of 7 µM (78.2 Ci/mmol) in 10 mM H_2SO_4/EtOH (9:1, v/v)), 50 mM HEPES pH 8.0, 10 mM NaCl, 1 mM DTT, and 5% glycerol in a final volume of 60 µL. Reactions were stopped, acid hydrolyzed, and analyzed with cation exchange chromatography as previously described (25). Given the specific radioactivity of the [*methyl*-^{3}H]-AdoMet of 78.2 Ci/mmol and a counting efficiency of 50%, one fmol of methyl groups corresponds to 86 cpm.

ACKNOWLEDGEMENTS

This work was supported by grants from the NIH, including Grant GM026020 (to S.G.C.) and Ruth L. Kirschstein National Service Award GM007185 (to K.J., R.A.W., and A.H.). EWD was a Frey Fellow of the Damon Runyon Cancer Research Foundation (DRG-1977-08). We thank H. Rust (The Scripps Research Institute) and P. Thompson (UMass Medical School) for providing the $H4^{1-21}$ and $H4^{1-21}$ R3MMA peptides and the human His-PRMT1 plasmid, J. Hevel (Utah State University, Logan, UT) for providing the rat His-PRMT1 M48F plasmid, M. Dzialo (University of Leuven, Belgium) for help with amino acid analysis, G. Blobel (Rockefeller University) for support, D. Berman (Rockefeller University) for help with protein expression and purification, D. King (UC Berkeley) for mass spectrometry analysis, and the High-Throughput Screening and Spectroscopy Resource Center at Rockefeller University for support.

Author contributions: Experiments were performed by K.J., R.A.W., E.W.D., and A.H.. K.J. and R.A.W. drafted the manuscript. All authors participated in the data analysis and interpretation, and all authors participated in manuscript revisions. All authors reviewed the results and approved the final version of the manuscript.

TABLES AND FIGURES

Table 1. Product analyses of wild-type and mutant *Tb*PRMT7 enzymes with the $H4^{1-21}$ R3MMA peptide. The number of experiments is indicated in parenthesis. As shown in the "Experimental Procedures" section, 86 cpm corresponds to 1 fmol of methyl groups.

***Tb*PRMT7 enzyme**	**^{3}H-methyl group radioactivity in MMA (average cpm)**	**^{3}H-methyl group radioactivity in ADMA (average cpm)**	**^{3}H-methyl group radioactivity in SDMA (average cpm)**
Wild-type (n=4)	11,093	0	0
Automethylation (n=4)	122	0	0
Double E loop mutants			
G180N (n=1)	6,648	0	0
G180Y (n=1)	5,365	0	0
E172Q (n=1)	0	0	0
E181D (n=3)	294	161	0
E181Q (n=1)	62	0	0
I173G (n=1)	0	0	0
I173A (n=1)	121	0	0
I173V (n=1)	7,231	0	0
I173P F174M (n=1)	0	0	0
I173L F174L (n=1)	29,487	0	0
G175D M177E (n=1)	0	0	0
E172D E181D (n=1)	0	0	0
E181D I173G (n=2)	64	0	0
THW loop mutants			
Q329A (n=1)	420	0	0
Q329F (n=1)	95	0	0
Q329H (n=1)	23,218	0	0
W330A (n=1)	437	0	0
Q329N (n=1)	3,322	0	0
Helix αY mutants			
F71A (n=1)	123	0	0
M75A (n=1)	205	0	0
M75F (n=1)	644	0	0
Double E loop and THW loop double mutants			
E181D W330A (n=1)	52	0	0
E181D Q329A (n=2)	89	0	500
E181D Q329N (n=1)	0	0	0
Double E loop and Helix αY double mutants			
E181D M75A (n=1)	65	0	0
E181D F71A (n=1)	143	0	0

Table 2. Root mean square deviation (RMSD) values for structural alignments of the active-site double E loop, the THW loop, and AdoHcy made in PyMOL for type I, II, and III PRMTs from the indicated crystal structures.

PRMTs		RMSD (Å)	
		Cα	all atoms
Type I	*Rn* PRMT1 (1ORI)	0	0
	Hs PRMT3 (4QQN)	0.5	1.2
	Hs PRMT4 (5DWQ)	0.6	1.3
	Hs PRMT6 (5EGS)	0.7	1.2
	Hs PRMT8 (5DST)	0.6	1.1
Type II	*Hs* PRMT5 (4GQB)	0	0
	Ce PRMT5 (3UA3)	0.3	0.6
	Xl PRMT5 (4G56)	0.4	1.6
Type III	*Tb* PRMT7 (4M38)	0	0
	Ce PRMT7 (3X0D)	0.7	1.0
	Mm PRMT7 (4C4A)	0.7	1.1

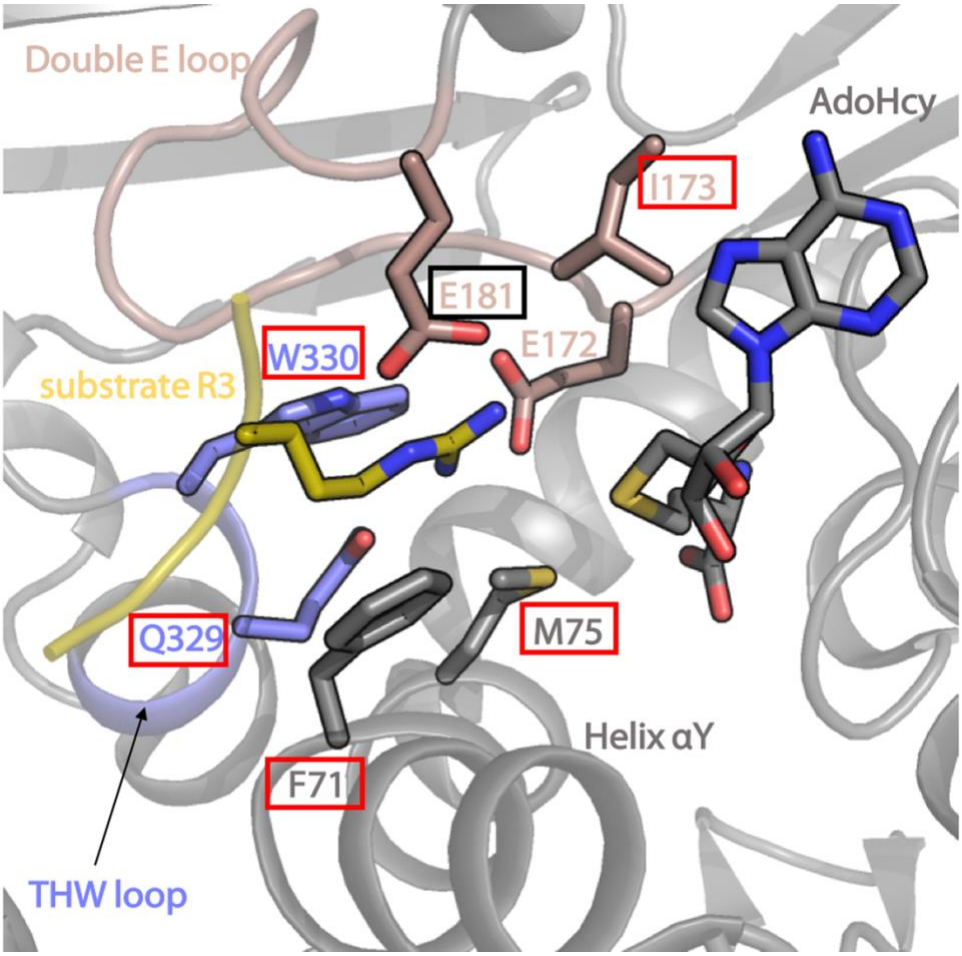

Figure 1. Active site of *Trypanosoma brucei* PRMT7. Residue E181, highlighted in the black box, is the site of mutation (E181D) shared by the six double mutants in this study with their second mutated residue highlighted in a red box (W330A, Q329A, Q329N, F71A, M75A, I173G). The double mutant E172D/E181D was previously analyzed and E172 is therefore not highlighted here (25). The double E loop is shown in dark salmon, the THW loop in slate, the substrate arginine residue in yellow, and the AdoHcy cofactor, helix αY, and adjacent residues of *Tb*PRMT7 (PDB 4M38) in gray.

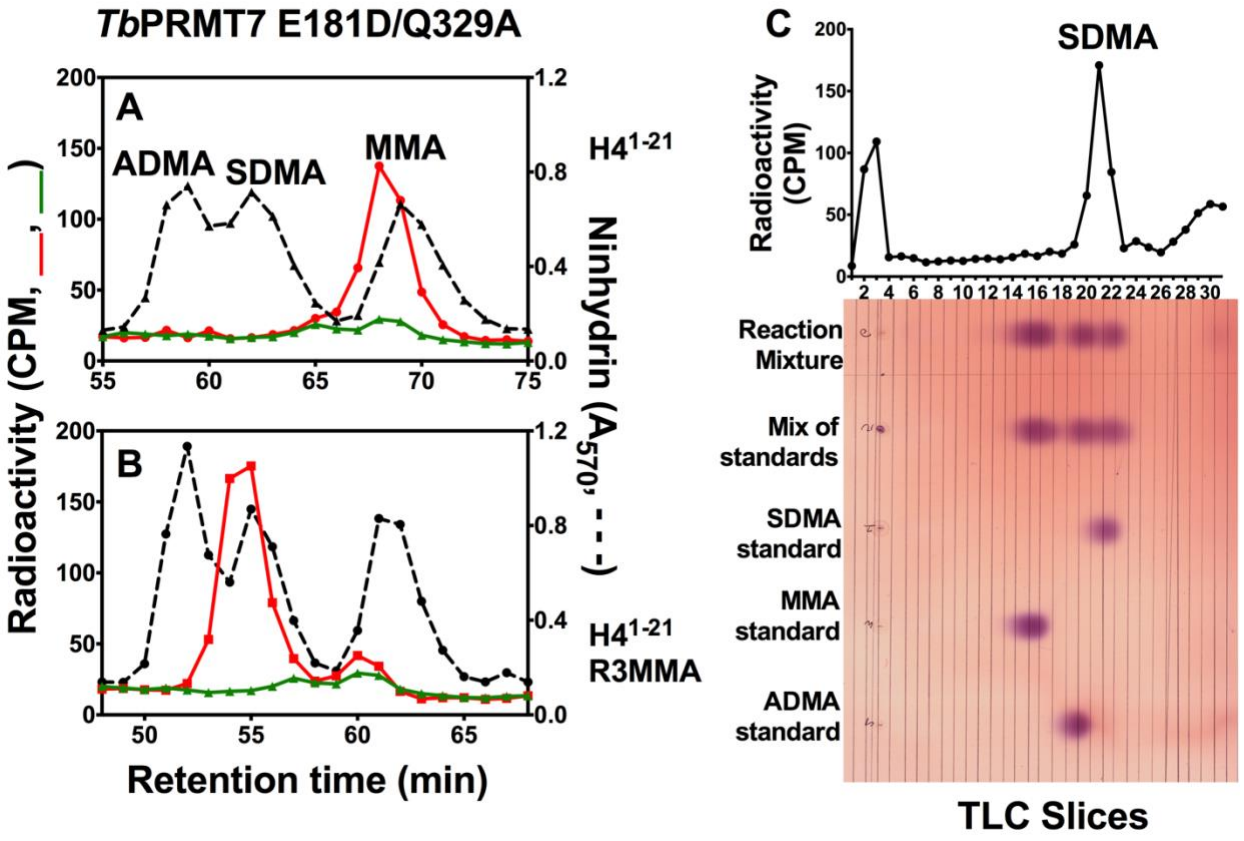

Figure 2. *TbPRMT7* E181D/Q329A double mutant produces SDMA with the H4$^{1-21}$ R3MMA peptide. The specificity of this mutant was determined using cation exchange chromatography and TLC as described in the "Experimental Procedures" section. *Tb*PRMT7 E181D/Q329A (4.8 µg protein) was incubated with the H4$^{1-21}$ or H4$^{1-21}$ R3MMA peptide (10 µM) and [*methyl*-^{3}H]AdoMet in a final volume of 60 µL. *A. Tb*PRMT7 E181D/Q329A double mutant with the H4$^{1-21}$ peptide. *B. Tb*PRMT7 E181D/Q329A with the H4$^{1-21}$ R3MMA peptide. The red lines in *A* and *B* represent radioactivity of the E181D/Q329A mutant with the different substrates and the green lines indicate radioactivity of the methylation reaction with no substrate. As noted previously (25), radioactive methylarginine derivatives elute one minute earlier than their non-radioactive counterparts due to the isotope effect (39, 40). As given in the "Experimental Procedures" section, 86 cpm corresponds to 1 fmol of methyl groups. For the number of biological replicates, see Table 1. *C.* Representative TLC for hydrolysates of the reaction mixture and individual and mixed

standards of ADMA, MMA, and SDMA. The lower portion shows the ninhydrin staining of the TLC plate; the upper portion shows the radioactivity corresponding to the TLC slices of the reaction mixture lane. Note: the ninhydrin standards on the TLC plate are the same as those shown in Fig 4*D* of Ref. 25 where a different reaction mixture was chromatographed adjacent to the ADMA standard lane. The experiment is one of two biological replicates.

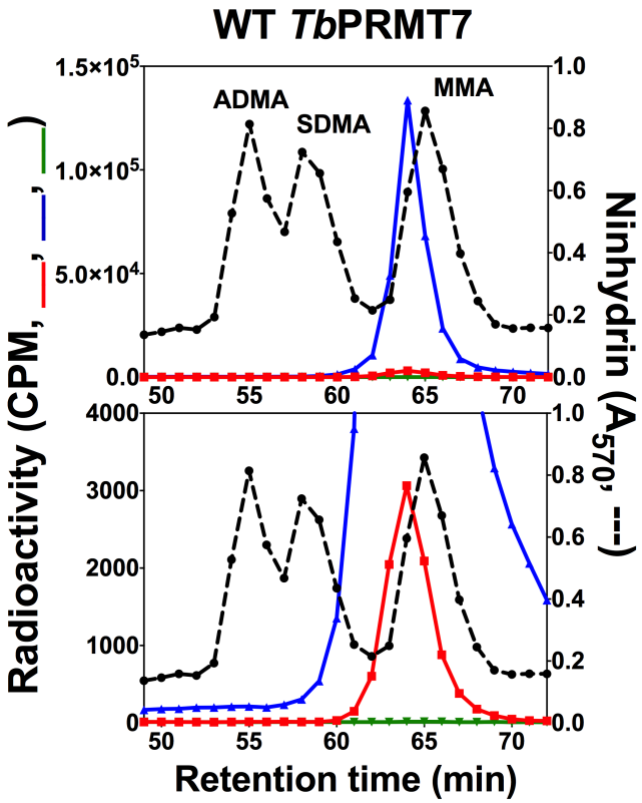

Figure 3. Wild-type *Tb*PRMT7 displays no dimethylarginine production with $H4^{1-21}$ and $H4^{1-21}$ R3MMA peptides. *In vitro* methylation and cation exchange chromatography were used as described in the “Experimental Procedures” section to assess wild-type *Tb*PRMT7 activity and product specificity with $H4^{1-21}$ (blue), $H4^{1-21}$ R3MMA peptides (red), or with the enzyme alone (green). Dashed black lines indicate elution profile of non-radioactive methylarginine species as measured by a ninhydrin assay (see “Experimental Procedures”). The *lower panel* represents enlargement of the radioactivity in the *upper panel* to show low levels of methylation. As given in the "Experimental Procedures" section, 86 cpm corresponds to 1 fmol of methyl groups. For the number of biological replicates, see Table 1.

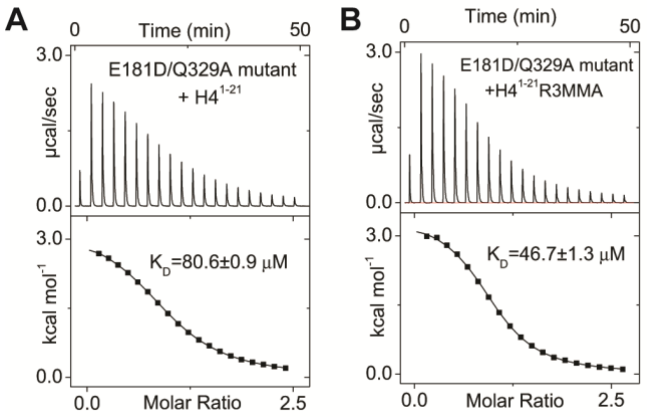

Figure 4. Isothermal titration calorimetry of the *Tb*PRMT7 E181D/Q329A mutant with $H4^{1-21}$ (*A*) and $H4^{1-21}$ R3MMA (*B*), respectively. Each titration was performed twice.

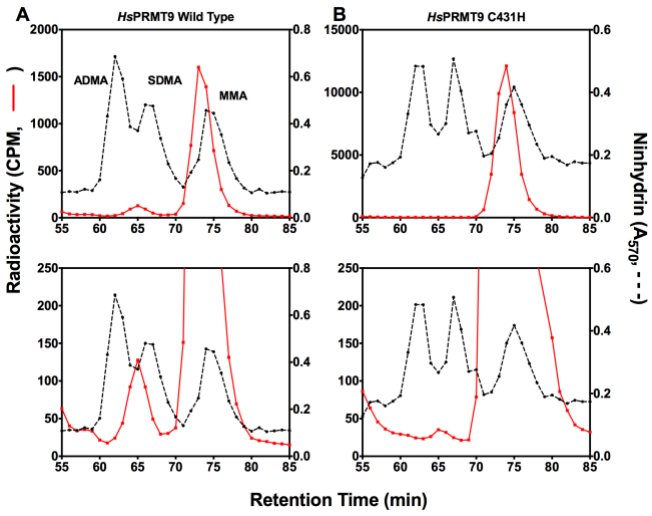

Figure 5. *Hs*PRMT9 C431H mutant displays diminished SDMA and greatly increased MMA production with GST-SF3B2. *(A)* Amino acid analysis of methylated arginine derivatives produced by the wild-type human GST-PRMT9 (*Hs*PRMT9) with substrate GST-SF3B2 as described in "Experimental Procedures". *(B)* Amino acid analysis of methylated arginine derivatives produced by the C431H mutant human GST-PRMT9 with substrate GST-SF3B2. In each case, the *lower panels* represent enlargement of the radioactivity in the *upper panels* to show low levels of methylation. As given in the "Experimental Procedures" section, 86 cpm corresponds to 1 fmol of methyl groups. This experiment is one of two biological replicates.

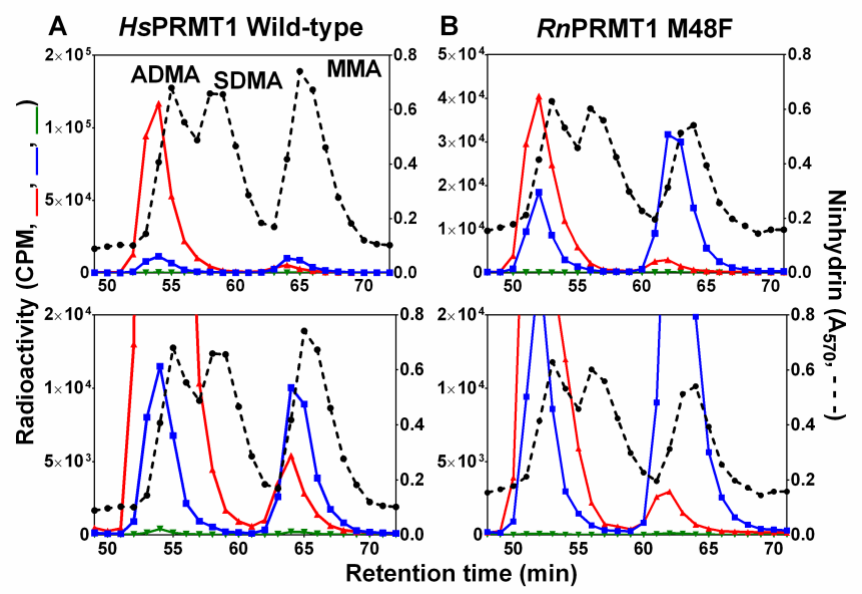

Figure 6. *Rn*PRMT1 M48F mutant enzyme does not produce SDMA with histone H4 peptides. *In vitro* methylation and cation exchange chromatography was used as described in the "Experimental Procedures" section to assess PRMT1 activity and product specificity with $H4^{1-21}$ (blue), $H4^{1-21}$ R3MMA (red), and the enzyme alone (green). Dashed black lines indicate elution profile of non-radioactive methylarginine species as measured by a ninhydrin assay (see "Experimental Procedures"). *(A)* Amino acid analysis of methylated arginine derivatives produced by human PRMT1 (*Hs*PRMT1). *(B)* Amino acid analysis of methylated arginine derivatives produced by rat PRMT1 (*Rn*PRMT1) M48F mutant. In each case, the *lower panels* represent enlargement of the radioactivity in the *upper panels* to show low levels of methylation. As given in the "Experimental Procedures" section, 86 cpm corresponds to 1 fmol of methyl groups. This experiment represents one of two biological replicates.

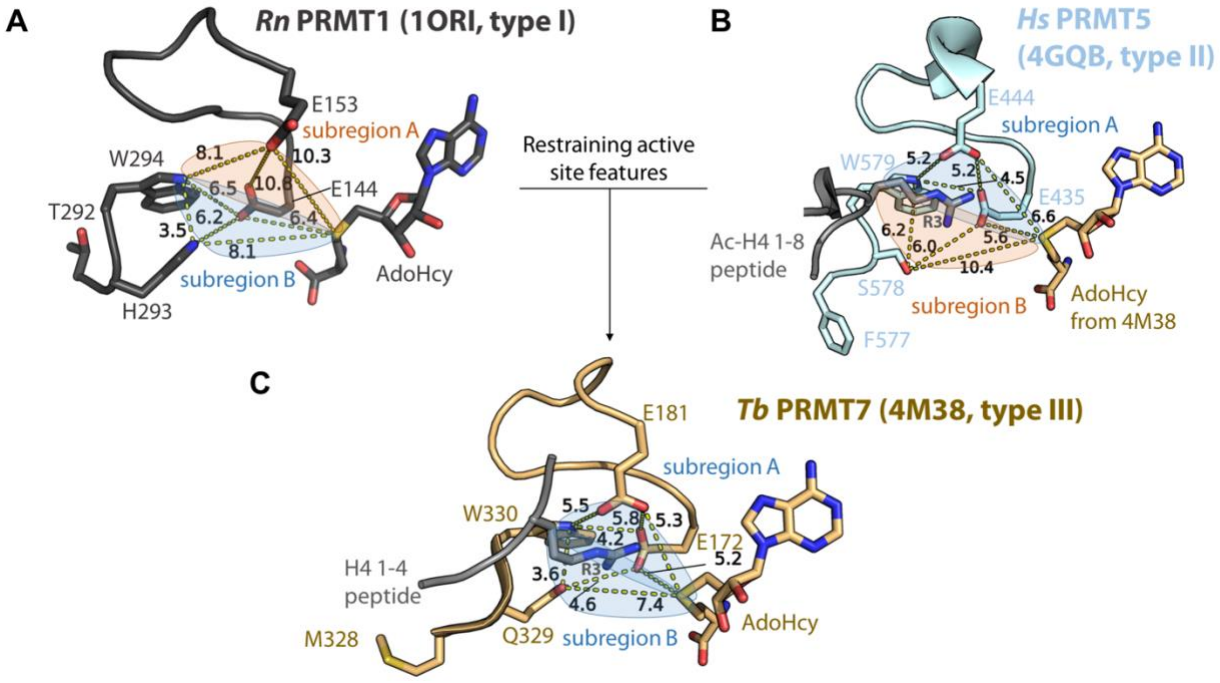

Figure 7. PRMT active sites display distinct spatial architectures. The active site (Double E loop, THW loop, and AdoHcy) from *A. Rn*PRMT1 (1ORI, Chain A; dark grey), *B. Hs*PRMT5 (4GQB, Chain A; cyan), and *C. Tb*PRMT7 (4M38, Chain A; wheat) are shown. Crowded subregions of the active sites are highlighted in light blue and open subregions are highlighted in orange. In *B* and *C*, substrate peptides co-crystallized with the enzyme are also shown. Distances between atoms are given in Ångströms and indicated by yellow dashed lines. Images were made using PyMOL (Schrödinger, LLC).

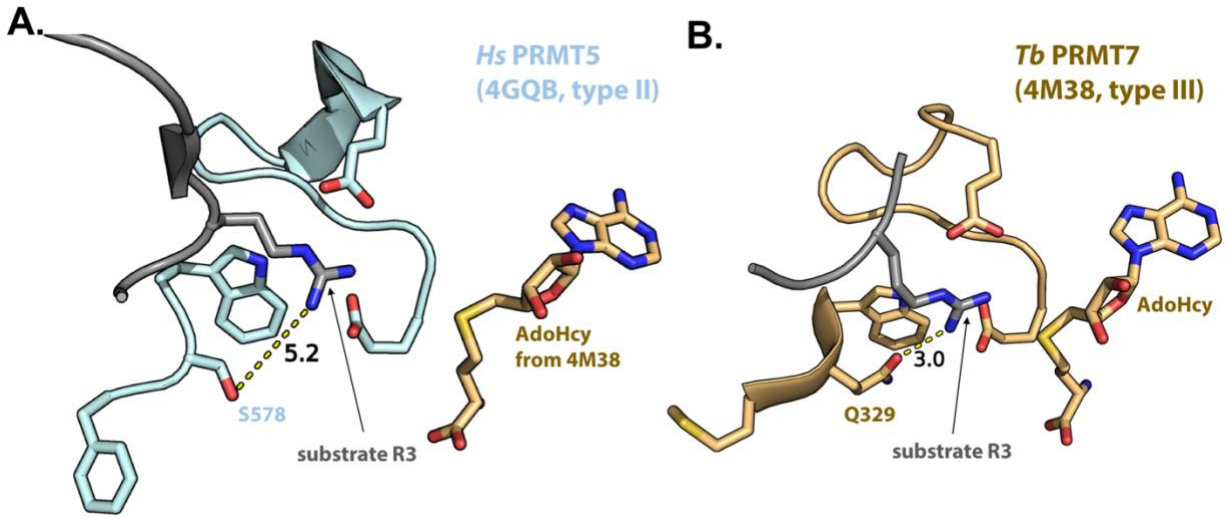

Figure 8. The THW loop of PRMT5 is farther away from the substrate arginine than the THW loop of PRMT7. *(A)* Active site of human PRMT5 (4GQB) is shown. *(B)* Active site of *Tb*PRMT7 (4M38) is shown. Distances between atoms are given in Ångströms and indicated by yellow dashed lines.

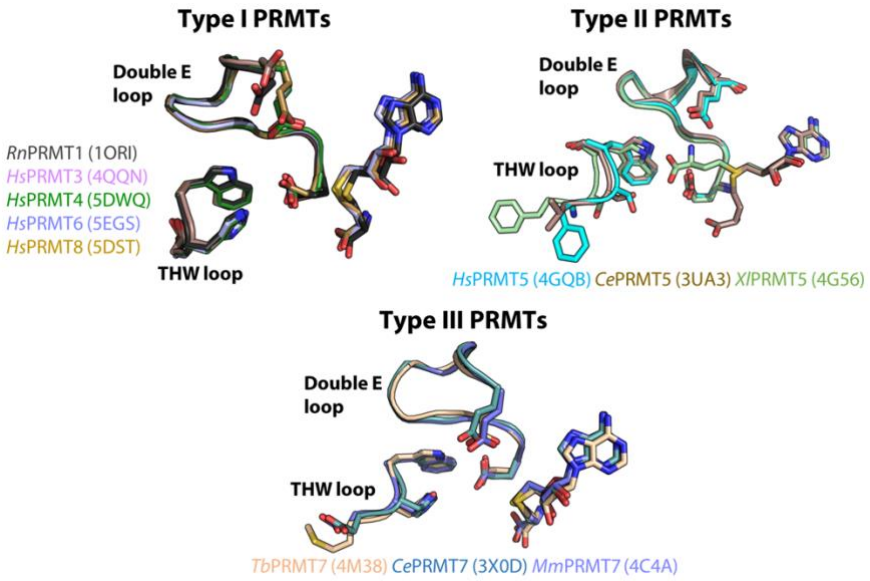

Figure 9. Structural alignment of PRMT active sites. Active sites of all three types of PRMTs are shown.

REFERENCES

1. Walsh, G., and Jefferis, R. (2006) Post-translational modifications in the context of therapeutic proteins. *Nat. Biotechnol.* **24**, 1241–52
2. Fuhrmann, J., Clancy, K. W., and Thompson, P. R. (2015) Chemical biology of protein arginine modifications in epigenetic regulation. *Chem. Rev.* **115**, 5413–5461
3. Morales, Y., Cáceres, T., May, K., and Hevel, J. M. (2016) Biochemistry and regulation of the protein arginine methyltransferases (PRMTs). *Arch. Biochem. Biophys.* **590**, 138–152
4. Baldwin, R. M., Haghandish, N., Daneshmand, M., Amin, S., Paris, G., Falls, T. J., Bell, J. C., Islam, S., and Côté, J. (2015) Protein arginine methyltransferase 7 promotes breast cancer cell invasion through the induction of MMP9 expression. *Oncotarget*. **6**, 3013–3032
5. Yao, R., Jiang, H., Ma, Y., Wang, L., Wang, L., Du, J., Hou, P., Gao, Y., Zhao, L., Wang, G., Zhang, Y., Liu, D.-X., Huang, B., and Lu, J. (2014) PRMT7 induces epithelial-to-mesenchymal transition and promotes metastasis in breast cancer. *Cancer Res.* **74**, 5656–5667
6. Yang, Y., and Bedford, M. T. (2013) Protein arginine methyltransferases and cancer. *Nat. Rev. Cancer*. **13**, 37–50
7. Karkhanis, V., Wang, L., Tae, S., Hu, Y. J., Imbalzano, A. N., and Sif, S. (2012) Protein arginine methyltransferase 7 regulates cellular response to DNA damage by methylating promoter histones H2A and H4 of the polymerase δ catalytic subunit gene, POLD1. *J. Biol. Chem.* **287**, 29801–29814
8. Wang, Y.-C., Peterson, S. E., and Loring, J. F. (2014) Protein post-translational modifications and regulation of pluripotency in human stem cells. *Cell Res.* **24**, 143–60
9. Lott, K., Zhu, L., Fisk, J. C., Tomasello, D. L., and Read, L. K. (2014) Functional interplay between protein arginine methyltransferases in Trypanosoma brucei. *Microbiologyopen*. **3**, 3595–3609
10. Ferreira, T. R., Alves-Ferreira, E. V. C., Defina, T. P. A., Walrad, P., Papadopoulou, B.,

and Cruz, A. K. (2014) Altered expression of an RBP-associated arginine methyltransferase 7 in L eishmania major affects parasite infection. *Mol. Microbiol.* **94**, 1085–1102

11. Bedford, M. T., and Clarke, S. G. (2009) Protein Arginine Methylation in Mammals: Who, What, and Why. *Mol. Cell*. **33**, 1–13
12. Martens-Lobenhoffer, J., Bode-Böger, S. M., and Clement, B. (2016) First detection and quantification of N(δ)-monomethylarginine, a structural isomer of N(G)-monomethylarginine, in humans using MS(3). *Anal. Biochem.* **493**, 14–20
13. Wang, H., Huang, Z. Q., Xia, L., Feng, Q., Erdjument-Bromage, H., Strahl, B. D., Briggs, S. D., Allis, C. D., Wong, J., Tempst, P., and Zhang, Y. (2001) Methylation of histone H4 at arginine 3 facilitating transcriptional activation by nuclear hormone receptor. *Science*. **293**, 853–57
14. Sun, L., Wang, M., Lv, Z., Yang, N., Liu, Y., Bao, S., Gong, W., and Xu, R.-M. (2011) Structural insights into protein arginine symmetric dimethylation by PRMT5. *Proc. Natl. Acad. Sci.* **108**, 20538–20543
15. Dhar, S. S., Lee, S.-H., Kan, P.-Y., Voigt, P., Ma, L., Shi, X., Reinberg, D., and Lee, M. G. (2012) Trans-tail regulation of MLL4-catalyzed H3K4 methylation by H4R3 symmetric dimethylation is mediated by a tandem PHD of MLL4. *Genes Dev.* **26**, 2749–2762
16. Migliori, V., Müller, J., Phalke, S., Low, D., Bezzi, M., Mok, W. C., Sahu, S. K., Gunaratne, J., Capasso, P., Bassi, C., Cecatiello, V., De Marco, A., Blackstock, W., Kuznetsov, V., Amati, B., Mapelli, M., and Guccione, E. (2012) Symmetric dimethylation of H3R2 is a newly identified histone mark that supports euchromatin maintenance. *Nat. Struct. Mol. Biol.* **19**, 136–144
17. Gayatri, S., and Bedford, M. T. (2014) Readers of histone methylarginine marks. *Biochim. Biophys. Acta - Gene Regul. Mech.* **1839**, 702–710
18. Suárez-Calvet, M., Neumann, M., Arzberger, T., Abou-Ajram, C., Funk, E., Hartmann, H.,

Edbauer, D., Kremmer, E., Göbl, C., Resch, M., Bourgeois, B., Madl, T., Reber, S., Jutzi, D., Ruepp, M.-D., Mackenzie, I. R. A., Ansorge, O., Dormann, D., and Haass, C. (2016) Monomethylated and unmethylated FUS exhibit increased binding to Transportin and distinguish FTLD-FUS from ALS-FUS. *Acta Neuropathol.* **131**, 587–604

19. Dhar, S., Vemulapalli, V., Patananan, A. N., Huang, G. L., Di Lorenzo, A., Richard, S., Comb, M. J., Guo, A., Clarke, S. G., and Bedford, M. T. (2013) Loss of the major Type I arginine methyltransferase PRMT1 causes substrate scavenging by other PRMTs. *Sci. Rep.* **3**, 1311
20. Fuhrmann, J., and Thompson, P. R. (2016) Protein arginine methylation and citrullination in epigenetic regulation. *ACS Chem. Biol.* **11**, 654–668
21. Schapira, M., and Ferreira de Freitas, R. (2014) Structural biology and chemistry of protein arginine methyltransferases. *Medchemcomm*. **5**, 1779–1788
22. Cura, V., Troffer-Charlier, N., Wurtz, J. M., Bonnefond, L., and Cavarelli, J. (2014) Structural insight into arginine methylation by the mouse protein arginine methyltransferase 7: a zinc finger freezes the mimic of the dimeric state into a single active site. *Acta Crystallogr. D. Biol. Crystallogr.* **70**, 2401–2412
23. Hasegawa, M., Toma-Fukai, S., Kim, J. D., Fukamizu, A., and Shimizu, T. (2014) Protein arginine methyltransferase 7 has a novel homodimer-like structure formed by tandem repeats. *FEBS Lett.* **588**, 1942–1948
24. Gui, S., Gathiaka, S., Li, J., Qu, J., Acevedo, O., and Hevel, J. M. (2014) A remodeled protein arginine methyltransferase 1 (PRMT1) generates symmetric dimethylarginine. *J. Biol. Chem.* **289**, 9320–9327
25. Debler, E. W., Jain, K., Warmack, R. A., Feng, Y., Clarke, S. G., Blobel, G., and Stavropoulos, P. (2016) A glutamate/aspartate switch controls product specificity in a protein arginine methyltransferase. *Proc. Natl. Acad. Sci. U. S. A.* **113**, 2068–2073
26. Fisk, J. C., Sayegh, J., Zurita-Lopez, C., Menon, S., Presnyak, V., Clarke, S. G., and Read,

L. K. (2009) A type III protein arginine methyltransferase from the protozoan parasite Trypanosoma brucei. *J. Biol. Chem.* **284**, 11590–11600

27. Wang, C., Zhu, Y., Caceres, T. B., Liu, L., Peng, J., Wang, J., Chen, J., Chen, X., Zhang, Z., Zuo, X., Gong, Q., Teng, M., Hevel, J. M., Wu, J., and Shi, Y. (2014) Structural determinants for the strict monomethylation activity by trypanosoma brucei protein arginine methyltransferase 7. *Structure*. **22**, 756–68
28. Hadjikyriacou, A., Yang, Y., Espejo, A., Bedford, M. T., and Clarke, S. G. (2015) Unique features of human protein arginine methyltransferase 9 (PRMT9) and its substrate RNA splicing factor SF3B2. *J. Biol. Chem.* **290**, 16723–16743
29. Yang, Y., Hadjikyriacou, A., Xia, Z., Gayatri, S., Kim, D., Zurita-Lopez, C., Kelly, R., Guo, A., Li, W., Clarke, S. G., and Bedford, M. T. (2015) PRMT9 is a type II methyltransferase that methylates the splicing factor SAP145. *Nat. Commun.* **6**, 6428
30. Feng, Y., Maity, R., Whitelegge, J. P., Hadjikyriacou, A., Li, Z., Zurita-Lopez, C., Al-Hadid, Q., Clark, A. T., Bedford, M. T., Masson, J. Y., and Clarke, S. G. (2013) Mammalian protein arginine methyltransferase 7 (PRMT7) specifically targets RXR sites in lysine- and arginine-rich regions. *J. Biol. Chem.* **288**, 37010–37025
31. Feng, Y., Xie, N., Jin, M., Stahley, M. R., Stivers, J. T., and Zheng, Y. G. (2011) A transient kinetic analysis of PRMT1 catalysis. *Biochemistry*. **50**, 7033–7044
32. Huang, S., Litt, M., and Felsenfeld, G. (2005) Methylation of histone H4 by arginine methyltransferase PRMT1 is essential in vivo for many subsequent histone modifications. *Genes Dev.* **19**, 1885–1893
33. Wang, M., Xu, R.-M., and Thompson, P. R. (2013) Substrate specificity, processivity, and kinetic mechanism of protein arginine methyltransferase 5. *Biochemistry*. **52**, 5430–5440
34. Bao, X., Zhao, S., Liu, T., Liu, Y. Y., Liu, Y. Y., and Yang, X. (2013) Overexpression of PRMT5 promotes tumor cell growth and is associated with poor disease prognosis in epithelial ovarian cancer. *J. Histochem. Cytochem.* **61**, 206–217

35. Tarighat, S. S., Santhanam, R., Frankhouser, D., Radomska, H. S., Lai, H., Anghelina, M., Wang, H., Huang, X., Alinari, L., Walker, A., Caligiuri, M. A., Croce, C. M., Li, L., Garzon, R., Li, C., Baiocchi, R. A., and Marcucci, G. (2016) The dual epigenetic role of PRMT5 in acute myeloid leukemia: gene activation and repression via histone arginine methylation. *Leukemia*. **30**, 789–99

36. Schapira, M., and Arrowsmith, C. H. (2016) Methyltransferase inhibitors for modulation of the epigenome and beyond. *Curr. Opin. Chem. Biol.* **33**, 81–87

37. Hu, H., Qian, K., Ho, M.-C., and Zheng, Y. G. (2016) Small molecule inhibitors of protein arginine methyltransferases. *Expert Opin. Investig. Drugs*. **25**, 335–358

38. Zhang, X., and Cheng, X. (2003) Structure of the predominant protein arginine methyltransferase PRMT1 and analysis of its binding to substrate peptides. *Structure*. **11**, 509–520

39. Zurita-Lopez, C. I., Sandberg, T., Kelly, R., and Clarke, S. G. (2012) Human protein arginine methyltransferase 7 (PRMT7) is a type III enzyme forming omega-NG-monomethylated arginine residues. *J. Biol. Chem.* **287**, 7859–7870

40. Gottschling, H., and Freese, E. (1962) A tritium isotope effect on ion exchange chromatography. *Nature*. **196**, 829–831

Chapter 5

Mammalian PRMT7's preference for sub-physiological temperatures is not due to gross structural changes

Mammalian PRMT7's preference for sub-physiological temperatures is not due to gross structural changes

Kanishk Jain, Martin L. Phillips, Troy L. Lowe, and Steven G. Clarke

ABSTRACT

Mammalian PRMT7's role as a regulator of crucial cellular functions including transcription, cell differentiation, and cancer metastasis has made it increasingly vital to thoroughly understand its biochemistry. Since PRMT7 appears to be emerging as a viable target for potential anti-cancer therapeutics, knowing the intricacies of how this enzyme works may help lead to the development of effective small-molecule inhibitors. One of the less well understood features of this enzyme is its preference for cold, sub-physiological temperatures in terms of methylating activity. In order to elucidate whether certain structural elements of human PRMT7 are being affected by changes in temperature, causing the enzyme to become relatively inactive at 37 °C, we employed biophysical techniques including analytical ultracentrifugation (AUC) and circular dichroism (CD) spectroscopy. Through AUC we determined that while temperature did not affect the overall sedimentation rate of human PRMT7, the enzyme did show a small but significant change in its rate of sedimentation in the presence of its product AdoHcy, implying a structural change occurring as a result of enzyme-cofactor binding. CD experiments revealed that the secondary structure of human PRMT7 does not change at different temperatures, unlike *Tb*PRMT7 and *Hs*PRMT1—enzymes most active at 37°C—highlighting new structural information on human PRMT7.

INTRODUCTION

PRMT7 has been somewhat of an oddball in the PRMT family for a number of reasons. In the first place, PRMT7 is the only enzyme in its family that is restricted to monomethylating arginine residues (1–4). Secondly, the mammalian PRMT7 enzymes seem to recognize distinctly different substrate motifs than their dimethylating cousins, implying that PRMT7 is not just a redundant monomethylating enzyme (5, 6). Finally, a truly peculiar trait of mammalian PRMT7 is its relative inactivity at temperatures that are physiologically relevant to mammals, namely 37°C (5). Most enzymes in mammalian systems optimally function in a narrow range around 37°C (7), but human and mouse PRMT7 seem to display activity over a wide range of temperatures that are significantly below physiological temperatures *in vitro* (5, 8).

Over the years, literature implicating mammalian PRMT7 as a crucial player in cellular regulation has been growing (9–14). Given the emerging biological significance of this protein, we have set out to understand how human PRMT7's enzymatic activity may be controlled through temperature. It is possible that *in vitro* experiments done thus far to assay human PRMT7 activity have lacked a certain element which is present in the cellular environment—an element necessary to activate the enzyme at 37 °C. We explored this possibility through the structural techniques of analytical ultracentrifugation (AUC) and circular dichroism (CD) spectroscopy to find out whether PRMT7 structure was affected by changing temperature. Structural elements often display instability at various temperatures *in vitro* where they might otherwise be stable *in vivo* due to protein-protein interactions, hydrogen bonds, and/or other molecular interactions. Through various biophysical methods, we report that while human PRMT7's structure does not seem to change drastically as a function of temperature, suggesting that structural dynamics that may be affecting this enzyme's activity are occurring at a very minute level and cannot be measured well with ensemble methods AUC and CD. However, the experiments in our current

study highlight these findings as yet another group of features that set mammalian PRMT7 apart from the rest of the PRMTs.

RESULTS

Isolation of recombinantly expressed human PRMT7-His at high purity

Previous *in vitro* studies on human PRMT7 have used an N-terminal glutathione S-transferase (GST)- PRMT7 fusion protein recombinant protein expressed in *E. coli* and purified on an affinity column with covalently-linked glutathione (1, 2, 5, 8). However, SDS gel analysis of this preparation indicated additional polypeptide bands in addition to the expected 105 kDa fusion polypeptide, possibly including the cleaved GST protein, nicked PRMT7, and *E. coli* contaminants. Creating a new human PRMT7 construct with a cleavable N-terminal maltose binding protein (MBP) tag and a C-terminal His-tag, along with a three-step purification of anion exchange chromatography (anIEC), immobilized metal affinity chromatography (IMAC), and gel filtration (GF) resulted in an enzyme preparation with no discernable degradation products (**Figure 1**).

Maximal enzymatic activity of *Hs*PRMT7-His at sub-physiological temperature

Previous studies in the lab have shown that GST-*Hs*PRMT7 is highly active between 10 °C to 25 °C and almost completely inactive at the physiological temperature of 37 °C (5). With a new, more robust method for purifying human PRMT7, it was necessary to re-examine whether the enzyme still showed the same temperature preference. By testing the activity of human PRMT7 with H2B (23-37) at two different temperatures and varying times, a linear range of 30 min to 3 h was determined (**Figure 2A**). Following this, with a reaction time of 1 h, PRMT7-mediated methylation of H2B (23-37) was measured at 5 °C, 15 °C, 23 °C, 30 °C, and 37 °C. Consistent with previous results (5), the His-tagged preparation of PRMT7 is most active at sub-37 °C temperatures (**Figure 2B**); additionally the methylation rate seems to be higher at 15 °C versus 37 °C (**Figure 2A**). Interestingly, unlike the almost complete lack of PRMT7 activity observed in previous work (5), the construct used in this study retains about 23% of its maximal activity at 37 °C.

***Hs*PRMT7-His sediments primarily as a monomer regardless of temperature**

One hypothesis for mammalian PRMT7's low temperature-high activity behavior is that some structural changes due to temperature may cause the enzyme to change its quaternary interactions (i.e. oligomerize or aggregate). Analytical ultracentrifugation was conducted with human PRMT7 at 4 °C, 20 °C, and 37 °C with or without a two-fold molar excess of AdoHcy over enzyme —used to mimic AdoMet-related effects without inducing automethylation. Observed sedimentation coefficients were corrected with density and viscosity factors to facilitate comparison of any temperature (15, 16). PRMT7 primarily sedimented as a monomeric species, irrespective of temperature, around 4.8 S (**Table 1**; **Figure 3A and 3B**). Additionally, because there was no significant difference in sedimentation of PRMT7 in terms of temperature, one can assume those data to be degenerate and analyze the differences between the average sedimentation of PRMT7 with or without AdoHcy (**Table 1**). When comparing these average values, the sedimentation coefficient for PRMT7 with AdoHcy is significantly higher (p = 0.0082) than the coefficient for PRMT7 without AdoHcy (**Figure 3C**): 4.96 versus 4.84. It is important to note that though this difference exists, there is no significant change in the oligomerization or aggregation of PRMT7 and it primarily exists as a monomer regardless of the presence of AdoHcy.

Human PRMT7 secondary structure is unaffected by changes in temperature

Further investigation into the effects of temperature on PRMT7 was done through circular dichroism (CD) spectroscopy. By measuring the CD signal of human PRMT7 at far-UV wavelengths (195-260), we noted that there was no significant change as a function of temperature from 10 °C to 37 °C (**Figure 4A and 4B**). Each spectrum represented and average of nine scans at each temperature. We similarly analyzed the secondary structure of two PRMTs known to be most active at 37 °C—*Tb*PRMT7 (17) and *Hs*PRMT1 (18). Interestingly, these

enzymes did seem to show some loosening of secondary structure, as evidenced by the slight decrease in CD signal between 205-225 nm (**Figure 4C-F**); this change is especially evident when comparing the lowest temperature to the highest one (**Figure 4D and 4F**). It is unclear why human PRMT7 secondary structure remains unchanged by temperature changes, while *Tb*PRMT7 and human PRMT1 show some flexibility in structure as temperatures approach 37 °C.

DISCUSSION

Most biological reactions, particularly those catalyzed by human enzymes, occur in a temperature range with maximal activity usually around 37 °C (19). As such, most of the mammalian PRMTs, including the primary dimethylating enzymes PRMT1 and PRMT5, are most active at physiological temperatures (18, 20). This made it difficult to initially characterize human PRMT7 activity, as it did not seem to be very active at 37 °C. Further analysis of enzymatic activity at different temperatures revealed that mammalian PRMT7 was highly active from 10 °C to 25 °C, but almost completely inactive around 37 °C (5). The discovery of human and mouse PRMT7's preference for sub-physiological temperatures was quite unexpected since the other members of the PRMT family seemed to be active at 37 °C (18, 20–26). Given the various studies which implicate PRMT7 as an important player in the regulation of vital cellular processes such as transcription and DNA damage repair (14), as well as the regulation of diseases such as cancer (9, 12, 27), it became crucial to understand how this enzyme's activity was being affected by temperature. Biophysical experiments require highly purified protein preparations, and so a new human PRMT7-his construct was prepared and purified to the required specifications (**Figure 1).** After confirming that a new human PRMT7 construct also exhibited similar behavior in terms of temperature relative to previous studies (**Figure 2**), we approached this question from a structural stand point and probed the effects of changing temperatures on human PRMT7's ability to oligomerize and aggregate through AUC and on its secondary structure through CD spectroscopy.

Analytical ultracentrifugation showed that human PRMT7 mainly exists as a monomer in solution, with or without AdoHcy. There does not seem to be any change in the way human PRMT7 aggregates as temperatures change from 4 °C to 37 °C (**Figure 3**). The first interesting thing we noted was that the sedimentation coefficient of about 4.8-4.9S (**Table 1**) was somewhat lower than would be expected of a spherical, hydrated protein with a similar molecular weight of

around 79.5 kDa. Using the Svedberg equations (28), we calculated the theoretical coefficient to be about 5.6 S with a hydration value of 0.5 g water/g protein, implying that the human PRMT7 particle was traveling slower than it would if it was a similarly hydrated, spherical protein. The PRMT7 monomer particle may have a rigid asymmetric shape, resulting in slower sedimentation; it may even have regions of disordered structure which create drag. The experimental sedimentation coefficients correspond to a calculated axial ratio of 3.6 assuming a prolate ellipsoid shape (using Perrin factors (29)); this correlates well with the toroidal shape observed in the crystal structure of mouse PRMT7 (30). Additionally, the presence of the AdoHcy cofactor appeared to increase the sedimentation coefficient from 4.84S to 4.96S—a statistically significant difference. This suggests that AdoHcy binding may have ordered certain regions of the enzyme, allowing it to achieve a more compact shape that could sediment faster.

Though there were no observable changes in the quaternary structure of human PRMT7 at different temperatures, more minute changes at the secondary structure level were probed for with CD spectroscopy. As with AUC, CD experiments showed little change in human PRMT7's structure—the secondary structural elements—when the enzyme was incubated at temperatures from 10 °C to 37 °C (**Figure 4A and 4B**). This further implies that if structural changes are indeed the cause of PRMT7's inactivity *in vitro* at 37 °C, such structural changes are indistinguishable from the overall dynamics of the protein where helices, sheets, and random coils are concerned. CD scans with AdoHcy were not conducted due to potential interference from the absorbance of the adenosine of AdoHcy in the far-UV range. We conducted similar experiments on similar PRMT enzymes known to be active at 37 °C (*Tb*PRMT7 and *Hs*PRMT1). Interestingly, both enzymes displayed slight changes in the far-UV CD spectra as temperatures went from 10 °C to 37 °C (**Figure 4C-F**). The data suggests that for these two enzymes, there is a slight loss in secondary structure, though it is difficult to say whether these differences are significant due to the relatively small changes in signal observed. Perhaps this means that a level of flexibility is

required for PRMTs to operate at 37 °C and human PRMT7 lacks that flexibility by itself. However, this would then mean that human PRMT7 would have similarly low activity at all temperatures by itself. Since that is clearly not the case (**Figure 2**), one may surmise that there are distinct features of the enzyme, both structurally and catalytically, which could be more finely manipulated in the cell and are indistinguishable through *in vitro* techniques. Through our series of biochemical and biophysical experiments, we have come closer to understanding this peculiar enzymatic behavior of human PRMT7, but further *in vivo* structural analysis may be necessary to get a complete picture of this enzyme's activity.

METHODS

Recombinant expression and protein purification

Human PRMT7 was cloned into a pMAPLE3 vector (31) as a maltose binding protein (MBP)-PRMT7-hexahistidine tag construct from a pGEX2T vector (5). This plasmid coexpresses TEV protease, which cleaves between MBP and PRMT7 to yield a PRMT7-hexahistidine (PRMT7-His) construct *in vivo*. The cleaved PRMT7-His construct contains an extra Ser residue on the N-terminus, and the hexahistidine tag is comprised of THHHHHH on the C-terminus. This plasmid was obtained from Dr. Mark Arbing in the Protein Expression Technology Center (UCLA).

PRMT7-His was expressed in *Escherichia coli* (*E. coli*) BL21(DE3) cells (Invitrogen) and grown in LB media with kanamycin (50 mg/L) at 37 °C and 225 rpm until an OD_{600} of ~0.6 was reached. Then expression was induced with the addition of 1 mM isopropyl-β-D-thiogalactoside (GoldBio) at 18 °C and 225 rpm for 20 h. The cells were then harvested through centrifugation at 5,000 x *g* at 4 °C. These cells were frozen at -20 °C for at least 24 h before being thawed and resuspended in a lysis buffer containing 50 mM HEPES-K (pH 8.0), 50 mM NaCl, 5 mM β-mercaptoethanol (β-ME; MP Biomedicals, Inc), 0.2 mM phenylmethylsulfonyl fluoride (Sigma), complete EDTA-free protease inhibitor mixture (1 tablet/50 mL of lysis buffer; Pierce A32965), and 0.2 mg/mL chicken egg-white lysozyme (Alfa Aesar). Resuspended cells were lysed in an EmulsiFlex homogenizer (Avestin) by passaging cells three times through the chamber at a pressure of 40 psi and the lysed cells were centrifuged at 15,000 rpm for 50 min at 4 °C.

The supernatant of the lysate was loaded onto a 20-mL DEAE FF anion exchange chromatography column at 4 °C (GE Healthcare). The column was washed with 10 column volumes of the lysis buffer before the protein was eluted with a 50-500 mM NaCl gradient. The eluted protein was dialyzed against 50 mM HEPES-K (pH 8.0), 300 mM NaCl, 20 mM imidazole-HCl (pH 8.0), and 5 mM β-ME at 4 °C overnight. Three 5-mL HisTrap HP Ni^{2+} columns (GE Healthcare) were joined in tandem and the dialyzed protein was applied to these columns—

equilibrated with 60 mL of the previous dialysis buffer—at room temperature. The column was then washed with 150 mL of 50 mM HEPES-K (pH 8.0), 300 mM NaCl, 40 mM imidazole-HCl (pH 8.0), and 5 mM β-ME before PRMT7-His was eluted in a 40-500 mM imidazole gradient (175 mL). The eluted PRMT7-His was further dialyzed against a buffer of identical composition to the wash buffer but lacking imidazole at 4 °C overnight. Finally, the protein was concentrated to about 500 μL using Amicon Millipore Centrifugal units (MWCO 10 kDa; Thermo Fisher Scientific) and purified on a Superdex 75pg (GE Healthcare) gel filtration column. Protein purity was assessed to be > 95% through SDS-PAGE.

Following this final purification step, PRMT7-His was buffer exchanged into three different solutions, depending on the experiments being carried out. For circular dichroism (CD) spectroscopy experiments, the protein was dialyzed into 0.5 X PBS (0.95 mM NaH_2PO_4, 4.05 mM Na_2HPO_4, and 77 mM NaCl at pH 7.4) and 0.5 mM tris(2-carboxyethyl)phosphine (TCEP; VWR). For analytical ultracentrifugation (AUC), the protein was buffer exchanged into 50 mM HEPES-K (pH 8.0), 150 mM NaCl, and 1 mM TCEP. For enzymatic assays and storage purposes, the enzyme was buffer exchanged into 50 mM HEPES-K (pH 8.0), 15% (v/v) glycerol, and 1 mM dithiothreitol (DTT; GoldBio).

Human PRMT1 (*Hs*PRMT1) was expressed and purified as described previously (3). PRMT7 from *Trypanosoma brucei* (*Tb*PRMT7) was obtained from Dr. Erik W. Debler (Thomas Jefferson University, Philadelphia, PA) as a generous gift and purified as described earlier (4).

Phosphocellulose-81 filter binding assays for PRMT7-His enzymatic assays

In order to determine optimal reaction times for initial velocities with human PRMT7-His and a histone H2B peptide from residues 23-37 of the human sequence: Ac-KKDGKKRKRSRKESY (H2B (23-37), GenScript), methylation was measured at 15 °C and 37 °C from 0 to 3 h. Specifically, the reaction mixtures contained 0.28 μM PRMT7-His, 10 μM H2B (23-37), a 5 μM mixture of *S*-adenosyl-L-methionine p-toluenesulfonate salt (AdoMet) (Sigma A2408;

≥80% purity) and *S*-adenosyl-L-[methyl-^{3}H]-methionine ([methyl-^{3}H]-AdoMet) (stock solution of 7 μM (78.2 Ci/mmol) in 10 mM H_2SO_4/EtOH (9:1, v/v)) with a specific activity of 10.7 cpm/fmol, 50 mM HEPES-K (pH 8.0), 10 mM NaCl, and 1 mM DTT. The reactions were incubated at the stated temperatures from 0 to 3 h and were quenched with 0.5 μL of 100% TFA. These reactions were done in triplicate and background reactions lacking 10 μM H2B (23-37) were done once. These reactions were bound to phosphocellulose-81 (P81) filter paper (Reaction Biology Corp.) and the assays were conducted as described previously (6) with the exception that the P81 papers were dried for 1.5 h after being washed instead of 0.75 h.

Once a linear range was determined for PRMT7-His activity, the same reactions were done for 1 h at 5 °C, 15 °C, 23 °C, 30 °C, and 37 °C. These reactions were done in triplicate. Reactions lacking substrate were also done in triplicate and the amount methylation observed in these reactions was subtracted from the methylation amount measured in reactions with H2B (23-37). The radioactivity was analyzed via P81 filter binding assays, as described earlier.

Analytical ultracentrifugation of PRMT7-His at varying temperatures

Sedimentation velocity runs were performed at 4 °C, 20 °C, and 37 °C in a Beckman Optima XL-A analytical ultracentrifuge in 12 mm pathlength double sector cells using absorption optics at 280 nm and a rotor speed of 52,000 rpm. Samples were in 50 mM HEPES-K (pH 8.0), 150 mM NaCl, and 1 mM TCEP at a protein concentration of about 0.5 mg/mL. For experiments containing *S*-adenosyl-L-homocysteine (AdoHcy, Cayman Chemicals), a two-fold molar excess of the small molecule over the enzyme was used at 16 μM. Partial specific volumes of 0.723 (4°C), 0.730 (20°C) and 0.737 (37°C) for PRMT7-His calculated from the amino acid composition and corrected for temperature were used (15, 16).

Apparent sedimentation coefficient distributions, uncorrected for diffusion, were determined as g(s) plots using the Beckman Origin based software (Version 3.01) and the sedimentation coefficients were determined from the main peak maximum. These plots display a function

proportional to the weight fraction of material with a given sedimentation coefficient, s. The function g(s) was calculated as

$$g(s) = \left(\frac{dc}{dt}\right)\left(\frac{1}{c_o}\right)\left(\frac{\omega^2 t^2}{\ln\left(\frac{r_m}{r}\right)}\right)\left(\frac{r^2}{{r_m}^2}\right)$$

where s is the sedimentation coefficient, ω is the angular velocity of the rotor, c_o is the initial concentration, r is the radius, r_m is the radius of the meniscus, and t is time.

The x-axis was converted to sedimentation coefficient by $s = \left(\frac{1}{\omega^2 t}\right)\left(\frac{1}{\ln\left(\frac{r}{r_m}\right)}\right)$ (32).

Far-UV circular dichroism spectroscopy of PRMTs at varying temperatures

Circular dichroism (CD) was conducted using a JASCO J-715 CD spectrophotometer and a pathlength of 1 mm from 10 °C to 37 °C. CD in the far-UV range (195-260 nm) was collected for *Hs*PRMT7-His, *Tb*PRMT7, and *Hs*PRMT1 at 0.2 mg/mL each in a solution of 0.5X PBS and 0.5 mM TCEP.

ACKNOWLEDGEMENTS

We thank Paul Thompson (University of Massachusetts Medical School) for providing the human his-PRMT1 plasmid. We thank members of the Clubb Lab (UCLA) –Ramsay Macdonald, Scott McConnell, Christopher Sue, and Orlando Martinez—for access to their gel filtration FPLC system. This work was supported by a grant from the National Science Foundation (MCB 17145690 to S.G.C.), grants from the NIH, including Grant GM026020 (S.G.C.) and a Ruth L. Kirschstein National Service Award GM007185 (to K.J.), and an Audree Fowler Fellowship in Protein Science (to K.J.).

TABLES AND FIGURES

Table 1. Sedimentation coefficients for human PRMT7 at various temperatures

	Temperature (°C)	Observed s (Svedbergs, S)	s20, w[a] (Svedbergs, S)	Average s20, w ± St. Dev. (Svedbergs, S)
-AdoHcy	4	3	4.83	4.84 ± 0.01
	20	4.6	4.84	
	37	6.6	4.85	
+AdoHcy	4	3.05	4.91	4.96 ± 0.03
	20	4.7	4.94	
	37	6.75	4.96	

a The s20, w values represent sedimentation coefficients derived by correcting observed values for viscosity and density changes relative to those of water at a temperature of 20 °C.

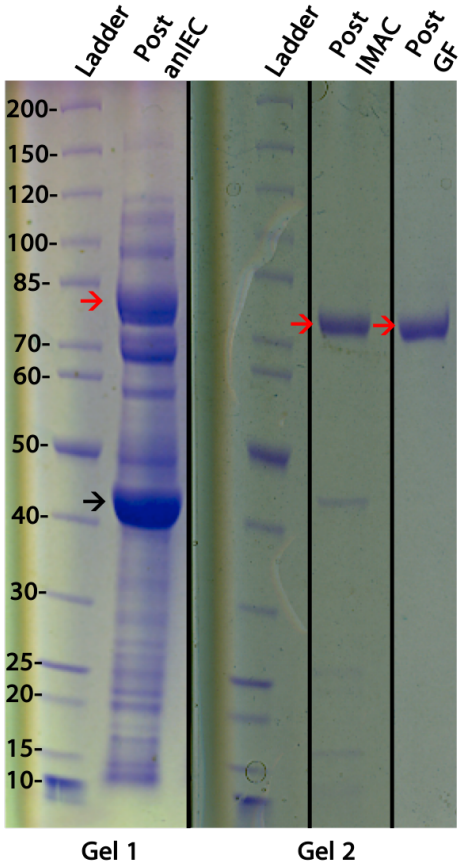

Figure 1. Purification gel of human PRMT7-His. Two Coomassie Blue-stained SDS gels depict the purity of the human PRMT7-construct at three different steps—after anion exchange chromatography (Post anIEC), after immobilized metal affinity chromatography (Post IMAC), and after gel filtration (Post GF). The red arrows indicate the increasingly pure PRMT7-his polypeptide at a molecular weight of about 79.5 kDa. In the Post anIEC, the MBP tag (cleaved *in vivo*) is indicated by a black arrow. The first two lanes on the left are on one gel (Gel 1) and the next three lanes are on another (Gel 2); the samples on Gel 2 were run on non-consecutive lanes and so are separated by black vertical lines. Note: lanes are not equally loaded in terms of amount of protein.

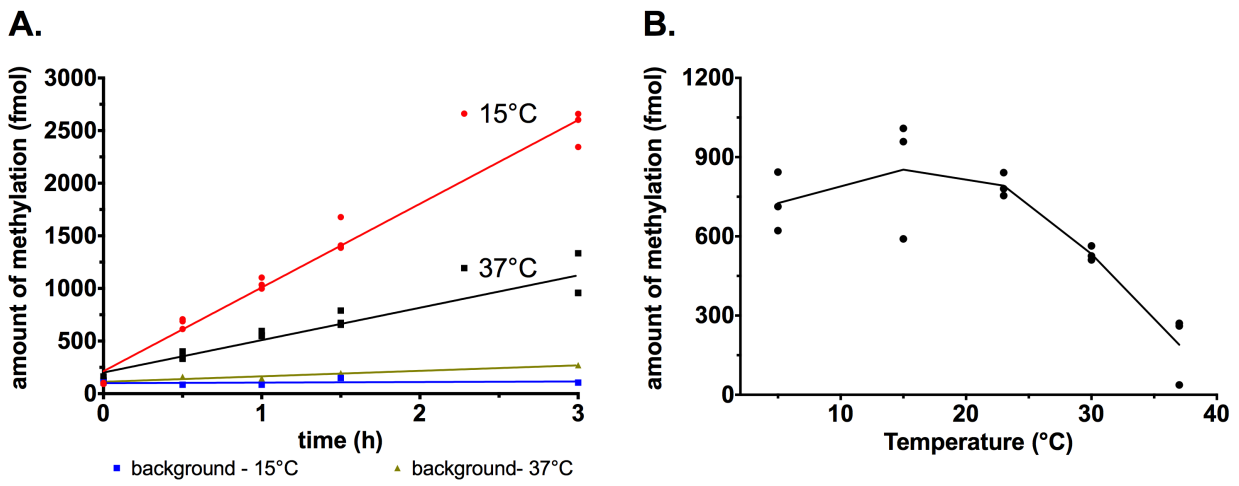

Figure 2. Human PRMT7-His displays a sub-physiological temperature preference. A) Reactions with PRMT7 and H2B (23-37) done at 15 °C are represented by red circles and those done at 37 °C are represented by black squares; these data were collected in triplicate and are shown as individual data points at each time point. The no-substrate reactions at 15°C are represented by "background-15°C" and blue squares, while those done at 37°C are represented by "background-37°C" and olive-green triangles. B) Reactions were conducted for one hour at the indicated temperatures in triplicate with human PRMT7 and H2B (23-37); reactions lacking H2B (23-37) were also done in triplicate and the amount of methylation observed was subtracted as background. Data was analyzed and graphed using GraphPad Prism 7.0. For reaction details, see "Methods."

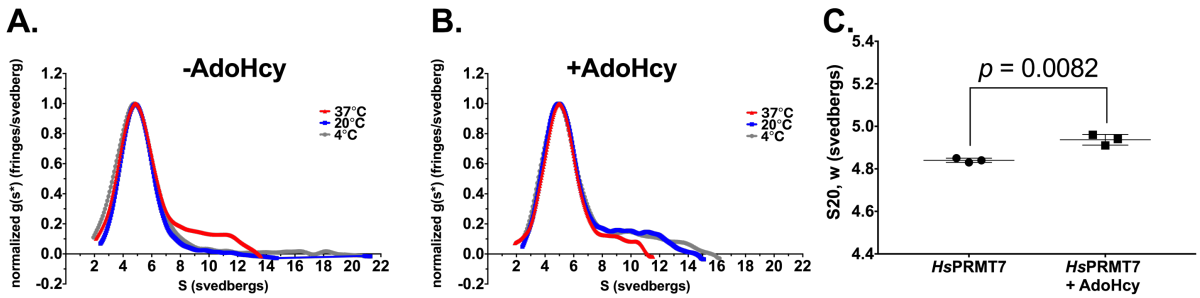

Figure 3. Human PRMT7 exists predominantly as a monomeric protein in solution regardless of temperature and cofactors. A) Sedimentation profile of PRMT7 without AdoHcy is shown at three temperatures: 4 °C (gray), 20 °C (blue), and 37 °C (red). B) Sedimentation profile of PRMT7 with two-fold AdoHcy is shown at three temperatures: 4 °C (gray), 20 °C (blue), and 37 °C (red). C) Corrected sedimentation coefficients of the monomer peak for PRMT7 with or without AdoHcy are graphed with each of the three temperatures as individual replicates. A paired t-test was used to determine statistical significance. Data was analyzed and graphed using GraphPad Prism 7.0. For details on how the AUC was performed, see “Methods.”

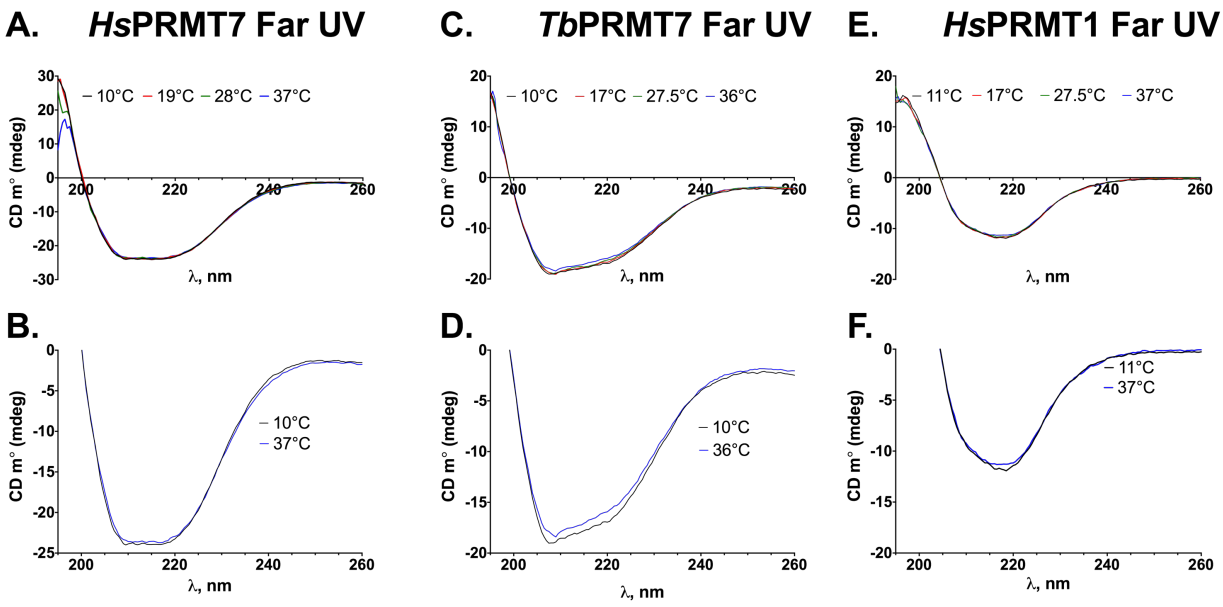

Figure 4. Circular Dichroism spectroscopy of various PRMTs shows no effect on human PRMT7 secondary structure. A) Far-UV CD of human PRMT7 at 10 °C (black), 19 °C (red), 28 °C (green), and 37 °C (blue); spectra shown here are averages of 9 scans at each temperature. B) a close-up of Panel A with human PRMT7 CD spectra at 10°C (black) and 37 °C (blue). C) Far-UV CD of *Tb*PRMT7 at 10 °C (black), 17 °C (red), 27.5 °C (green), and 36 °C (blue); spectra shown here are averages of 9 scans at each temperature. D) a close-up of Panel C with human PRMT7 CD spectra at 10 °C (black) and 36 °C (blue). E) Far-UV CD of human PRMT1 at 11°C (black), 17 °C (red), 27.5 °C (green), and 37 °C (blue); spectra shown here are averages of 9 scans at each temperature. F) a close-up of Panel E with human PRMT7 CD spectra at 11°C (black) and 37 °C (blue). For details on the how CD spectra were collected, see "Methods."

REFERENCES

1. Miranda, T. B., Miranda, M., Frankel, A., and Clarke, S. (2004) PRMT7 is a member of the protein arginine methyltransferase family with a distinct substrate specificity. *J. Biol. Chem.* **279**, 22902–22907
2. Zurita-Lopez, C. I., Sandberg, T., Kelly, R., and Clarke, S. G. (2012) Human protein arginine methyltransferase 7 (PRMT7) is a type III enzyme forming omega-NG-monomethylated arginine residues. *J. Biol. Chem.* **287**, 7859–7870
3. Jain, K., Warmack, R. A., Debler, E. W., Hadjikyriacou, A., Stavropoulos, P., and Clarke, S. G. (2016) Protein arginine methyltransferase product specificity Is mediated by distinct active-site architectures. *J. Biol. Chem.* **291**, 18299–18308
4. Debler, E. W., Jain, K., Warmack, R. A., Feng, Y., Clarke, S. G., Blobel, G., and Stavropoulos, P. (2016) A glutamate/aspartate switch controls product specificity in a protein arginine methyltransferase. *Proc. Natl. Acad. Sci. U. S. A.* **113**, 2068–2073
5. Feng, Y., Hadjikyriacou, A., and Clarke, S. G. (2014) Substrate specificity of human protein arginine methyltransferase 7 (PRMT7): the importance of acidic residues in the double E loop. *J. Biol. Chem.* **289**, 32604–32616
6. Jain, K., Jin, C. Y., and Clarke, S. G. (2017) Epigenetic control via allosteric regulation of mammalian protein arginine methyltransferases. *Proc. Natl. Acad. Sci. U. S. A.* **114**, 10101–10106
7. Held, C., and Sadowski, G. (2016) Thermodynamics of Bioreactions. *Annu. Rev. Chem. Biomol. Eng.* **7**, 395–414
8. Feng, Y., Maity, R., Whitelegge, J. P., Hadjikyriacou, A., Li, Z., Zurita-Lopez, C., Al-Hadid, Q., Clark, A. T., Bedford, M. T., Masson, J. Y., and Clarke, S. G. (2013) Mammalian protein arginine methyltransferase 7 (PRMT7) specifically targets RXR sites in lysine- and arginine-rich regions. *J. Biol. Chem.* **288**, 37010–37025
9. Yao, R., Jiang, H., Ma, Y., Wang, L., Wang, L., Du, J., Hou, P., Gao, Y., Zhao, L., Wang,

G., Zhang, Y., Liu, D.-X., Huang, B., and Lu, J. (2014) PRMT7 induces epithelial-to-mesenchymal transition and promotes metastasis in breast cancer. *Cancer Res.* **74**, 5656–5667

10. Blanc, R. S., Vogel, G., Chen, T., Crist, C., and Richard, S. (2016) PRMT7 preserves satellite cell regenerative capacity. *Cell Rep.* **14**, 1528–1539
11. Ying, Z., Mei, M., Zhang, P., Liu, C., He, H., Gao, F., and Bao, S. (2015) Histone arginine methylation by PRMT7 controls germinal center formation via regulating Bcl6 transcription. *J. Immunol.* **195**, 1538–1547
12. Dhar, S. S., Lee, S.-H., Kan, P.-Y., Voigt, P., Ma, L., Shi, X., Reinberg, D., and Lee, M. G. (2012) Trans-tail regulation of MLL4-catalyzed H3K4 methylation by H4R3 symmetric dimethylation is mediated by a tandem PHD of MLL4. *Genes Dev.* **26**, 2749–2762
13. Blanc, R. S., and Richard, S. (2017) Regenerating muscle with arginine methylation. *Transcription*. 10.1080/21541264.2017.1291083
14. Karkhanis, V., Wang, L., Tae, S., Hu, Y. J., Imbalzano, A. N., and Sif, S. (2012) Protein arginine methyltransferase 7 regulates cellular response to DNA damage by methylating promoter histones H2A and H4 of the polymerase δ catalytic subunit gene, POLD1. *J. Biol. Chem.* **287**, 29801–29814
15. Brown, P. H., Balbo, A., Zhao, H., Ebel, C., and Schuck, P. (2011) Density Contrast Sedimentation Velocity for the Determination of Protein Partial-Specific Volumes. *PLoS One*. **6**, e26221
16. Laue, T. M., Shah, B. D., Ridgeway, T. M., and Pelletier, S. L. (1992) Computer-aided interpretation of analytical sedimentation data for proteins. in *Analytical ultracentrifugation in biochemistry and polymer science*, pp. 90–125, 10.1006/abio.1995.1030
17. Fisk, J. C., Sayegh, J., Zurita-Lopez, C., Menon, S., Presnyak, V., Clarke, S. G., and Read, L. K. (2009) A type III protein arginine methyltransferase from the protozoan parasite Trypanosoma brucei. *J. Biol. Chem.* **284**, 11590–11600

18. Feng, Y., Xie, N., Jin, M., Stahley, M. R., Stivers, J. T., and Zheng, Y. G. (2011) A transient kinetic analysis of PRMT1 catalysis. *Biochemistry*. **50**, 7033–7044

19. Barton, J. S. (1979) Denaturation at the optimum temperature. *Biochem. Educ.* **7**, 13–14

20. Sun, L., Wang, M., Lv, Z., Yang, N., Liu, Y., Bao, S., Gong, W., and Xu, R.-M. (2011) Structural insights into protein arginine symmetric dimethylation by PRMT5. *Proc. Natl. Acad. Sci.* **108**, 20538–20543

21. Pak, M. L., Lakowski, T. M., Thomas, D., Vhuiyan, M. I., Hüsecken, K., and Frankel, A. (2011) A Protein Arginine *N* -Methyltransferase 1 (PRMT1) and 2 Heteromeric Interaction Increases PRMT1 Enzymatic Activity. *Biochemistry*. **50**, 8226–8240

22. Frankel, A., and Clarke, S. (2000) PRMT3 is a distinct member of the protein arginine N-methyltransferase family. Conferral of substrate specificity by a zinc-finger domain. *J. Biol. Chem.* **275**, 32974–32982

23. Schurter, B. T., Koh, S. S., Chen, D., Bunick, G. J., Harp, J. M., Hanson, B. L., Henschen-Edman, A., Mackay, D. R., Stallcup, M. R., and Aswad, D. W. (2001) Methylation of histone H3 by coactivator-associated arginine methyltransferase 1. *Biochemistry*. **40**, 5747–5756

24. Lakowski, T. M., and Frankel, A. (2008) A kinetic study of human protein arginine N-methyltransferase 6 reveals a distributive mechanism. *J. Biol. Chem.* **283**, 10015–10025

25. Hadjikyriacou, A., Yang, Y., Espejo, A., Bedford, M. T., and Clarke, S. G. (2015) Unique features of human protein arginine methyltransferase 9 (PRMT9) and its substrate RNA splicing factor SF3B2. *J. Biol. Chem.* **290**, 16723–16743

26. Dillon, M. B. C., Rust, H. L., Thompson, P. R., and Mowen, K. A. (2013) Automethylation of protein arginine methyltransferase 8 (PRMT8) regulates activity by impeding S-adenosylmethionine sensitivity. *J. Biol. Chem.* **288**, 27872–27880

27. Baldwin, R. M., Haghandish, N., Daneshmand, M., Amin, S., Paris, G., Falls, T. J., Bell, J. C., Islam, S., and Côté, J. (2015) Protein arginine methyltransferase 7 promotes breast cancer cell invasion through the induction of MMP9 expression. *Oncotarget*. **6**, 3013–3032

28. Correia, J. J., and Stafford, W. F. (2015) Sedimentation Velocity. in *Methods in enzymology*. **562**, 49–80

29. Perrin, F. (1934) Mouvement brownien d'un ellipsoide - I. Dispersion diélectrique pour des molécules ellipsoidales. *J. Phys. le Radium*. **5**, 497–511

30. Cura, V., Troffer-Charlier, N., Wurtz, J. M., Bonnefond, L., and Cavarelli, J. (2014) Structural insight into arginine methylation by the mouse protein arginine methyltransferase 7: a zinc finger freezes the mimic of the dimeric state into a single active site. *Acta Crystallogr. D. Biol. Crystallogr.* **70**, 2401–2412

31. Arbing, M. A., Chan, S., Harris, L., Kuo, E., Zhou, T. T., Ahn, C. J., Nguyen, L., He, Q., Lu, J., Menchavez, P. T., Shin, A., Holton, T., Sawaya, M. R., Cascio, D., and Eisenberg, D. (2013) Heterologous Expression of Mycobacterial Esx Complexes in Escherichia coli for Structural Studies Is Facilitated by the Use of Maltose Binding Protein Fusions. *PLoS One*. **8**, e81753

32. Stafford, W. F. (1992) Boundary analysis in sedimentation transport experiments: a procedure for obtaining sedimentation coefficient distributions using the time derivative of the concentration profile. *Anal. Biochem.* **203**, 295–301

Chapter 6

Epigenetic control via allosteric regulation of mammalian protein arginine methyltransferases

The work described in this chapter has been reproduced from:

Kanishk Jain, Cyrus Y. Jin, and Steven G. Clarke. “Epigenetic control via allosteric regulation of mammalian protein arginine methyltransferases.” *Proc. Natl. Acad. Sci. U.S.A*. 2017 Sep 114(38):10101-10106.

ABSTRACT

Arginine methylation on histones is a central player in epigenetics and in gene activation and repression. Protein arginine methyltransferase (PRMT) activity has been implicated in stem cell pluripotency, cancer metastasis, and tumorigenesis. The expression of one of the nine mammalian PRMTs, PRMT5, affects the levels of symmetric dimethylarginine (SDMA) at Arg-3 on histone H4 leading to the repression of genes which are related to disease progression in lymphoma and leukemia. Another PRMT, PRMT7, also affects SDMA levels at the same site in spite of its unique monomethylating activity and the lack of any evidence for PRMT7-catalyzed histone H4 Arg-3 methylation. We present evidence that PRMT7-mediated monomethylation of histone H4 Arg-17 regulates PRMT5 activity at Arg-3 in the same protein. We analyzed the kinetics of PRMT5 over a wide range of substrate concentrations. Significantly, we discovered that PRMT5 displays positive cooperativity *in vitro*, suggesting that this enzyme may be allosterically regulated *in vivo* as well. Most interestingly, monomethylation at Arg-17 in histone H4 not only raised the general activity of PRMT5 with this substrate, but also ameliorated the low activity of PRMT5 at low substrate concentrations. These kinetic studies suggest a biochemical explanation for the interplay between PRMT5 and PRMT7-mediated methylation of the same substrate at different residues and also suggest a general model for regulation of PRMTs. Elucidating the exact relationship between these two enzymes when they methylate two distinct sites of the same substrate may aid in developing therapeutics aimed at reducing PRMT5/7 activity in cancer and other diseases.

SIGNIFICANCE STATEMENT

There is increasing literature that links the overexpression of protein arginine methyltransferases PRMT5 and PRMT7 to cancer metastasis and tumorigenesis and that suggests these enzymes may be good therapeutic targets. An important question remaining is how PRMT7 may control PRMT5 activity in mammalian cells. In this work, we demonstrate that PRMT7-dependent monomethylation at one site in histone H4 can activate another site for methylation by PRMT5. Such allosteric regulation has not been previously seen in this class of protein modification enzymes.

INTRODUCTION

Posttranslational modifications (PTMs) of proteins such as histones and transcription factors have been shown to regulate gene expression and contribute to epigenetic control (1–4). PTMs that occur on histones commonly include methylation marks on lysine and arginine residues. Histone arginine methylation has been recently linked to stem cell pluripotency (5), DNA damage repair (6), and cancer metastasis and tumorigenesis (7–10). As such, the enzymes that catalyze these modifications have become popular targets for therapeutic treatments (11–14).

In mammals, there are nine enzymes in the seven-β-strand family of protein arginine methyltransferase, designated PRMT1 – 9 (3, 4). These PRMTs are further divided into three types based on the different methylarginine derivatives they produce: type I PRMTs (PRMT1-4, 6, and 8) catalyze the production of ω-monomethylarginine (MMA) and asymmetric dimethylarginine (ADMA), type II PRMTs (PRMT5 and 9) catalyze MMA and symmetric dimethylarginine (SDMA) production, and type III enzymes (PRMT7) catalyze only the production of MMA residues (3, 4).

PRMT5, often in complex with methylosome protein 50 (MEP50), is the most prolific type II mammalian PRMT and is responsible for almost all of the SDMA marks in the cell (4, 15–18). Studies of the symmetric dimethylation of arginine-3 in histone H4 indicate that this modification is affected by the expression of PRMT5 (15, 16, 19–21). Since R3 SDMA is a repressive mark, changes in this modification can lead to the loss of tumor suppressor proteins and contribute to proliferative diseases such as lymphoma (8), mixed-lineage leukemia (MLL) (22), and acute myeloid leukemia (AML) (20).

Recently, similar observations of a link between protein arginine symmetric dimethylation of histone H4 at position 3 and a distinct enzyme, PRMT7, have been made (4, 6, 22–26). Initially, PRMT7 was incorrectly identified as an SDMA catalyzing enzyme due to contamination with PRMT5 (3, 10, 27, 28). As such, PRMT7 was reported to symmetrically dimethylate histone H4

at R3 (29, 30). However, since those initial studies, it has been clearly shown that PRMT7 does not catalyze dimethylarginine production and that it is only able to produce MMA (27, 31, 32). The corrected characterization of PRMT7 as a type III PRMT does not explain, however, why PRMT7 expression levels also seem to affect SDMA levels at R3 on histone H4 (4, 6, 22, 24, 26) and R2 on histone H3 (23). One hypothesis suggests that PRMT7 monomethylates substrates for PRMT5 to subsequently symmetrically dimethylate; thus, a depletion of PRMT7 may result in fewer "primed" arginine residues, causing lower PRMT5-mediated SDMA (10). This hypothesis, however, has not been experimentally supported (4, 26). In fact, it has been shown that PRMT7 has distinctly different substrate recognition from PRMT5 and specifically does not methylate R3 on histone H4 *in vitro* (27). Nevertheless, PRMT7 is able to monomethylate arginine-17 and 19 on the same histone H4 N-terminal tail (27). A recent proteomic study documented the presence of monomethylation at R17 on histone H4 in mice testes (33). These observations lend themselves to another hypothesis: monomethylation of R17 and/or R19 by PRMT7 may direct PRMT5 activity on R3 of histone H4.

Kinetic studies on PRMT5 and different forms of histone H4, including peptides with variable numbers of residues and amino acid substitution and modifications, have demonstrated the sensitivity of the enzyme activity to the residues downstream (distal site) of the methylatable R3 site (15). Similar studies have been done with PRMT1 and they generally also demonstrate the importance of residues, and their modifications, downstream from the primary methylation site for PRMT-mediated activity (34–36). For example, lysine acetylation at K5, K8, K12, and K16 on histone H4 significantly effects PRMT1 activity at residue R3 (36). Likewise, a study of *C. elegans* PRMT5 revealed the importance of the chemical properties of residues downstream from R3 for catalytic activity (15), indicating that a second or "distal" site on substrates and enzymes alike might exist as a means for regulation of methylation activity. Interestingly, with one recent exception (37), none of these studies reported effects of distal substrate recognition sites on the type of kinetics displayed by PRMT5 and PRMT1 such as allostery (cooperativity). The

experiments in our current study, however, demonstrate not only the allosteric nature of PRMT5 and PRMT1, key regulators of gene transcription, but also that downstream methylation of histone H4 (R17MMA) can significantly affect the methylation by PRMT5 of R3, an important gene repression marker, on the same protein.

RESULTS

Histone H4 monomethylation at R17 affects methylation of R3 by *Hs*PRMT5/MEP50

Symmetric dimethylation of histone H4 residue R3 in mammals has been reported to be affected by the expression levels of PRMT7 (4, 6, 22–26). However, *in vitro* assays of PRMT7 show that it monomethylates residues R17 and R19 in histone H4 and does not modify R3 (27, 31). Methylation of R17 and R19 in histone H4 from intact cells has not been observed with the exception of monomethylation at R17 in one proteomic study of mouse testes (33). To resolve this apparent paradox, we investigated the effect of the methylation state of histone H4 R17 in an N-terminal peptide (H4 (1-21)) on the activity of *Hs*PRMT5/MEP50. Cation exchange chromatography on the acid hydrolysates of the methylation products of reactions with *Hs*PRMT5/MEP50 and the H4 (1-21) peptide, tested either with unmodified sequence (WT) or with R17 monomethylated (R17MMA) (Fig. 1), was performed. When the R17MMA peptide was used as a substrate, we found significantly higher MMA (~2-fold increase) and SDMA production (~3-fold increase) than with the unmodified peptide (Fig. 1A-C). Additionally, the ratio of SDMA to MMA was also significantly higher with the R17MMA peptide (Fig. 1D). These results suggest that the methylation state of a distal residue can markedly affect the activity of PRMT5 on this peptide.

*Hs*PRMT5/MEP50 methylation displays positive cooperativity

To confirm that R3 and not R17/R19 is the site of methylation carried out by *Hs*PRMT5/MEP50, we demonstrated that no methylation by this enzyme was observed with the R3K modified H4 (1-21) peptide (Fig. 2A). We then determined the kinetic parameters of *Hs*PRMT5/MEP50 with the cofactor AdoMet and the substrate H4 (1-21), finding that this enzyme showed typical Michaelis-Menten kinetics as a function of AdoMet concentration with a K_M of 1.66 ± 0.37 μM (Fig. S1A and Table S1), a value that is consistent with previous measurements (15, 21). However, a different result was found when the peptide substrate concentration was varied. Importantly, these kinetic data revealed that *Hs*PRMT5/MEP50 does not follow simple Michaelis-

Menten kinetics but appears to show positive cooperativity with the H4 (1-21) WT substrate and a Hill coefficient (n) $>$ 1 (Fig. 2A and B). Cooperativity has not been observed for PRMT5 in previous studies. These findings suggest a possible allosteric mechanism for the regulation of PRMT5 via binding of second site arginine residues. The kinetic data best fits the Hill equation (38) for positive cooperativity, with k_{cat}, $K_{0.5}$, $k_{cat}/K_{0.5}$, and Hill coefficients shown in Table 1. We note that the k_{cat} of the human enzyme measured here is about 10-fold lower than that of the *C. elegans* enzyme (15), though its $k_{cat}/K_{0.5}$ is about 3-fold greater.

Monomethylation of histone H4 R17 has significant effects on the kinetics of *Hs*PRMT5 and its allosteric enzymatic activity

Having observed the increase in methylation of H4 (1-21) in the presence of MMA at position R17 (Fig. 1) and the cooperative nature of PRMT5 with the unmodified H4 (1-21) peptide (Fig. 2), we then tested the effect of monomethylation at position R17 on the activity of *Hs*PRMT5/MEP50. We were able to determine kinetic parameters and characterize the activity of *Hs*PRMT5/MEP50 as a function of R17 methylation (Fig. 2; Table 1). When presented with the H4 (1-21) peptide synthetically monomethylated at position 17 (H4 (1-21) R17MMA), *Hs*PRMT5/MEP50 exhibits about a two-fold increase in maximal activity relative to the WT peptide and a much larger— five-fold or more — increase in activity at substrate concentrations below 0.5 μM (Fig. 2 brown v. blue; Table 1), consistent with the data from the cation exchange experiments (Fig. 1). This methyltransferase also shows positive cooperativity with the modified H4 (1-21) peptides described below (Fig. S2A and B; Table 1).

Given the positive cooperativity of PRMT5 with H4 (1-21) (Fig. 2), we characterized the kinetics of this enzyme with the R17MMA modification and either alanine or lysine substitutions at positions R17 and R19 on H4 (1-21) (Fig. S2A-B). To determine significant differences in kinetic parameters with the H4 (1-21) peptides used, we compared the value of each parameter relative to the WT peptide value (Fig. 2C-E). There was a significant decrease in $K_{0.5}$ relative to

WT when H4 (1-21) R17MMA was used, indicating an increase in binding affinity (Fig. 2A-C; Table 1); a similar effect was seen for the R17A derivative (Fig. 2C). The R19A peptide exhibited a significant decrease in binding affinity while the other peptides did not have a significant effect on the $K_{0.5}$. Enzymatic activity, k_{cat}, appeared to vary significantly for most of the H4 (1-21) derivatives relative to WT; notably, the R17MMA peptide had the highest activity at 2.31 ± 0.20 hr^{-1} and a *p*-value of 0.0001 (Fig. 2D; Table 1). The statistical analysis of Hill coefficients revealed that PRMT5 had maximal cooperativity with H4 (1-21) WT with an n value of nearly 3. On the other hand, the Hill coefficient for the R17MMA peptide was significantly lower (about 1.3), indicating that the PRMT5 exhibited mostly non-cooperative (Michaelis-Menten) kinetics with this peptide (Table 1).

***Hs*PRMT1 also exhibits positive cooperativity**

To see if the results observed with PRMT5 were unique for that enzyme, kinetics experiments were conducted with *Hs*PRMT1, an enzyme that also targets R3 on histone H4 for ADMA formation (4, 39, 40), and the various H4 (1-21) peptides. Significantly, we also observed positive cooperativity with this enzyme (Fig. 3). A comparison of PRMT1 kinetics with the WT H4 peptide and the R3K derivative shows similar results as with PRMT5; PRMT1 only methylates residue R3 on the H4 (1-21) peptide (Fig. 3). *Hs*PRMT1 also exhibits about a two-fold increase in overall activity relative to the wild-type peptide with H4 (1-21) R17MMA as a substrate (Fig. 3 and Table 1), though there is no apparent increase in activity at the low substrate concentrations, unlike PRMT5. Again, as with PRMT5, PRMT1 showed positive cooperativity with H4 (1-21) WT (Fig. 3E and Table 1). While PRMT1 did display similar kinetics to PRMT5 with histone H4 (1-21) WT, the difference between the degree of cooperativity for the R17MMA and WT peptide was greater for PRMT5 than for PRMT1 (Fig. 2E and 3E; Table 1). In fact, none of the modified H4 peptides had a significant effect on PRMT1 cooperativity; this indicates that the R17MMA modification may more selectively affect PRMT5 kinetics than those for PRMT1. Experiments to assess kinetic parameters of PRMT1 with AdoMet as the varying substrate gave similar results

as seen with PRMT5; no cooperativity was observed (Fig. S1B and Table S1). The results of these kinetic studies indicate PRMT1 to be an allosteric enzyme as well, whose activity can be modulated by binding downstream residues, albeit to a more minor degree than PRMT5.

DISCUSSION

As the molecular mechanisms of PRMT5 and PRMT7 have become clearer and their impact on the biological landscape of disease more pronounced, the need to understand how these enzymes engage in crosstalk has become more important. Several studies have already demonstrated that PRMT7 expression levels influence the amount of PRMT5-catalyzed methylation of histone H4 R3 (4, 6, 22–26). Both of these enzymes are involved in major biological functions such as DNA damage repair and cellular proliferation as well as being dysregulated in diseases such as cancer (7–9). With the knowledge that PRMT7 prefers to methylate histone H4 downstream from position R3 (27) and that chemical changes in such regions—distal sites—can, in general, affect PRMT activity (15, 34–36), we set out to determine if there was a link between PRMT5- and PRMT7-mediated methylation of different residues on the same protein.

With the exception of on recent study of PRMT1 (37), previous studies have not reported PRMT5 and PRMT1 to behave in a cooperative fashion (15, 16, 21, 34–36). Our experiments, however, not only show that PRMT5 and PRMT1 each demonstrate positive cooperativity when methylating one of their endogenous substrates, but that the allosteric activity of PRMT5—very low enzyme activity at lower substrate concentrations—is alleviated when R17 on the same peptide substrate is monomethylated (Fig. 2B and E; Table 1). For both enzymes, we found that the degree of cooperativity, as well as the level of activity, is affected by the chemical make-up of residues R17 and 19 on the histone H4 peptide. Intriguingly, monomethylation of R17 in histone H4 had the largest effect on the activity of PRMT5 at low substrate concentrations (Fig. 2). Given the fact that both PRMT1 and PRMT5 are highly active and promiscuous enzymes, there has been surprisingly little uncovered about how their activity is regulated. Allosteric dependence on “distal sites” of methylation substrates may help highlight a mode of regulation through which the activity of PRMT5 and PRMT1 activity is modulated.

We know from our previous work that PRMT7 does not methylate R3 on histone H4 and instead catalyzes MMA production on R17 and/or R19 (27). Recent literature, however, links changes in SDMA levels at R3 on histone H4 with expression of PRMT7 (4, 6, 22–26), suggesting that this enzyme may be responsible for aiding PRMT5-mediated methylation at this residue. We thus propose that methylation of R17 by PRMT7 may be responsible for the indirect activation of PRMT5-mediated methylation of R3 on histone H4 in mammals (Fig. 4). Because R17MMA appears to be an allosteric regulator of PRMT5 activity, it is possible that this methylated residue binds to PRMT5 at an allosteric site, causing conformational changes in the enzyme which increase its activity towards its native substrate, residue R3. In fact, similar binding phenomena have previously been suggested (35) for PRMT1, though not in the context of allosteric regulation.

By looking at the electrostatic potentials for PRMT5 and PRMT1 structures, it may be possible to identify potential allosteric binding regions (Fig. S3 and S4, respectively). The sequence around histone H4 R17 contains basic residues, so allosteric binding sites on the enzyme would ideally be negatively charged. It is interesting, therefore, that PRMT5 appears to have a negatively charged cavity on the face opposite to its active site (solid black enclosure in Fig. S3A) and on part of the post-methyltransferase domain β-barrel (dashed black enclosure in Fig. S3B); none such regions appear on the same face as the active site (Fig. S3). The large negatively charged furrow illustrated in Fig. S3B is unlikely to be potential allosteric binding site because the ~ 70 Å distance from the active site greater that the ~ 50 Å distance from R3 to R17 in the most extended conformation. PRMT1's structure also reveals similar allosteric sites at negatively charged regions after its methyltransferase domain (dashed black enclosures in Fig. S4A). However, due to its simpler oligomeric structure, PRMT1 may have more surface area accessible, making other allosteric sites possible as well (Fig. S4B).

Although both PRMT5 and PRMT1 exhibit positive cooperativity in the presence of the unmodified histone H4 (1-21) peptide, it is unclear whether this occurs in a symmetrical/concerted fashion, as theorized by the Monod-Wyman-Changeux (MWC) model (41), or in a sequential

manner, as theorized by the Koshland-Nemethy-Filmer (KNF) model (42). However, our data suggests that when residue R17 is monomethylated, there is likely to be an altered conformation of PRMT5 which results not only in higher affinity binding of the substrate, but also higher maximal velocity. Further structural studies must be undertaken to determine where in the methyltransferase such allosteric sites are and the nature of the different conformational states.

Until recently, PRMTs were thought to behave like canonical Michaelis-Menten enzymes (15, 21, 34–36), but our work has shown that at least PRMT1 and PRMT5 can catalyze methylation via positive cooperativity. As these enzymes are key players in controlling gene transcription, it is logical to assume that there are mechanisms to regulate their activity. Furthermore, the PRMTs' role in disease-related processes such as cancer metastasis and tumorigenesis has been established. Recently there has been considerable work in the development of small molecular inhibitors of these enzymes (11, 43). Regulation of methyltransferase activity by crosstalk with other modifications has been seen in a number of other systems (22, 44–46), such as in the interactions between methylation on histone H3 K27 and K36 by PRC2 and Setd2/Ash1 respectively. Specifically, our studies show how positive cooperativity can play an integral part in crosstalk between PRMTs. With this new understanding of PRMT behavior and regulation, it may be possible to generate new and more selective types of drugs which target a previously unexplored facet of arginine methyltransferases—their allosteric kinetics.

METHODS

Peptide substrates

H4 (1-21) WT and R17MMA peptides were purchased as trifluoroacetic acid (TFA) salts from GenScript Inc. at >95% purity by HPLC. Histone H4 (1-21) R17A/K and R19A/K peptides were generous gifts from Dr. Paul Thompson (University of Massachusetts Medical School, Worcester, MA). All of the peptide masses were confirmed by MALDI-TOF mass spectrometry (Table S1).

Protein expression and purification

His-tagged human PRMT1 (*Hs*PRMT1) was obtained in a pET28b plasmid from Dr. Paul Thompson (University of Massachusetts Medical School, Worcester, MA) and was expressed and purified as previously described (47). Human PRMT5/MEP50 (*Hs*PRMT5/MEP50) complex protein was purchased from BioSciences as recombinantly co-expressed and purified proteins in HEK293T cells (0.65 mg/mL, BPS Biosciences 51045, Lot 150126).

Phosphocellulose-81 paper kinetics assay

Methylation reactions were performed with 2.45 nM *Hs*PRMT5/MEP50 (calculated as the tetramer complex) or 10 nM PRMT1 (calculated as the dimer) buffered with 50 mM HEPES (pH 8.0), 10 mM NaCl, and 1 mM DTT containing 20 μM of a 20:1 molar ratio of *S*-adenosyl-L-methionine *p*-toluenesulfonate salt (AdoMet) (Sigma A2408; ≥ 80% purity) to *S*-adenosyl-L-[*methyl*-^{3}H]-methionine ([*methyl*-^{3}H]-AdoMet) (PerkinElmer Life Sciences; stock solution of 7 μM (78.2 Ci/mmol) in 10 mM H_2SO_4/EtOH (9:1, v/v)) as a methyl donor. A H4 (1-21) peptide substrate concentration range of 0.05-2 μM was used in each reaction with PRMT5 and a concentration range of 0.05-5 μM for PRMT1 reactions. When determining the kinetic parameters for the enzymes with AdoMet as the varying substrate, a range of 0-3 μM AdoMet (20:1 molar ratio of AdoMet to [*methyl*-^{3}H]-AdoMet) and 10 μM H4 (1-21) WT were used. The reaction volume was brought up to 30 μL with deionized water. Reactions were incubated for 1 h for *Hs*PRMT5/MEP50

and 1.5 h for *Hs*PRMT1 at 37°C, and then quenched with 0.5 µL 100 % (v/v) TFA. Each reaction was run in triplicate.

25 µL of the reaction products were spotted onto 1.5 cm x 1.5 cm P81 phosphocellulose ion exchange filter paper (Reaction Biology Corp IEP-01, Malvern, PA) and air dried for 30 min. The papers were subsequently washed in 1 L of 50 mM $NaHCO_3$ at pH 9.0 for 45 min. The papers were placed in scintillation vials and allowed to further air dry for 45 minutes. Radioactivity was counted with 5 mL of Safety-Solve scintillation mixture (Research Products International, 111177) for three cycles of 5 minutes using a Beckman LS6500 instrument.

Amino acid analysis of protein and peptide substrates

In vitro methylation assays with 12.3 nM *Hs*PRMT5/MEP50 tetramer, 10 µM H4 (1-21) peptide (WT and R17MMA), and 0.7 µM of [*methyl*-^{3}H]-AdoMet were carried out in 50 mM K-HEPES (pH 8.0), 10 mM NaCl, 1 mM DTT, and 5% glycerol at 37 °C for 2 h. Reactions were quenched with 0.5 µL 100% TFA and peptides were purified via RP-HPLC and acid hydrolyzed as described previously (47, 48). Acid hydrolysates were also analyzed through cation exchange chromatography as previously described (47, 48).

Statistical analysis

All error bars indicate the standard deviation of triplicate measurements. Data was analyzed using the GraphPad Prism 6.0 software. The one-way ANOVA test was used to compare kinetic parameters with a Dunnett test for multiple comparisons (49). A two-tailed t-test was used to compare MMA and SDMA levels from cation exchange chromatography.

ACKNOWLEDGEMENTS

We thank Paul Thompson (UMass Medical School) for providing the $H4^{1-21}$ R17A/K, R19A/K, and R17/19A/K peptides and the human His-PRMT1 plasmid. We also thank Jon Lowenson for thoughtful discussions and critique of the manuscript and Duilio Cascio for aiding in generating electrostatic potential maps (UCLA). This work was supported by grants from the NIH, including Grant GM026020 (to S.G.C.), Ruth L. Kirschstein National Service Award GM007185 (to K.J), and a Faculty Research Grant from the UCLA Academic Senate (to S.G.C.), and a Zymo Summer Research Scholarship (C.Y.J).

TABLES AND FIGURES

Table 1.

Initial Kinetic Parameters

Substrate	*Hs*PRMT5/MEP50				*Hs*PRMT1			
	$K_{0.5}$ (μM)	k_{cat} (hr^{-1})	$k_{cat}/K_{0.5}$ (hr^{-1} μM^{-1})	n (Hill coefficient)	$K_{0.5}$ (μM)	k_{cat} (hr^{-1})	$k_{cat}/K_{0.5}$ (hr^{-1} μM^{-1})	n (Hill coefficient)
H4 (1-21) WT[a]	0.39 ± 0.033	5.63 ± 0.36	14.44	2.83 ± 0.66	0.58 ± 0.083	4.90 ± 0.34	8.45	1.54 ± 0.29
H4 (1-21) R17A[a]	0.11 ± 0.015	6.80 ± 0.34	61.82	1.17 ± 0.18	1.22 ± 0.26	3.11 ± 0.37	2.55	1.85 ± 0.44
H4 (1-21) R17K[a]	0.48 ± 0.048	2.72 ± 0.26	5.67	3.87 ± 1.45	0.50 ± 0.048	3.26 ± 0.18	6.52	2.46 ± 0.56
H4 (1-21) R17MMA[a]	0.13 ± 0.029	9.25 ± 0.79	71.15	1.3 ± 0.33	0.38 ± 0.040	7.85 ± 0.39	20.66	1.98 ± 0.40
H4 (1-21) R19A[a]	0.49 ± 0.065	3.28 ± 0.41	6.69	3.86 ± 1.87	1.34 ± 0.29	4.25 ± 0.53	3.17	1.73 ± 0.37
H4 (1-21) R19K[a]	0.30 ± 0.034	7.02 ± 0.57	23.4	4.90 ± 2.28	0.95 ± 0.15	4.53 ± 0.35	4.77	1.43 ± 0.21
H4 (1-21) R3K[a]	nd[b]	nd[b]	nd[b]	nd[b]	nd[b]	nd[b]	nd[b]	nd[b]

[a] 20 μM AdoMet used (20:1 molar ratio of AdoMet: [*methyl*-^{3}H]-AdoMet)

[b] amount of product formation was too low to accurately measure kinetic parameters

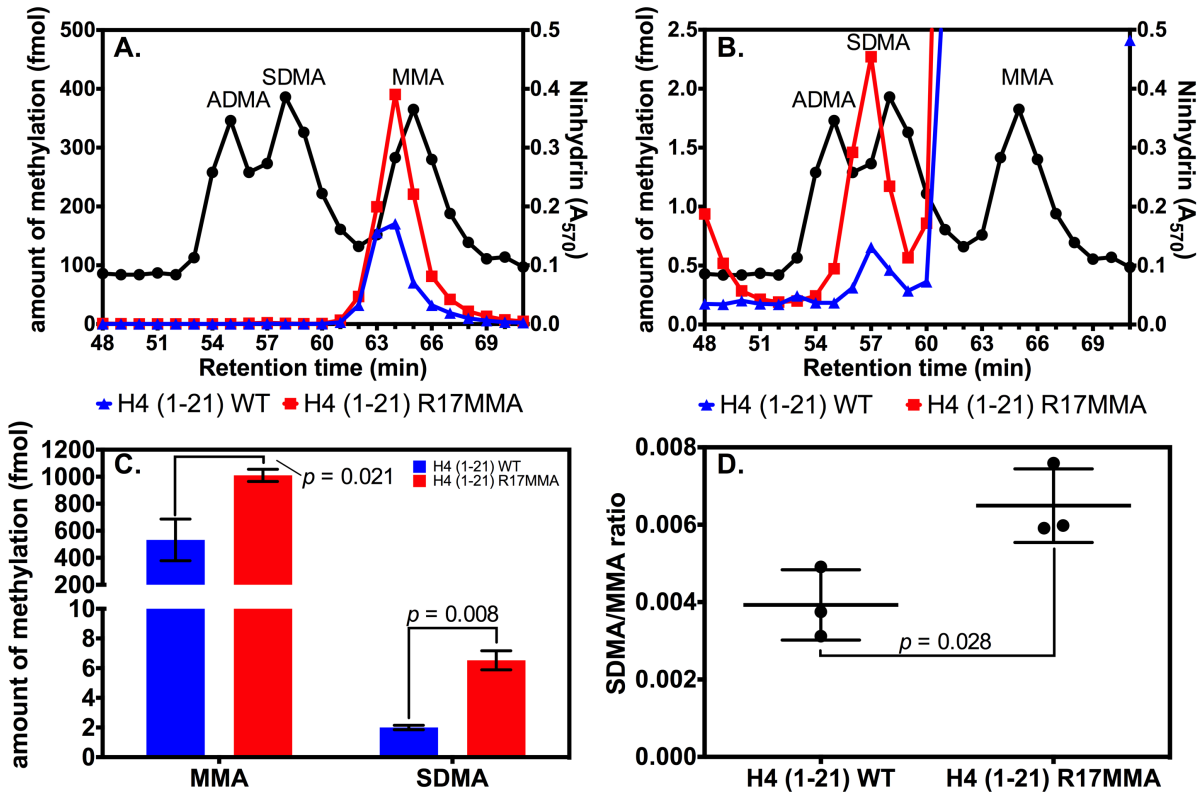

Figure 1. Analysis of methylarginine production by *Hs*PRMT5/MEP50 on histone H4 (1-21) peptide. (A) A representative cation exchange chromatogram (n = 3) for hydrolysates of reactions with H4 (1-21) WT (blue) and H4 (1-21) R17MMA (red) as substrates with [*methyl*-^{3}H]-AdoMet. Fractions (one minute) were collected and analyzed for the presence of non-radioactive methylarginine standards and radioactivity. The black line indicates the retention profile of the standards as determined by ninhydrin assays (47, 48). The colored lines represent radioactive methylarginine derivatives which elute about one minute before the non-radioactive standards due to the isotope effect (50). For details of the reaction and chromatography conditions, see "Methods". (B) An expanded view of panel A to emphasize the differences in SDMA levels. (C) Data from three replicate experiments were used to show changes in ^{3}H-MMA and ^{3}H-SDMA produced with H4 (1-21) WT (blue bars) or its R17MMA derivative (red bars); the *p*-values were determined through two-tailed t-tests. The error bars represent standard deviations. (D) The

SDMA/MMA ratio was calculated from the data in panel C. The *p*-value was determined as for panel C and the error bars represent standard deviations.

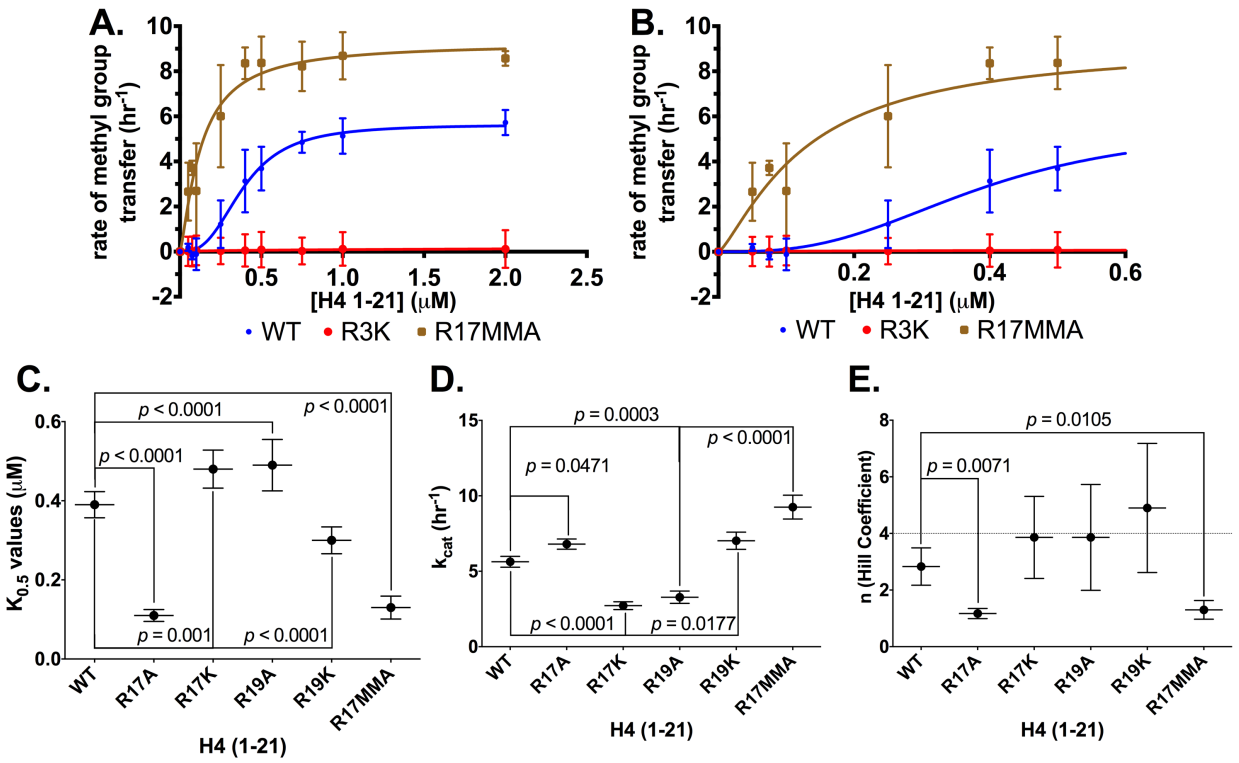

Figure 2. Monomethylation of H4 R17 affects the positive cooperativity exhibited by *Hs*PRMT5/MEP50. Initial kinetic measurements were made and the data was fit to the Hill equation (38). (A) Enzyme activity of *Hs*PRMT5/MEP50 with H4 (1-21) WT (blue), H4 (1-21) R17MMA (brown), and H4 (1-21) R3K (black) is shown for triplicate assays (error bars represent standard deviation). (B) An expanded view of panel A at the low substrate concentrations. Best fit curves are shown for $K_{0.5}$, k_{cat}, and Hill coefficient values for the H4 (1-21) WT substrate of 0.39 μM, 5.63 h^{-1}, and 2.83 respectively. For H4 (1-21) R17MMA, the parameters were 0.13 μM, 9.25 h^{-1}, and 1.3 respectively. For details about reaction conditions and concentrations, see "Methods." (C) statistical analysis of $K_{0.5}$ values, (D) statistical analysis of k_{cat} values, (E) statistical analysis of the Hill coefficient values. The dashed line represents a Hill coefficient of 4. Data was taken from the triplicate assays shown in Fig. 2A and B; error bars represent standard deviation. The *p*-values were calculated using a one-way ANOVA test with a Dunnett test for multiple comparisons using the GraphPad Prism 6.0 software.

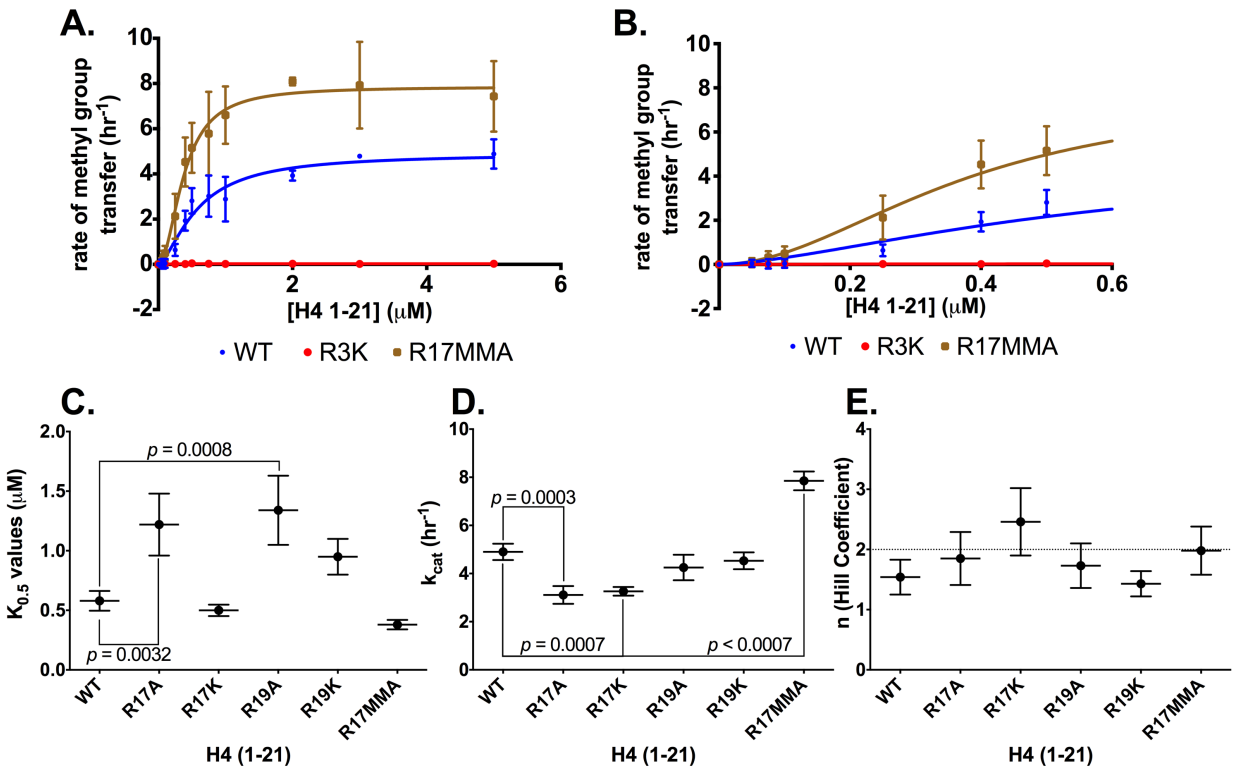

Figure 3. *Hs*PRMT1 exhibits positive cooperativity. Initial kinetic measurements were made and the data was fit to the Hill equation (38). (A) Enzyme activity of *Hs*PRMT1 with H4 (1-21) WT (blue), H4 (1-21) R17MMA (brown), and H4 (1-21) R3K (black) is shown for triplicate assays (error bars represent standard deviation). (B) An expanded view of panel A at the low substrate concentrations. Best fit curves are shown for $K_{0.5}$, k_{cat}, and Hill coefficient values for the H4 (1-21) WT substrate of 0.58 μM, 4.90 h^{-1}, and 1.54 respectively. For H4 (1-21) R17MMA, the parameters were 0.38 μM, 7.85 h^{-1}, and 1.98 respectively. For details about reaction conditions and concentrations, see "Methods." (C) statistical analysis of $K_{0.5}$ values, (D) statistical analysis of k_{cat} values, (E) statistical analysis of the Hill coefficient values. The dashed line represents a Hill coefficient of 2. Data was taken from the triplicate assays shown in Fig. 3A and B; error bars represent standard deviation. The *p*-values were calculated using a one-way ANOVA test with a Dunnett test for multiple comparisons using the GraphPad Prism 6.0 software.

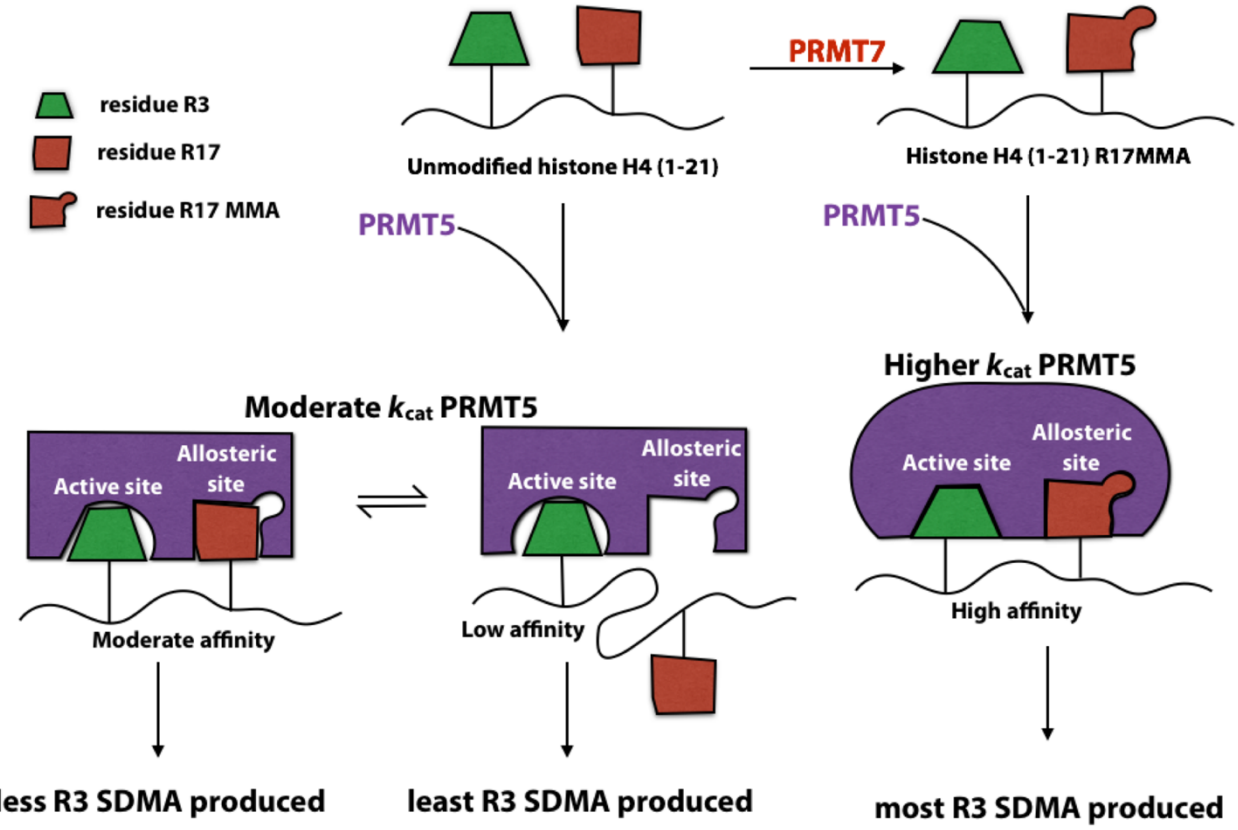

Figure 4. Model for allosteric regulation of PRMT5/MEP50 activity by PRMT7. The green blocks represent residue R3 on histone H4 (1-21), while the red blocks represent residue R17. PRMT5/MEP50 is shown in purple.

SUPPORTING INFORMATION

Table S1.

Histone Peptide Derivatives

Peptide	Sequence	Expected Mass (Da)	Observed Mass (Da)[a]
H4 (1-21) WT	Ac-SGRGKGGKGLGKGGAKRHRKV	2,133	2,133
H4 (1-21) R17A	Ac-SGRGKGGKGLGKGGAK**A**HRKV	2,048	2,049
H4 (1-21) R17K	Ac-SGRGKGGKGLGKGGAK**R**HRKV	2,105	2,106
H4 (1-21) R17MMA	Ac-SGRGKGGKGLGKGGAK**R(me)**HRKV	2,147	2,148
H4 (1-21) R19A	Ac-SGRGKGGKGLGKGGAKRH**A**KV	2,048	2,049
H4 (1-21) R19K	Ac-SGRGKGGKGLGKGGAKRH**K**KV	2,105	2,106
H4 (1-21) R3K	Ac-SG**K**GKGGKGLGKGGAKRHRKV	2,105	2,106

[a] Data from MALDI-TOF analysis show monoisotopic M + 1 values; bold residues indicate the modified positions in each peptide

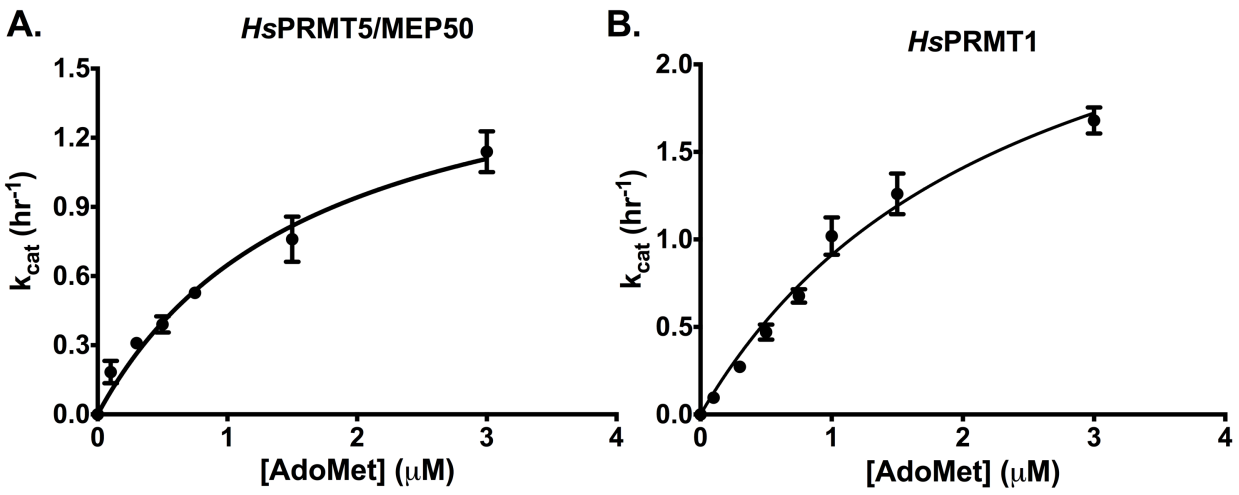

Figure S1. Binding affinity of AdoMet with *Hs*PRMT5/MEP50 and *Hs*PRMT1. Initial kinetic measurements were made and the data was fit to the Michaelis-Menten equation. (A) Enzyme activity of *Hs*PRMT5/MEP50 with varying [AdoMet] and 10 μM H4 (1-21) WT peptide in triplicate (error bars represent standard deviation). The solid line was best fit to the Michaelis-Menten equation with the following parameters: a K_M of 1.66 μM and a k_{cat} of 1.72 h^{-1}. (B) Enzyme activity of *Hs*PRMT1 with varying [AdoMet] and 10 μM H4 (1-21) WT peptide in triplicate (error bars represent standard deviation). The solid line was best fit to the Michaelis-Menten equation with the following parameters: a K_M of 2.41 μM and a k_{cat} of 3.11 h-1. For details about reaction conditions and concentrations, see "Methods."

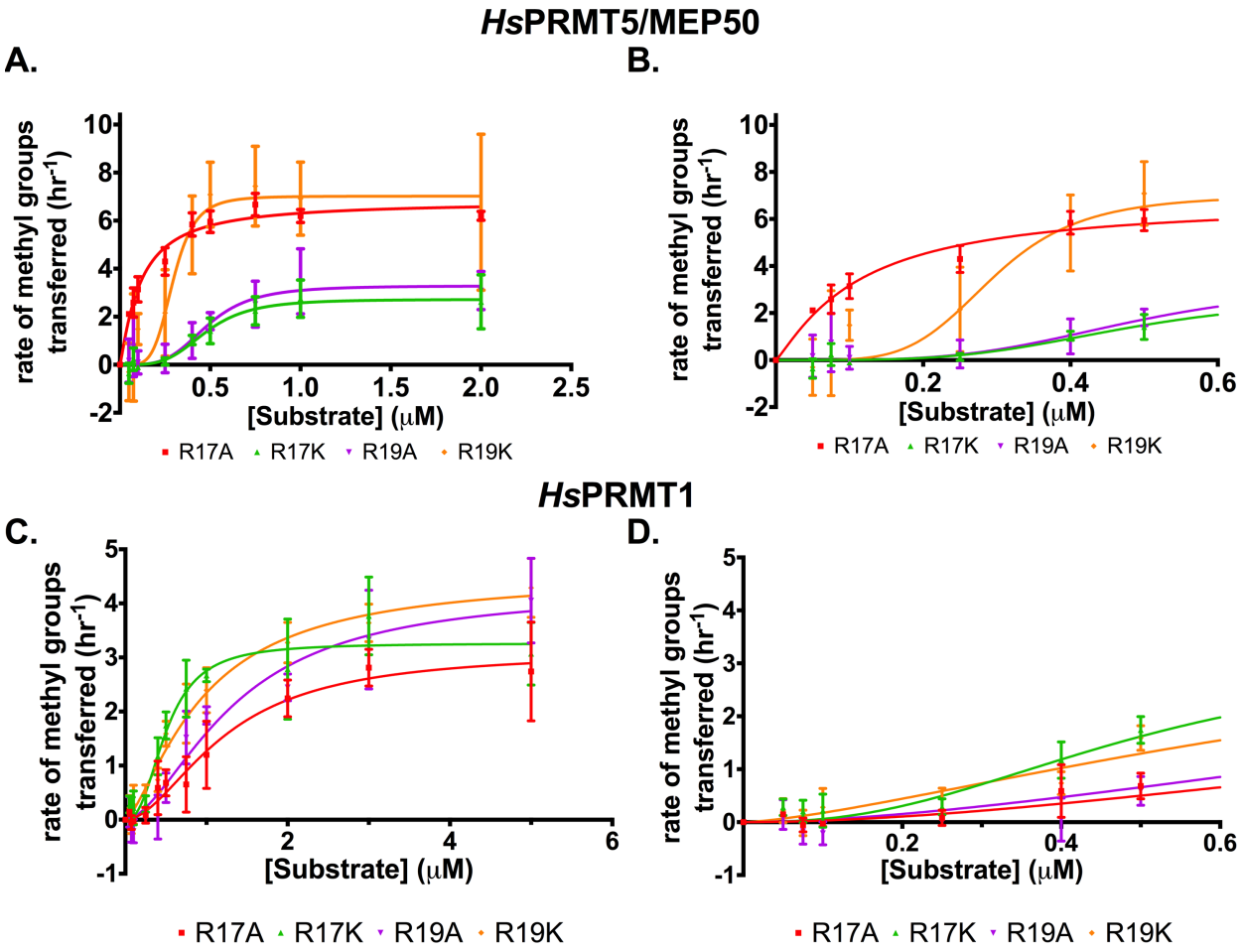

Figure S2. *Hs*PRMT5/MEP50 and *Hs*PRMT1 exhibit positive cooperativity as a function of modifications on the substrate H4 peptide. Initial kinetic measurements were made and the data was fit to the Hill equation (37). (A) Enzyme activity of *Hs*PRMT5/MEP50 with H4 (1-21) R17A (red), H4 (1-21) R17K (green), H4 (1-21) R19A (purple), and H4 (1-21) R19K (orange) in triplicate assays (error bars represent standard deviation). (B) A close-up of the graph from panel A to make differences at low [substrate] clearer. (C) Enzyme activity of *Hs*PRMT1 with H4 (1-21) R17A (red), H4 (1-21) R17K (green), H4 (1-21) R19A (purple), and H4 (1-21) R19K (orange) in triplicate assays (error bars represent standard deviation). (D) A close-up of the graph from panel C to make differences at low [substrate] clearer. For details about reaction conditions and concentrations, see "Methods."

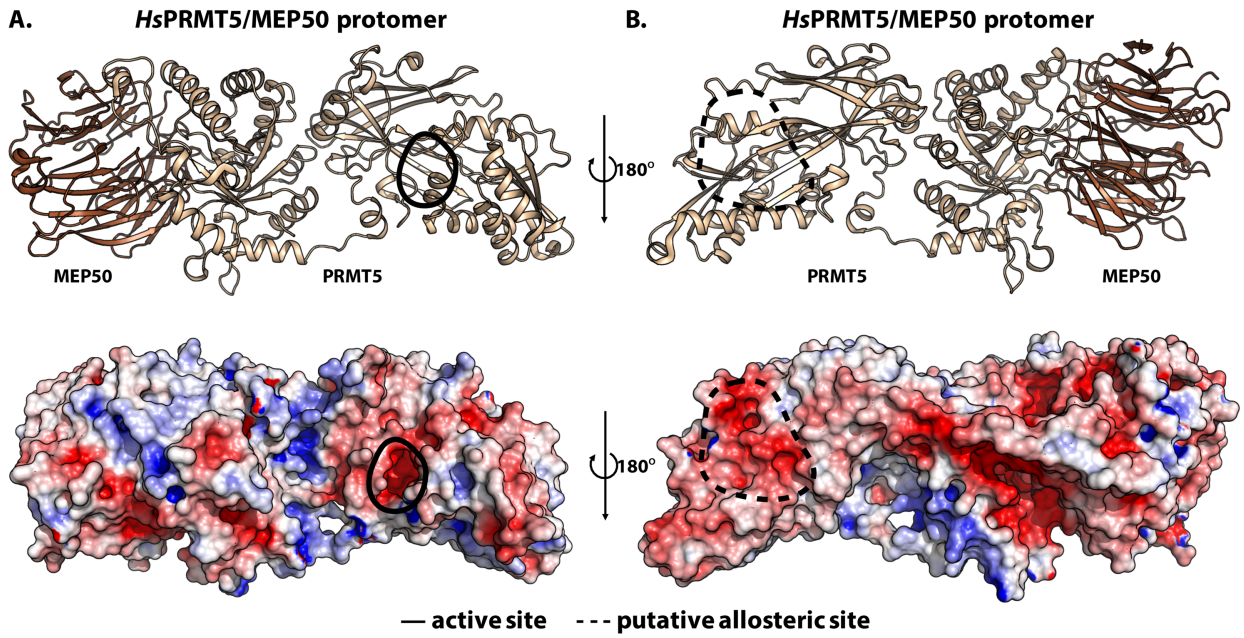

Figure S3. Electrostatic potential map of *Hs*PRMT5/MEP50 protomer reveals potential allosteric sites. A. The protomer of *Hs*PRMT5/MEP50 (PDB ID: 4GQB) is shown; the beige subunit represents PRMT5, while the brown subunit represents MEP50. The active is highlighted by a solid black enclosure. B. Dashed black enclosures on the opposite face of the structure in panel A indicate negatively charged cavities as potential allosteric binding sites on the electrostatic potential map, generated using APBS in PyMOL (red to blue corresponds to -5 kT/e to 5 kT/e).

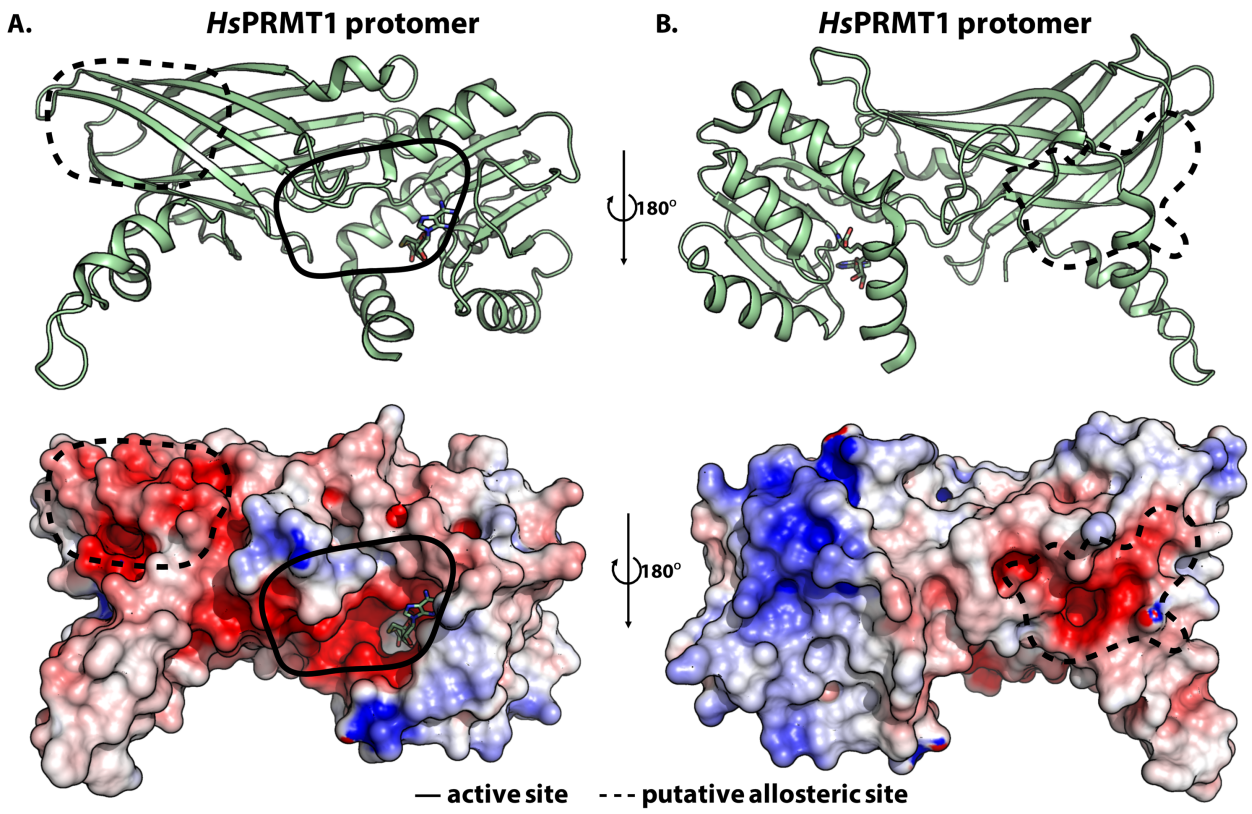

Figure S4. Electrostatic potential map of *Hs*PRMT1 homodimer reveals potential allosteric sites. The protomer of *Hs*PRMT1 (PDB ID: 1ORI) is shown. A. The cartoon representation and electrostatic map for the PRMT1 dimer with the active site (solid black enclosure) facing forward; the dashed black enclosure indicates a negatively charged cavity as potential allosteric binding site on the electrostatic potential map. B. A 180° rotation of the molecules in panel A about the y-axis shows an additional putative allosteric site. Electrostatic potentials were generated using APBS in PyMOL (red to blue corresponds to -5 kT/e to 5 kT/e).

REFERENCES

1. Walsh G, Jefferis R (2006) Post-translational modifications in the context of therapeutic proteins. *Nat Biotechnol* 24(10):1241–12452.
2. Fuhrmann J, Clancy KW, Thompson PR (2015) Chemical biology of protein arginine modifications in epigenetic regulation. *Chem Rev* 115(11):5413–5461.
3. Bedford MT, Clarke SG (2009) Protein arginine methylation in mammals: who, what, and why. *Mol Cell* 33(1):1–13.
4. Blanc RS, Richard S (2017) Arginine methylation: the coming of age. *Mol Cell* 65(1):8–24.
5. Wang Y-C, Peterson SE, Loring JF (2014) Protein post-translational modifications and regulation of pluripotency in human stem cells. *Cell Res* 24(2):143–160.
6. Karkhanis V, et al. (2012) Protein arginine methyltransferase 7 regulates cellular response to DNA damage by methylating promoter histones H2A and H4 of the polymerase δ catalytic subunit gene, POLD1. *J Biol Chem* 287(35):29801–29814.
7. Baldwin RM, et al. (2015) Protein arginine methyltransferase 7 promotes breast cancer cell invasion through the induction of MMP9 expression. *Oncotarget* 6(5):3013–3032.
8. Koh CM, et al. (2015) MYC regulates the core pre-mRNA splicing machinery as an essential step in lymphomagenesis. *Nature* 523(7558):96–100.
9. Hu D, et al. (2015) Interplay between arginine methylation and ubiquitylation regulates KLF4-mediated genome stability and carcinogenesis. *Nat Commun* 6:8419.
10. Yang Y, Bedford MT (2013) Protein arginine methyltransferases and cancer. *Nat Rev Cancer* 13(1):37–50.
11. Ferreira de Freitas R, et al. (2016) Discovery of a potent class I protein arginine methyltransferase fragment inhibitor. *J Med Chem* 59(3):1176–11783.
12. Eram MS, et al. (2016) A Potent, Selective, and Cell-Active Inhibitor of Human Type I Protein Arginine Methyltransferases. *ACS Chem Biol* 11(3):772–781.
13. Kaniskan HÜ, et al. (2015) A potent, selective and cell-active allosteric inhibitor of protein

arginine methyltransferase 3 (PRMT3). *Angew Chemie Int Ed* 54(17):5166–5170.

14. Chan-Penebre E, et al. (2015) A selective inhibitor of PRMT5 with in vivo and in vitro potency in MCL models. *Nat Chem Biol* 11(6):432–437.
15. Wang M, Xu R-M, Thompson PR (2013) Substrate specificity, processivity, and kinetic mechanism of protein arginine methyltransferase 5. *Biochemistry* 52(32):5430–5440.
16. Antonysamy S, et al. (2012) Crystal structure of the human PRMT5:MEP50 complex. *Proc Natl Acad Sci* 109(44):17960–17965.
17. Antonysamy S (2017) The structure and function of the PRMT5:MEP50 complex. *Sub-Cellular Biochemistry*, pp 185–194.
18. Yang Y, et al. (2015) PRMT9 is a type II methyltransferase that methylates the splicing factor SAP145. *Nat Commun* 6:6428.
19. Ho MC, et al. (2013) Structure of the arginine methyltransferase PRMT5-MEP50 reveals a mechanism for substrate specificity. *PLoS One* 8. doi:10.1371/journal.pone.0057008.
20. Tarighat SS, et al. (2016) The dual epigenetic role of PRMT5 in acute myeloid leukemia: gene activation and repression via histone arginine methylation. *Leukemia* 30(4):789–799.
21. Sun L, et al. (2011) Structural insights into protein arginine symmetric dimethylation by PRMT5. *Proc Natl Acad Sci* 108(51):20538–20543.
22. Dhar SS, et al. (2012) Trans-tail regulation of MLL4-catalyzed H3K4 methylation by H4R3 symmetric dimethylation is mediated by a tandem PHD of MLL4. *Genes Dev* 26(24):2749–2762.
23. Migliori V, et al. (2012) Symmetric dimethylation of H3R2 is a newly identified histone mark that supports euchromatin maintenance. *Nat Struct Mol Biol* 19(2):136–144.
24. Blanc RS, Vogel G, Chen T, Crist C, Richard S (2016) PRMT7 preserves satellite cell regenerative capacity. *Cell Rep* 14(6):1528–1539.
25. Ying Z, et al. (2015) Histone arginine methylation by PRMT7 controls germinal center formation via regulating Bcl6 transcription. *J Immunol* 195(4):1538–1547.

26. Blanc RS, Richard S (2017) Regenerating muscle with arginine methylation. *Transcription*:e1291083.

27. Feng Y, et al. (2013) Mammalian protein arginine methyltransferase 7 (PRMT7) specifically targets RXR sites in lysine- and arginine-rich regions. *J Biol Chem* 288(52):37010–37025.

28. Nishioka K, Reinberg D (2003) Methods and tips for the purification of human histone methyltransferases. *Methods* 31(1):49–58.

29. Lee J-H, et al. (2005) PRMT7, a new protein arginine methyltransferase that synthesizes symmetric dimethylarginine. *J Biol Chem* 280(5):3656–3664.

30. Gonsalvez GB, et al. (2007) Two distinct arginine methyltransferases are required for biogenesis of Sm-class ribonucleoproteins. *J Cell Biol* 178(5):733–740.

31. Feng Y, Hadjikyriacou A, Clarke SG (2014) Substrate specificity of human protein arginine methyltransferase 7 (PRMT7): the importance of acidic residues in the double E loop. *J Biol Chem* 289(47):32604–32616.

32. Zurita-Lopez CI, Sandberg T, Kelly R, Clarke SG (2012) Human protein arginine methyltransferase 7 (PRMT7) is a type III enzyme forming omega-NG-monomethylated arginine residues. *J Biol Chem* 287(11):7859–7870.

33. Luense LJ, et al. (2016) Comprehensive analysis of histone post-translational modifications in mouse and human male germ cells. *Epigenetics Chromatin* 9(1):24.

34. Obianyo O, Osborne TC, Thompson PR (2008) Kinetic mechanism of protein arginine methyltransferase 1. *Biochemistry* 47(39):10420–10427.

35. Osborne TC, Obianyo O, Zhang X, Cheng X, Thompson PR (2007) Protein arginine methyltransferase 1: positively charged residues in substrate peptides distal to the site of methylation are important for substrate binding and catalysis. *Biochemistry* 46(46):13370–13381.

36. Feng Y, et al. (2011) Histone H4 acetylation differentially modulates arginine methylation by an in Cis mechanism. *J Biol Chem* 286(23):20323–20334.

37. Fulton MD, Zhang J, He M, Ho M-C, Zheng YG (2017) The intricate effects of alpha-amino and lysine modifications on arginine methylation on the N-terminal tail of histone H4. *Biochemistry* 56:3539–3548.

38. Weiss JN (1997) The Hill equation revisited: uses and misuses. *FASEB J* 11(11):835–841.

39. Feng Y, et al. (2011) A transient kinetic analysis of PRMT1 catalysis. *Biochemistry* 50(32):7033–7044.

40. Zhang X, Cheng X (2003) Structure of the predominant protein arginine methyltransferase PRMT1 and analysis of its binding to substrate peptides. *Structure* 11(5):509–520.

41. Monod J, Wyman J, Changeux J-P (1965) On the nature of allosteric transitions: A plausible model. *J Mol Biol* 12(1):88–118.

42. Koshland DE, Némethy G, Filmer D (1966) Comparison of experimental binding data and theoretical models in proteins containing subunits. *Biochemistry* 5(1):365–385.

43. Ye Y, et al. (2017) Discovery and optimization of selective inhibitors of protein arginine methyltransferase 5 by docking-based virtual screening. *Org Biomol Chem* 15(17):3648–3661.

44. Lu C, et al. (2016) Histone H3K36 mutations promote sarcomagenesis through altered histone methylation landscape. *Science* 352(6287):844–849.

45. Molina-Serrano D, Schiza V, Kirmizis A (2013) Cross-talk among epigenetic modifications: lessons from histone arginine methylation. *Biochem Soc Trans* 41(3):751–759.

46. Yuan W, et al. (2011) H3K36 methylation antagonizes PRC2-mediated H3K27 methylation. *J Biol Chem* 286(10):7983–7989.

47. Jain K, et al. (2016) Protein arginine methyltransferase product specificity Is mediated by distinct active-site architectures. *J Biol Chem* 291(35):18299–18308.

48. Debler EW, et al. (2016) A glutamate/aspartate switch controls product specificity in a protein arginine methyltransferase. *Proc Natl Acad Sci U S A* 113(8):2068–2073.

49. Dunnett CW (1955) A multiple comparison procedure for comparing several treatments

with a control. *J Am Stat Assoc* 50(272):1096.

50. Gottschling H, Freese E (1962) A tritium isotope effect on ion exchange chromatography. *Nature* 196(4857):829–831

Chapter 7

Future Research and Concluding Remarks

What are the physiological substrates of mammalian PRMT7?

The fact that histone proteins and peptides are good substrates for PRMT7 in *in vitro* experiments has suggested that these proteins may also be the *in vivo* substrates (1–4). Additionally, observations on the methylation status of histones in intact cells as a function of PRMT7 expression have also indicated that mammalian PRMT7 may be methylating proteins involved in transcriptional regulation (5, 6). In fact, it is becoming clearer that mammalian PRMT7's methylating activity may be crucial in the regulation of various types of cancers as well (7–10). Taken together however, there is still a significant lack of understanding in terms of the direct substrates that PRMT7 is methylating in the cell. *In vitro* experiments identify histone H2B to be a robust substrate for this enzyme (3, 4), but so far, no direct studies of PRMT7 methylation have been able to identify substrates *in vivo*. However, some proteomic evidence does suggest that H4 R17, also an *in vitro* site of methylation (3), is monomethylated in mouse testes (11). The issue in identifying PRMT7 substrates in intact cells may be largely because of PRMT7's low activity (4) relative to the major dimethylating enzymes, PRMT1 and PRMT5 (12); methods such as mass spectrometry, which readily detect modifications at a stoichiometric level, may not be sensitive enough to detect methylation catalyzed by PRMT7 at only a small sub-fraction of protein sites. However, some studies show that even a 5% change in histone content can lead to the onset of diseases such as chondroblastoma (13), suggesting that while PRMT7-mediated methylation might be an uncommon event in cells, it may still occur to levels that can affect epigenetic pathways involved in chromatin regulation. In fact, with some 19,000 human genes, the modification of histones by PRMT7 in associated with chromatin from only a few genes may be physiologically important while still resulting in the overall methylation of less than one histone in a thousand.

There is also some evidence that PRMT7 may have non-histone substrates. The methylation state of proteins such as Sm proteins and elongation factors have been shown to be affected by the expression of PRMT7 (14, 15). Evidence associating PRMT7 in the regulation of

the function of skeletal muscles (5), stem cells (10, 16), and immune cells (17) also suggests the possibility of non-histone PRMT7 substrates, although it is possible that these phenotypes may be indirectly due to histone methylation. To approach the question of non-histone PRMT7 substrates, I conducted preliminary studies with collaborators Dr. Romeo S. Blanc and Dr. Stefane Richard from McGill University (Montreal, Canada) to determine PRMT7-specific substrates from mouse tissues. My collaborators were able to produce a PRMT7-knockout (PRMT7KO) mouse line and harvest and fractionate cells from various organs. Since radioactivity is a highly sensitive method to detect methylation, I conducted radioactive methylation assays with wild-type (WT) and KO tissue lysates by adding recombinant human PRMT7 and S-adenosyl-[*methyl-*^{3}*H*]-methionine to the mixture. By running these reactions on a gel and analyzing the radioactivity through fluorography, I was able to identify a unique radiolabelled polypeptide in cytoplasmic and nuclear fraction around 35 kDa that only appeared in the PRMT7KO recombinant PRMT7 reaction mixture, implicating this species as a unique non-histone PRMT7 substrate. This species, however, was in significantly lower abundance than surrounding proteins around 35 kDa on the Coomassie blue-stained gel. This made the identification of the novel substrate impossible though MS techniques, as proteins higher in abundance, but not necessarily methylated by PRMT7, in proximity to the species of interest obscured any relevant peptides from being seen in the MS analysis.

Furthermore, mass spectrometry techniques have historically been difficult to use in order to identify posttranslational modifications (PTMs) on histones due to their highly basic amino acid content—leading proteases such as trypsin to digest peptides into individual amino acids, dipeptides or other species too small for typical MS analyses—and have limited the understanding of non-abundantly occurring PTMs. However, in the last few years, with the emergence of middle-down proteomic techniques, the ability to leverage MS techniques to probe non-abundantly occurring PTMs, particularly those occurring in basic regions, has gained significant momentum (18). With a combination of biochemical and mass spectrometric approaches, it will vital to

elucidate the direct substrates of mammalian PRMT7 so that this enzyme's exact role in the epigenetic landscape may be more clearly understood.

Determination of the human PRMT7 structure and understanding the biophysical features that affect PRMT7 activity

Over the last decade, a great deal of effort has been put into solving the structures of the mammalian PRMTs, but structural studies on PRMT7 have really only emerged within the last few years with solution of PRMT7 from *Trypanosoma brucei* (*Tb*PRMT7) (19, 20), then the *Caenorhabditis elegans* ortholog (*Ce*PRMT7) (21), followed by the mouse structure (*Mm*PRMT7) (22). Interestingly, all three PRMT7 structures were published in 2014 and no other structural studies on PRMT7, human or otherwise, have been done since. Obviously missing from this list is the structure of human PRMT7. The mouse ortholog bears high sequence similarity (85.1% identical) to human PRMT7 and contains a duplicated methyltransferase domain like human PRMT7 but solving and uncovering the structural properties of *Hs*PRMT7 are still crucial to understanding the potentially distinct characteristics of this enzyme. Additionally, work described in Chapter 5 highlights that human PRMT7's peculiar preference for sub-physiological temperatures *in vitro* are most likely not due to large ensemble changes in structure. This makes it even more important to clearly outline what the structure of this enzyme is, as identifying potential subtle protein-protein interactions through structural analysis may answer how human PRMT7 works in the cell. Pull-down studies and co-crystallization studies should also be undertaken to better understand the role of potential PRMT7-specific binding partners/chaperones. Specifically, elucidating structures of human PRMT7 in the presence of AdoMet, AdoHcy, and/or substrate molecules like histone peptides will be highly illuminating.

Do other PRMTs exhibit cooperativity and/or engage in crosstalk?

Chapter 6 outlines experiments which highlight for the first time PRMT5's and PRMT1's cooperative kinetic activity (12). Having established that these major dimethylating PRMTs function through positive cooperativity and that PRMT5's methylation of histone H4 R3 may be

significantly affected by PRMT7-mediated methylation of histone H4 R17, it behooves us to ask whether other members of the PRMT family participate in similar kinetic and regulatory behavior. Substantial enzymatic analysis on some of the PRMTs has been done (3, 4, 23–30), but at relatively high substrate and enzyme concentrations, suggesting that these studies may have missed any evidence of cooperativity and allosteric behavior exhibited by these enzymes. If other PRMTs do indeed display positive cooperativity, this will be a new avenue to target this class of enzymes for therapeutics. Allostery is a hallmark of many oligomeric proteins (31), and since most PRMTs functions as homo-oligomers (24–29, 32), it is also important to explore the role of oligomerization in affecting potential cooperativity. Furthermore, the implication that PRMTs can influence the activity of other PRMTs by indirect methylation of the same protein presents a fascinating opportunity to study the regulation of arginine methyltransferase family.

Concluding Remarks

Over the course of the last five years, I have worked to better understand the biochemical nature of PRMT catalysis and how these enzymes can be regulated mechanistically in light of their emerging relevance in the medical field. One of the major findings in my graduate years has been the development of an active-site architecture-based model for PRMT product specificity. In the landscape of burgeoning drug development, understanding the minute structural differences that allow PRMTs to produce varying methylarginine derivatives will be crucial for the synthesis of highly specific and potent therapies. Another exciting discovery from my research was the observation that two major PRMTs—PRMT5 and PRMT1—exhibit positive cooperativity and that PRMT5's activity can be regulated by the activity of another arginine methyltransferase—PRMT7. The epigenetic regulatory field is quite a complex and intricate one. As such, protein-protein interactions and crosstalk among epigenetic readers, writers, and erasers have been a popular subject of study. PRMTs, however, have largely remained untouched in this respect. Thus, evidence for PRMT regulation through allostery may have exciting implications in our knowledge of chromatin biochemistry.

REFERENCES

1. Miranda, T. B., Miranda, M., Frankel, A., and Clarke, S. (2004) PRMT7 is a member of the protein arginine methyltransferase family with a distinct substrate specificity. *J. Biol. Chem.* **279**, 22902–22907
2. Zurita-Lopez, C. I., Sandberg, T., Kelly, R., and Clarke, S. G. (2012) Human protein arginine methyltransferase 7 (PRMT7) is a type III enzyme forming omega-NG-monomethylated arginine residues. *J. Biol. Chem.* **287**, 7859–7870
3. Feng, Y., Maity, R., Whitelegge, J. P., Hadjikyriacou, A., Li, Z., Zurita-Lopez, C., Al-Hadid, Q., Clark, A. T., Bedford, M. T., Masson, J. Y., and Clarke, S. G. (2013) Mammalian protein arginine methyltransferase 7 (PRMT7) specifically targets RXR sites in lysine- and arginine-rich regions. *J. Biol. Chem.* **288**, 37010–37025
4. Feng, Y., Hadjikyriacou, A., and Clarke, S. G. (2014) Substrate specificity of human protein arginine methyltransferase 7 (PRMT7): the importance of acidic residues in the double E loop. *J. Biol. Chem.* **289**, 32604–32616
5. Blanc, R. S., Vogel, G., Chen, T., Crist, C., and Richard, S. (2016) PRMT7 preserves satellite cell regenerative capacity. *Cell Rep.* **14**, 1528–1539
6. Karkhanis, V., Wang, L., Tae, S., Hu, Y. J., Imbalzano, A. N., and Sif, S. (2012) Protein arginine methyltransferase 7 regulates cellular response to DNA damage by methylating promoter histones H2A and H4 of the polymerase δ catalytic subunit gene, POLD1. *J. Biol. Chem.* **287**, 29801–29814
7. Yao, R., Jiang, H., Ma, Y., Wang, L., Wang, L., Du, J., Hou, P., Gao, Y., Zhao, L., Wang, G., Zhang, Y., Liu, D.-X., Huang, B., and Lu, J. (2014) PRMT7 induces epithelial-to-mesenchymal transition and promotes metastasis in breast cancer. *Cancer Res.* **74**, 5656–5667
8. Baldwin, R. M., Haghandish, N., Daneshmand, M., Amin, S., Paris, G., Falls, T. J., Bell, J. C., Islam, S., and Côté, J. (2015) Protein arginine methyltransferase 7 promotes breast

cancer cell invasion through the induction of MMP9 expression. *Oncotarget*. **6**, 3013–3032

9. Migliori, V., Müller, J., Phalke, S., Low, D., Bezzi, M., Mok, W. C., Sahu, S. K., Gunaratne, J., Capasso, P., Bassi, C., Cecatiello, V., De Marco, A., Blackstock, W., Kuznetsov, V., Amati, B., Mapelli, M., and Guccione, E. (2012) Symmetric dimethylation of H3R2 is a newly identified histone mark that supports euchromatin maintenance. *Nat. Struct. Mol. Biol.* **19**, 136–144

10. Dhar, S. S., Lee, S.-H., Kan, P.-Y., Voigt, P., Ma, L., Shi, X., Reinberg, D., and Lee, M. G. (2012) Trans-tail regulation of MLL4-catalyzed H3K4 methylation by H4R3 symmetric dimethylation is mediated by a tandem PHD of MLL4. *Genes Dev.* **26**, 2749–2762

11. Luense, L. J., Wang, X., Schon, S. B., Weller, A. H., Lin Shiao, E., Bryant, J. M., Bartolomei, M. S., Coutifaris, C., Garcia, B. A., and Berger, S. L. (2016) Comprehensive analysis of histone post-translational modifications in mouse and human male germ cells. *Epigenetics Chromatin*. **9**, 24

12. Jain, K., Jin, C. Y., and Clarke, S. G. (2017) Epigenetic control via allosteric regulation of mammalian protein arginine methyltransferases. *Proc. Natl. Acad. Sci. U. S. A.* **114**, 10101–10106

13. Jayaram, H., Hoelper, D., Jain, S. U., Cantone, N., Lundgren, S. M., Poy, F., Allis, C. D., Cummings, R., Bellon, S., and Lewis, P. W. (2016) S-adenosyl methionine is necessary for inhibition of the methyltransferase G9a by the lysine 9 to methionine mutation on histone H3. *Proc. Natl. Acad. Sci. U. S. A.* **113**, 6182–6187

14. Lee, J.-H., Cook, J. R., Yang, Z.-H., Mirochnitchenko, O., Gunderson, S. I., Felix, A. M., Herth, N., Hoffmann, R., and Pestka, S. (2005) PRMT7, a new protein arginine methyltransferase that synthesizes symmetric dimethylarginine. *J. Biol. Chem.* **280**, 3656–3664

15. Jung, G. A., Shin, B. S., Jang, Y. S., Sohn, J. B., Woo, S. R., Kim, J. E., Choi, G., Lee, K. M., Min, B. H., Lee, K. H., and Park, G. H. (2011) Methylation of eukaryotic elongation

factor 2 induced by basic fibroblast growth factor via mitogen-activated protein kinase. *Exp. Mol. Med.* **43**, 550–560

16. Blanc, R. S., and Richard, S. (2017) Regenerating muscle with arginine methylation. *Transcription*. 10.1080/21541264.2017.1291083
17. Ying, Z., Mei, M., Zhang, P., Liu, C., He, H., Gao, F., and Bao, S. (2015) Histone arginine methylation by PRMT7 controls germinal center formation via regulating Bcl6 transcription. *J. Immunol.* **195**, 1538–1547
18. Sidoli, S., and Garcia, B. A. (2017) Middle-down proteomics: a still unexploited resource for chromatin biology. *Expert Rev. Proteomics*. **14**, 617–626
19. Debler, E. W., Jain, K., Warmack, R. A., Feng, Y., Clarke, S. G., Blobel, G., and Stavropoulos, P. (2016) A glutamate/aspartate switch controls product specificity in a protein arginine methyltransferase. *Proc. Natl. Acad. Sci. U. S. A.* **113**, 2068–2073
20. Wang, C., Zhu, Y., Caceres, T. B., Liu, L., Peng, J., Wang, J., Chen, J., Chen, X., Zhang, Z., Zuo, X., Gong, Q., Teng, M., Hevel, J. M., Wu, J., and Shi, Y. (2014) Structural determinants for the strict monomethylation activity by trypanosoma brucei protein arginine methyltransferase 7. *Structure*. **22**, 756–768
21. Hasegawa, M., Toma-Fukai, S., Kim, J.-D. D., Fukamizu, A., and Shimizu, T. (2014) Protein arginine methyltransferase 7 has a novel homodimer-like structure formed by tandem repeats. *FEBS Lett.* **588**, 1942–1948
22. Cura, V., Troffer-Charlier, N., Wurtz, J. M., Bonnefond, L., and Cavarelli, J. (2014) Structural insight into arginine methylation by the mouse protein arginine methyltransferase 7: a zinc finger freezes the mimic of the dimeric state into a single active site. *Acta Crystallogr. D. Biol. Crystallogr.* **70**, 2401–2412
23. Feng, Y., Xie, N., Jin, M., Stahley, M. R., Stivers, J. T., and Zheng, Y. G. (2011) A transient kinetic analysis of PRMT1 catalysis. *Biochemistry*. **50**, 7033–7044
24. Pak, M. L., Lakowski, T. M., Thomas, D., Vhuiyan, M. I., Hüsecken, K., and Frankel, A.

(2011) A Protein Arginine *N* -Methyltransferase 1 (PRMT1) and 2 Heteromeric Interaction Increases PRMT1 Enzymatic Activity. *Biochemistry*. **50**, 8226–8240

25. Frankel, A., and Clarke, S. (2000) PRMT3 is a distinct member of the protein arginine N-methyltransferase family. Conferral of substrate specificity by a zinc-finger domain. *J. Biol. Chem.* **275**, 32974–32982

26. Schurter, B. T., Koh, S. S., Chen, D., Bunick, G. J., Harp, J. M., Hanson, B. L., Henschen-Edman, A., Mackay, D. R., Stallcup, M. R., and Aswad, D. W. (2001) Methylation of histone H3 by coactivator-associated arginine methyltransferase 1. *Biochemistry*. **40**, 5747–5756

27. Sun, L., Wang, M., Lv, Z., Yang, N., Liu, Y., Bao, S., Gong, W., and Xu, R.-M. (2011) Structural insights into protein arginine symmetric dimethylation by PRMT5. *Proc. Natl. Acad. Sci.* **108**, 20538–20543

28. Lakowski, T. M., and Frankel, A. (2008) A kinetic study of human protein arginine N-methyltransferase 6 reveals a distributive mechanism. *J. Biol. Chem.* **283**, 10015–10025

29. Dillon, M. B. C., Rust, H. L., Thompson, P. R., and Mowen, K. A. (2013) Automethylation of protein arginine methyltransferase 8 (PRMT8) regulates activity by impeding S-adenosylmethionine sensitivity. *J. Biol. Chem.* **288**, 27872–27880

30. Hadjikyriacou, A., Yang, Y., Espejo, A., Bedford, M. T., and Clarke, S. G. (2015) Unique features of human protein arginine methyltransferase 9 (PRMT9) and its substrate RNA splicing factor SF3B2. *J. Biol. Chem.* **290**, 16723–16743

31. Monod, J., Wyman, J., and Changeux, J.-P. (1965) On the nature of allosteric transitions: A plausible model. *J. Mol. Biol.* **12**, 88–118

32. Zhang, X., and Cheng, X. (2003) Structure of the predominant protein arginine methyltransferase PRMT1 and analysis of its binding to substrate peptides. *Structure*. **11**, 509–520